AD-A158 293 MODELING A LARGE RING RESONATOR GYROSCOPE(U) OKLAHOMA 1/2
STATE UNIV STILLWATER SCHOOL OF ELECTRICAL AND CMMPUTER
ENGINEERING H R BILGER 30 MAR 85 AFOSR-TR-85-0526
UNCLASSIFIED AFOSR-84-0058 F/G 3/1 NL

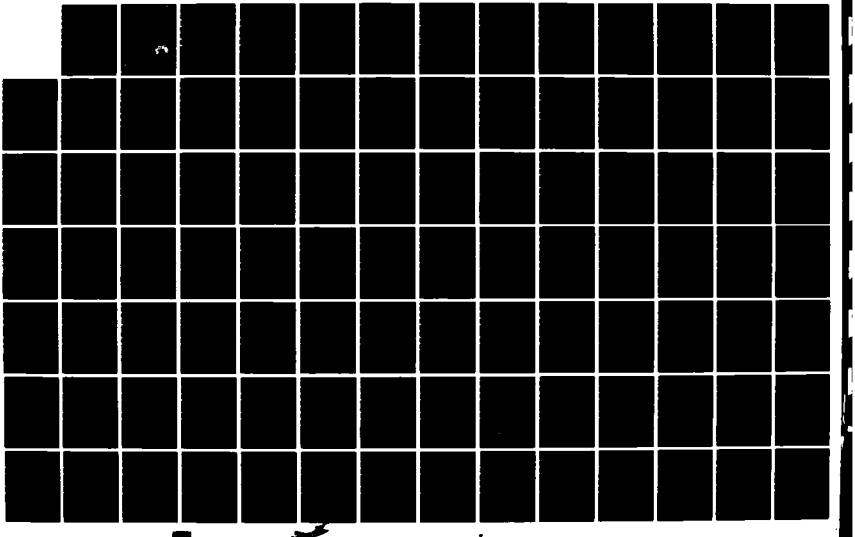

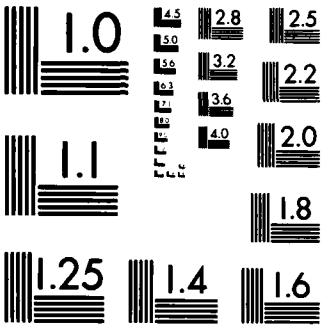

MICROCOPY RESOLUTION TEST CHART
NATIONAL BUREAU OF STANDARDS-1963-A

AD-A158 293

This document has been approved for public release and sale; its distribution is unlimited.

UNCLASSIFIED

SECURITY CLASSIFICATION OF THIS PAGE

AD-A158 293

REPORT DOCUMENTATION PAGE

1a. REPORT SECURITY CLASSIFICATION: UNCLASSIFIED	1b. RESTRICTIVE MARKINGS
2a. SECURITY CLASSIFICATION AUTHORITY	3. DISTRIBUTION/AVAILABILITY OF REPORT: Approved for public release; distribution unlimited.
2b. DECLASSIFICATION/DOWNGRADING SCHEDULE	
4. PERFORMING ORGANIZATION REPORT NUMBER(S)	5. MONITORING ORGANIZATION REPORT NUMBER(S): AFOSR-TR- 3526
6a. NAME OF PERFORMING ORGANIZATION: Oklahoma State University; 6b. OFFICE SYMBOL (If applicable)	7a. NAME OF MONITORING ORGANIZATION: Air Force Office of Scientific Research
6c. ADDRESS (City, State and ZIP Code): Dept of Elec & Eng, Stillwater OK 74078	7b. ADDRESS (City, State and ZIP Code): Bldg 410, Bolling AFB DC 20332-6448
8a. NAME OF FUNDING/SPONSORING ORGANIZATION: AFOSR; 8b. OFFICE SYMBOL (If applicable): NE	9. PROCUREMENT INSTRUMENT IDENTIFICATION NUMBER: AFOSR-84-0058
8c. ADDRESS (City, State and ZIP Code): Bldg 410, Bolling AFB DC 20332-6448	10. SOURCE OF FUNDING NOS. — PROGRAM ELEMENT NO.: 61102F; PROJECT NO.: 2305; TASK NO.: B2; WORK UNIT NO:

11. TITLE (Include Security Classification): MODELING A LARGE RING RESONATOR GYROSCOPE

12. PERSONAL AUTHOR(S): Professor Bilger

13a. TYPE OF REPORT	13b. TIME COVERED	14. DATE OF REPORT (Yr., Mo., Day)	15. PAGE COUNT
Final	FROM 01 FEB 84 TO 31 JAN 85	Mar Feb 1985	138

16. SUPPLEMENTARY NOTATION

17. COSATI CODES		
FIELD	GROUP	SUB. GR.

18. SUBJECT TERMS (Continue on reverse if necessary and identify by block number): Quantum Noise and Low Frequency Noise; Basic Modeling of the ring with Gaussian Beam & ray Matrices

19. ABSTRACT (Continue on reverse if necessary and identify by block number)

Attach

Rept. Date verified per call. DC

A-1

20. DISTRIBUTION/AVAILABILITY OF ABSTRACT: UNCLASSIFIED/UNLIMITED ☒ SAME AS RPT. ☐ DTIC USERS ☐	21. ABSTRACT SECURITY CLASSIFICATION: UNCLASSIFIED
22a. NAME OF RESPONSIBLE INDIVIDUAL: [illegible]	22b. TELEPHONE NUMBER (Include Area Code): (202) 767-4906; 22c. OFFICE SYMBOL: NE

DD FORM 1473, 83 APR — EDITION OF 1 JAN 73 IS OBSOLETE.

UNCLASSIFIED

SECURITY CLASSIFICATION OF THIS PAGE

A recent survey, although incomplete, is ref. 1. It has been shown that a high sensitivity ring project would become worthwhile if rotation sensitivities of better than 10(-9) x the earth's rotational rate can be reached. In this case it can potentially surpass in sensitivity not only the most advanced techniques for measuring absolute rotation of the earth, i.e. Lunar ranging, Lageos, VLBI (ref. 2), but it offers exciting possibilities: 1) it measures in "real time", directly a component of rotation rate, 2) it is a local sensor of absolute rotation, 3) it can basically be adjusted to be most sensitive for slow events (daily-monthly changes of the earth rotation vector) or fast events (microseisms, earth quakes, local disturbances of earth surface), 4) since it is a local method, the beam can naturally be circulated in vacuum, atmospheric disturbances are eliminated from the beam path.

Modeling a large ring resonator gyroscope

AFOSR grant No. 84-0058

(1 Feb. 1984-31 Jan. 1985)

H.R. Bilger
Electrical and Computer Engineering
310 ES
Oklahoma State University
Stillwater, OK 74078

30 March 1985

A[illegible] SCIENTIFIC RESEARCH (AFSC)
[illegible] is
[illegible].
MATTHEW [illegible]
Chief, Technical Information Division

Accession For
NTIS GRA&I ☑
DTIC TAB ☐
Unannounced ☐
Justification
By
Distribution/
Availability Codes
Dist | Avail and/or Special
A-1

DTIC COPY INSPECTED

Approved for public release;
distribution unlimited.

Foreword

The project of constructing a large laser ring is an end result of several questions, the more important of them being: a) Why should one do it? (motivation, expected benefits, comparison with competitive methods), b) Is the project feasible? (sensitivity, costs, compatibility of expected results with a)) c) What is the design? (technical parameters, stability considerations, output).

Ample literature is available on a). A recent survey, although incomplete, is ref. 1. It had become clear that the project would become worthwhile if rotation sensitivities of better than $10^{-9}\Omega_E$ (Ω_E="earth rate" = 2π/day) can be reached. In this case it can potentially surpass in sensitivity not only the most advanced techniques for measuring absolute rotation of the earth, i.e. Lunar ranging, Lageos, VLBI (ref. 2), but it offers exciting possibilities: 1) it measures in "real time", directly a component of rotation rate, 2) it is a local sensor of absolute rotation, 3) it can basically be adjusted to be most sensitive for slow events (daily-monthly changes of the earth rotation vector) or fast events (microseisms, earth quakes, local disturbances of earth surface), 4) since it is a local method, the beam can naturally be circulated in vacuum; atmospheric disturbances are eliminated from the beam path.

The extrapolation to an expected sensitivity of $<10^{-9}\Omega_E$ is done from data presently available, of the order of $10^{-6}\Omega_E$ (with averaging times of 1 day), with the theory of laser noise which is reasonably well in hand at this time. Much of the data on noise were measured by the author during several summer jobs in industry. The 1/f-noise becoming overseeable (ref. 3), we may now be able to predict $<10^{-9}\Omega_E$ for

averaging times much less than 1d. Technological improvements in making high-quality mirrors do continually push back the limits due to white noise and 1/f noise. The finished ring should become a formidable sensor of $\Omega_E(t)$, for Fourier frequencies larger than about a reciprocal year.

This report provides a variety of technical details on the basic noise limitations in a laser ring and on how to remove obstacles to reach the required sensitivities; some of the basic calculations on rings are collected as well as several novel insights into the setting up are reported. The major results have already been, or are in the process of being, published.

As a summary of the first year of involvement with the Seiler ring project, we state that none of the results have yet negated the proposed performance of it.

Modeling a large ring resonator gyroscope
Grant No. AFOSR-84-0058
Contract period 1 Feb. 1984-31 Jan. 1985

Report

Summary: The results obtained can be divided into three categories: a) A feasibility study with focus on quantum noise and low frequency noise b) Basic modeling of the ring with Gaussian beam and ray matrices c) Technical design: Effect of residual gas in ring on quality factor and light drag, scanning of beam, effect of misalignment and mismatch of source to ring, calibration procedures.

The results show no obstacle yet to the goal of achieving a sensitivity of rotation rate of better than 10^{-9} (earth rate) in rings of 60 m^2 size. Such a sensitivity which corresponds to a change of earth surface velocity of smaller than 4 cm/day, should surpass Lunar ranging methods, Lageos methods as well as VLBI-methods in accuracy, besides being a "real-time" observational method for earth rotation.

Content

I. Introduction

The content of this report is mainly intended to facilitate the design of large laser rings which act as gyros: They sense, via Sagnac effect, the absolute rotation of their structure. Versions with sizes up to square meters are by now well-known in industry as R(ing) L(aser) G(yro)'s. They have been pushed to better performance ever since the basic proposal of Rosenthal [4] was published. To guide the reader: two basic equations govern signal and noise of such a gyro:

Signal: $$\Delta f=(4/\lambda L)\vec{A}\circ\vec{\Omega} \qquad 1)$$

This equation translates an absolute rotation rate $\vec{\Omega}(t)$ of the ring into a beat frequency Δf (t);

Noise: $$S_{\Delta f}=hf_0^3/Q^2P \qquad 2)$$

which represents white quantum noise fluctuations per mode. Hereby, $S_{\Delta f}$ is the power spectral density of the output frequency noise Δf [5].

This report can be visualized as a study to realize the promise of equations 1 and 2. Most of the results were obtained with a view on designing the Seiler ring at the AF Academy, but they are of course generally applicable to large rings. In certain cases calculations were done on an active ringlaser. The equivalence in performance of active and passive rings [6] justifies such a procedure, although the design calls for a "passive" ring at this time.

Whenever a certain topic treated here appeared as a publication, the latter was substituted for the original text. A rough draft of this report was handed out to Seiler lab personnel on 2 Nov. 1984.

II. Contributions to basic theory of ringlaser

II. A. Low-frequency noise in ring laser gyros

II. A. 1 Reprint from SPIE - The International Society for Optical Engineering (ref. 7)

A Reprint from the

PROCEEDINGS

Of SPIE-The International Society for Optical Engineering

Volume 487

Physics of Optical Ring Gyros

7-10 January 1984
Snowbird, Utah

Low frequency noise in ring laser gyros

H. R. Bilger
School of Electrical and Computer Engineering
310ES, Oklahoma State University
Stillwater, Oklahoma 74078

©1984 by the Society of Photo Optical Instrumentation Engineers
Box 10, Bellingham, Washington 98227 USA Telephone 206 676-3290

Low frequency noise in ring laser gyros

H. R. Bilger

[illegible] Computer Engineering, ECEN, Oklahoma State University
Stillwater, Oklahoma 74078

Abstract

[illegible] spectral densities $S_{\Delta f}$ of ringlaser beat frequencies $\Delta f(t)$ consist mainly [illegible] laser noise is $1/f^2$ noise. Consequently, experimental results [illegible] of the Fourier frequency f,

[illegible] noise, h_{-1} is usually somewhat above the Jagnepain- [illegible] vary widely between devices. The most important 1/f [illegible] of ring laser performance. All analyzed noise [illegible] of the magnitudes of the noise involved.

[illegible] of frequency noise in oscillators

[illegible] its ragged appearance on TV screens, scopes, [illegible] spectral densities are plotted versus Fourier [illegible] spikes (δ-functions) are essentially absent in [illegible] the evaluation of spectra versus frequency [illegible] averaging time τ, proper account is taken of the [illegible] with arbitrary frequency dependence), discrete [illegible] individual power spectral density components [illegible] individual errors $\Delta S/S = 1$. Averaging of m [illegible] to $\Delta S/S = m^{-1/2}$. In many published spectra, [illegible] could simply be fitted by smooth spectra if the [illegible] approximately obeyed even in small sampling theory[1,2], [illegible] the two-sample variances (Allan variances).

[illegible] makes no exception. We will restrict our discussion [illegible] with their usual extreme spectral purity, such that the [illegible] sources in the lasing system rarely leads to excursions [illegible] Here, f_0 is the average oscillation frequency for which [illegible] taken. In the particular case of a ringlaser, two or more [illegible] are excited in the same cavity, and the difference frequency Δf is [illegible]. Therefore, a noise source producing correlated effects on the oscillations may not appear in Δf. This is the major reason ring laser outputs show frequency noise which is orders of magnitude below even the best maser clocks. Indeed the irreducible quantum noise limit[3] has been reached in good ring lasers (gyros) over many hours of observation which is quite a remarkable feat.

In keeping with the remarks above and with common practice in oscillator work we propose[4] a simple empirical power law series for the (one-sided) power spectral density $S_{\Delta f}$ of the observed beat frequency $\Delta f(t)$ between two (or more) optical oscillations versus Fourier frequency

$$S_{\Delta f}(f) = h_0 + h_{-1}f^{-1} + h_{-2}f^{-2} + \ldots + (h_1 f^{+1} + h_2 f^{+2} + \ldots) \quad (1)$$

with an equivalent Allan variance[5]

$$\sigma_A^2(\tau) = (h_0/2)\tau^{-1} + (2\ln 2\, h_{-1})\tau^0 + (4\pi^2 h_{-2}/6)\tau^{+1} + \ldots \quad (2)$$

A given power law in S corresponds to a power law in σ_A^2. Note in particular that a noise spectral density proportional to h_{-1} (flicker noise) produces a minimum Allan variance versus τ which is called flicker floor, a main characteristic in oscillators which is always observed, with the possible exception of hydrogen masers[6].

To avoid possible confusion it may be noted here that the noise discussed in this paper is strictly frequency noise which is measured by counting the output over a given time interval, or alternately by comparing the frequency directly with a frequency reference.

Any amplitude noise is disregarded in practice, although in principle it would have to be included in a thorough discussion of oscillator noise.

In the following we present data obtained from optical oscillators over the last two decades. They are shown either as a frequency deviation versus time from a reference, as a power spectral density of the beat frequency, or as an Allan variance of the beat frequency versus averaging time. They form the empirical basis for the classification scheme above. We then provide some thoughts on theoretical explanations of the observed noise. Finally, projected data on noise of large rings are included.

Experimental evidence of laser frequency fluctuations

Some preliminary information is given in ref. 7. Time-domain representations are dicussed in detail in ref. 8. One of the earliest documentations of optical frequency fluctuations by Jaseja et al.[9] is given in figure 1.

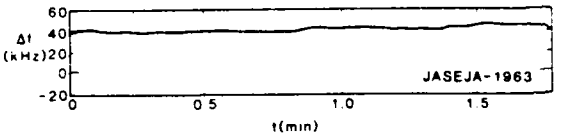

Figure 1. Fluctuation of frequency difference between two lasers at $\lambda = 1.15\mu m$ observed by Jaseja et al. in 1963.

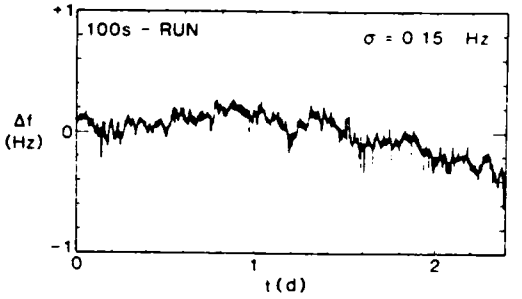

Figure 2. Fluctuation of frequency difference between two countercirculating modes at $\lambda = 633$ nm in a ring laser gyro (1982).

The beat note stayed audible over several minutes, i.e. it was of the order of kilohertz. In contrast to this is figure 2[7] obtained on a ring laser in 1982, where the beat was observed not to exceed ± 0.7 Hz over 2 1/2 days. The beat frequency has to be counted over a sampling period of 100 s to avoid significant quantization errors. The resulting rms-deviation was $\sigma = 0.15$ Hz over the whole period.

Turning to power spectral measurements: S versus power input P into a mode was studied by Kuvatova[10] in 1976 where a P^{-1} dependence was clearly observed over more than a decade of power, at Fourier frequencies where the laser noise was white, fig. 3.
As early as 1967, Siegman[11] had already succeeded in separating the noise in a white part and a f^{-2}-part, with a transition frequency of about 1 kHz, using two separate lasers under very careful conditions, fig. 4.

The following figures (5 through 10) were taken from data on a commercial ringlaser between 1980 and 1982.

Figure 5 shows a spectrum with a clear 1/f part over one decade. The transition frequency is at 5 millihertz. The open circles show the effect of quantization noise as an additional noise power spectral density for this run with sampling period 10 s. Correcting for it gave the white noise as indicated. A different run with 100 s sampling interval shows exclusively 1/f noise, fig. 6. The error bars are the statistical (rms) errors of clusters of 100 points (± 10%). In fig. 7, a long run (over 9½ days) shows f^{-2}, f^{-1} and white noise exclusively. The noise has a f^{-2} behavior over an impressive five decades of power density, with no discernible deviation from equation (1) except possibly below 3 μHz. Figure 8 gives a quantitative account of the relative spectral purity of ringlaser outputs ($S_{\Delta f/f_0}$) compared to data on hydrogen masers given by Vessot et al.[12] in 1977. Note that the state of the art in both hydrogen masers and ringlasers has considerably improved since; the flicker floors are estimated to be about two orders of magnitude lower in both types of devices. One of the better results achieved in ringlasers is given in figure 9, where white noise prevails at frequencies above 400μHz, with a spectral density of $S_{\Delta f} = h_0 =$

9×10^{-3} Hz^2/Hz; again, the overall spectrum can very well be represented by equation (1). Note also that the magnitudes are up to a factor 600 different from those given in figure 7.

A representative Allan variance versus τ is given in figure 10. Since the transformation between S and σ^2 is known[5], the curve σ_A^2 versus τ can be quantitatively predicted from power spectral densities, and vice versa. The flicker floor from figure 7 corresponds to $\sigma_A/f_o = 4.6 \times 10^{-17}$, whereas the flicker floor from figure 9 is $\sigma_A/f_o = 5.8 \times 10^{-13}$.

Theoretical support of equation (1)

White noise term h_o

Literature abounds at this time in calculations on white noise[13]. It is calculated from quantum noise considerations. According to arguments on quantum fluctuations of a system far from threshold, with complete inversion, at Fourier frequencies not exceeding $f = f_o/2Q$ (Q = quality factor of passive optical cavity), at quantum-dominated oscillation frequencies $f_o >> kT/h$, the (one-sided) power spectral density of one oscillation is [13,14]

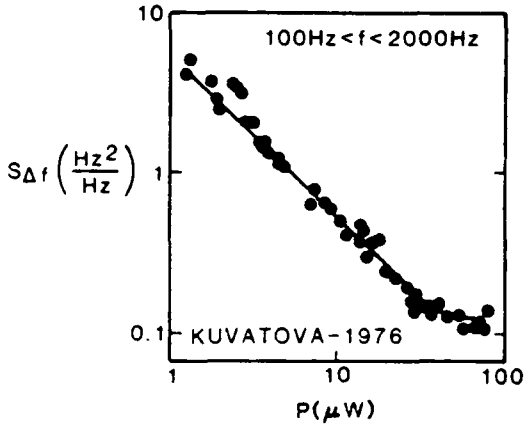

Figure 3. Power spectral density of a ringlaser output at $\lambda = 1.15$ μm.

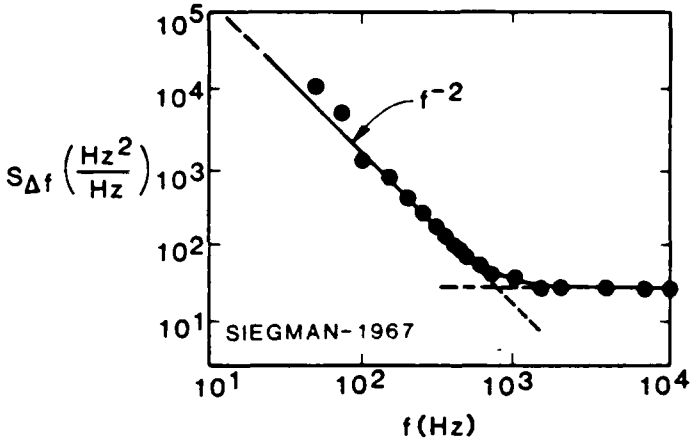

Figure 4. Power spectral density of the beat frequency between two lasers at $\lambda = 633$ nm.

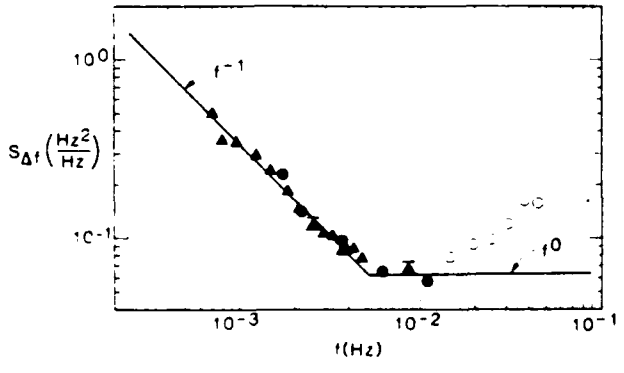

Figure 5. Run with sampling interval 10 s, showing quantization noise at high frequencies (open circles). The line f^0 (white noise) is obtained after correction for the quantization noise. At lower frequencies, f^{-1} noise is apparent. Note the size of the errors of the data.

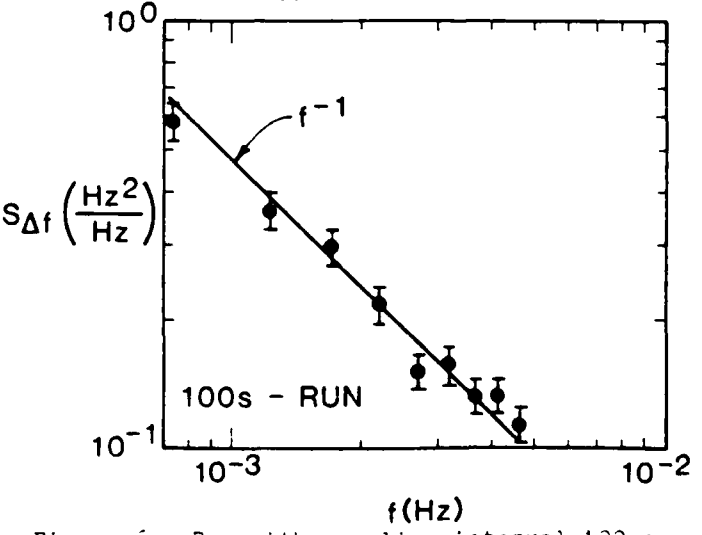

Figure 6. Run with sampling interval 100 s. Pure 1/f noise prevails, well documented via the error bars of the points which are averages of 100 neighboring individual power spectral densities.

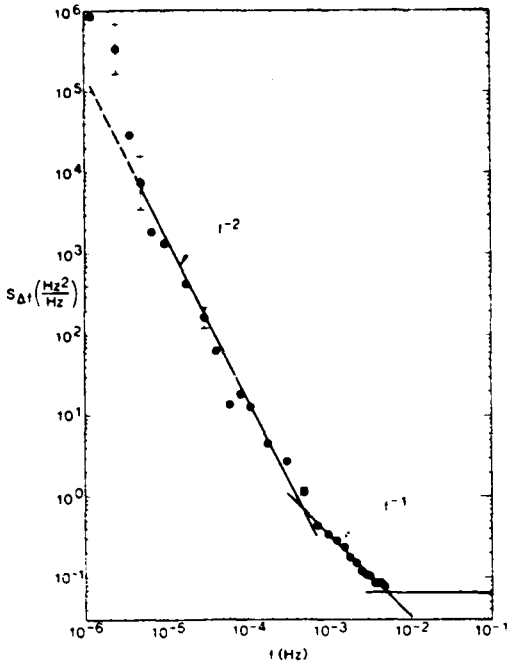

Figure 7. Power spectral density of a 9 1/2 day run. The bottom line is the white noise after subtraction of quantization noise.

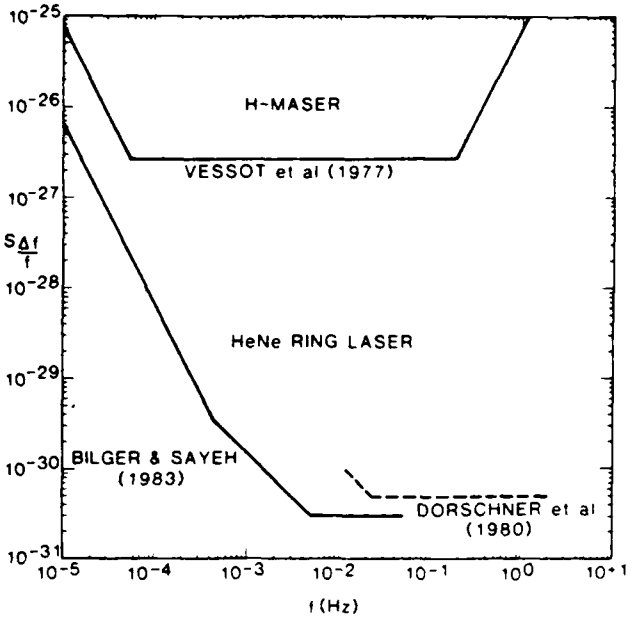

Figure 8. Comparison of noise spectral densities of relative frequency fluctuations of a state-of-the art hydrogen maser in 1977 and a ring laser in 1980.

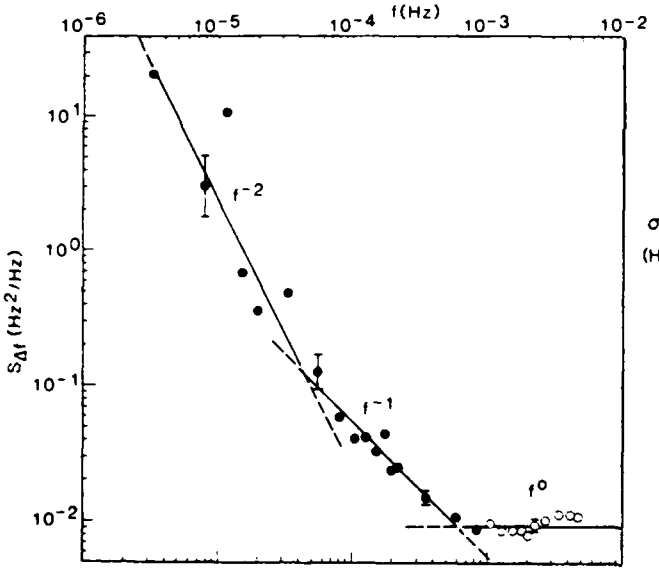

Figure 9. Power spectral density of a composite 5-day run. Equation (1) fits very well into the data. Quantization noise has been removed (open circles).

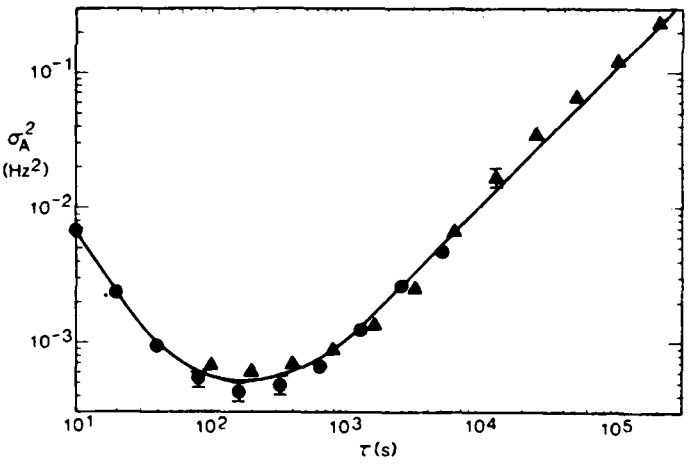

Figure 10. Allan variance of two runs on the same ringlaser. The broad minimum indicates presence of 1/f noise.

$$S_{\Delta f} = hf_0^3/Q^2P = h_0, \tag{3}$$

h = Planck's constant = 6.63×10^{-34} VAs^2.

At difference frequencies large compared to lock-in frequencies, the quantum noise of the two (or more) oscillations leading to the beat frequency are considered uncorrelated, at least in second order, so that the power spectral densities simply add. For example for a four-mode ring laser the observed beat frequency is expected to have a power spectral

density $S_{\Delta f}$, four modes = 4 $S_{\Delta f}$, if quality factor and power input are assumed to be the same for each mode. Published comparisons of theory and experiment are given by Dorschner et al[14], by Hammons and Ashby[15], and by Bilger and Sayeh[7]. The quality factor of a passive cavity can be determined with reasonable accuracy (error < 10%), and the power lost in the cavity can be estimated with about the same accuracy. In references 7 and 14 the measured white noise level was about 50% larger than the one calculated through equation (3). The difference is considered larger than the measurement errors; incomplete conversion in the lasing levels N_2 and N_1 has been suggested. A ratio $N_2/N_1 = 3$ would account for the observed difference. More precise comparisons of white noise observations with calculations are clearly important.

As things stand at this time, we may argue that good ring lasers operate at "high frequencies" within a factor two of the white noise given by equation (3). This is, in itself, a remarkable statement, as very few macroscopic phenomena have been shown to possess quantum-noise limited behavior (superconducting devices is another example). In designs of future ringlaser systems we may indeed use equation (3) to predict the "high frequency" lower limit, which actually may be correct down to frequencies of the order of a reciprocal day, see ref. 8. We do not anticipate any dramatic reduction of this level.

Flicker noise term h_{-1}

As opposed to the term h_0, the magnitude of h_{-1} has not been assessed adequately as to the dependence on parameters of the laser system. Low frequency fluctuations of this kind are sometimes called "bias instability," from the misguided notion that flicker noise may be separable from bias fluctuations.

A quick comparison with maser clocks (figure 8) would have us predict flicker floors vastly in excess of the ones actually observed in ringlasers (see refs. 4 and 7); no doubt some cancelling of correlated flicker noise is responsible.

In an attempt to look for reasons for flicker noise, quartz oscillators may serve as an example. Vagnepain et al[16] investigated a large variety of quartz oscillators, at resonance frequencies 1 MHz to 25 MHz, and at temperatures from 1 K to 300 K. They found the remarkable Q^{-4} dependence given in figure 11

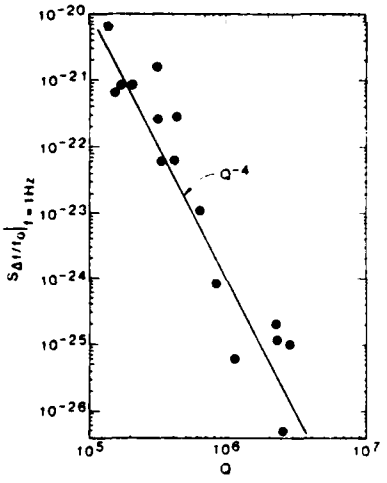

Figure 11. 1/f component of power spectral density observed at f = 1Hz in quartz oscillators versus the quality factor of the quartz crystals.

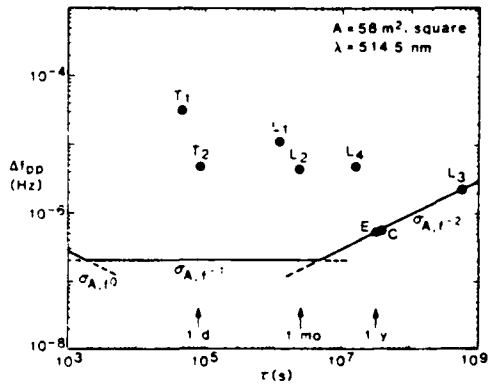

Figure 12. Estimated Allan standard deviation σ_A of a large ring (58 m²), and anticipated sizes of variations in the earth rate at time scales of 10^3s (1/4h) to 10^9s (30 y). T = tidal effects, L = various lunar effects, E, C = Euler resp. Chandler wobbles.

which extends over six decades of S, suggesting a fundamental role of the quality factor in the 1/f noise. The theoretical approach to explain this dependence rests on the hypothesis[17] that phonon relaxation times τ_p in a lattice have a 1/f power spectral density by themselves, i.e. $S_{\Delta\tau_p} \propto f^{-1}$. But the quality factor in a quartz cavity is related to the losses via τ_p, viz.

$$\delta f/f_0 = [(\omega_0\tau_p)^2/(1+\omega_0^2\tau_p^2)^2]\,\delta\tau_p/\tau_p \propto Q^{-2}\,\delta\tau_p/\tau_p. \quad (4)$$

Taking the power spectral densities on both sides produces indeed a Q^{-4}-law. Gagnepain et al. moreover propose that the proportionality factor be in the neighborhood of one, i.e.

$$S_{\Delta f/f} = AQ^{-4}/f \qquad \text{with } A = 1. \quad (5)$$

Whether this hypothesis can be successfully transplanted into laser systems remains to be seen. An investigation of the following aspects of observed 1/f noise is desirable:
1. Dependence on the losses, or quality factor (is Q^{-4} apparent?)
2. Dependence on beam power (which way to enter the losses?)
3. Dependence on bias (is 1/f largely compensated?)
4. Dependence on cavity construction (temperature coefficient, elastic properties, mass?)

At this time, comparing observed 1/f noises in figures 7 and 9 tentatively with the Gagnepain-Uebersfeld law

$$S_{\Delta f} = f_0^2\, Q^{-4}\, f^{-1}, \quad (6)$$

we note that equation (6) predicts lower 1/f noise by about an order of magnitude.

Indirect evidence of the crucial role of the laser cavity quality factor is the fact that commercial ringlasers with lossy elements in the cavity (Faraday rotators, e.g.) are inferior in 1/f noise ("bias stability") to ringlasers without intracavity elements.

Random walk term h_{-2}

This term is known to be quite apparatus-dependent[11], as opposed to the idea that the atomic system itself may produce it. As an example, temperature fluctuations may possess a relaxation spectrum of the type

$$S_{\Delta T} \propto \tau_T[1+\omega^2\tau_T^2]^{-1}. \quad (7)$$

For large thermal relaxation times this spectrum essentially provides a f^{-2} source which may be transduced through the temperature sensitivity of the system into beat frequency noise with an f^{-2} - dependence. Quantitative estimates of this effect depend crucially on details of the construction of the laser cavity.

Summary

Three major noise phenomena are well documented in ring lasers: White noise, flicker noise, and random walk noise. The white noise is reasonably well linked to quantum noise of the oscillator. The second type is tentatively linked to the quality factor of the cavity via 1/f spectra of the losses; the latter play a major role in most theories trying to explain 1/f noise in physical systems. In ringlasers, a large power law dependence on Q would lend support to Handel's[17] theory on 1/f noise. The random walk can be linked to fluctuations in the support, e.g. due to transduced temperature fluctuations.

Conclusions and suggestions

From the foregoing it is clear that very high Q cavities should be attempted, not only to decrease the quantum noise but even more so to decrease the 1/f noise. The application of these ideas to large ringlasers, e.g. to the 58 m^2 ring presently in the design stage at the Beiler lab (AF Academy, CO) may prove useful. Estimated Allan standard deviations for such a ring are shown in figure 12: At Fourier frequencies of 1 mHz down to, say, 0.1 mHz, the dominating role is not played by quantum noise but by 1/f noise. Quantum noise is expected to be negligible in this range. The various points in figure 12 indicate anticipated magnitudes of variations in the rotation vector of the earth at the periods indicated. They may then become visible in the ring output, should the estimated noise materialize.

Acknowledgement

This work is supported by grant No. AFOSR-84-0053 from OSR which agency is, to our delight, interested in supporting such basic scientific research. I would like to acknowledge the cooperation of the Beiler Lab, AF Academy, CO which led to this paper.

References

1. Benlat, J. S., and Piersol, A. G., Random Data: Analysis and Measurement Procedures, Wiley 1971.

2. Lesage, P., and Audoin, C., "Estimation of the two-sample variance with a limited number of data," Proc. 31st Ann. Freq. Contr. Symp. 1977, pp. 311-318.

3. We do not discuss here possible clever uses of the uncertainty relations by redistributing errors of canonically conjugated variables, as proposed in ref. 14.

4. Bilger, H. R., "Possibility of flicker floor in laser gyros," 11th Winter Colloq. Quant. El., Snowbird, UT, Jan. 1981.

5. Barnes, J. A., Chi, A. R., Cutler, L. S., Healey, D. J., Leeson, D. B., McGunigal, T. E., Mullen, J. A., Smith, W. L., Sydnor, R. L., Vessot, R. F. C., and Winkler, G. M. R., "Characterization of Frequency Stability," IEEE Trans. Instr. Meas. IM-20, pp. 105-120, 1971.

6. Walls, F. (NBS, Boulder, CO), private communication.

7. Bilger, H. R., and Sayeh, M., "Noise phenomena in ring lasers," in Noise in physical systems and 1/f noise (eds. M. Savelli, G. Lecoy, and J.-P. Nougier), Elsevier Science Publ. B.V. 1983, pp. 325-328.

8. Tehrani, M. M., "Ring laser gyro data analysis with cluster sampling techniques," SPIE symposium on fiberoptic and laser sensors, Arlington, VA, April 1983.

9. Jaseja, T. J., Javan, A., and Townes, C. H., "Frequency stability of HeNe masers and measurements of length," Phys. Rev. Lett. 10, pp. 165-167, 1963.

10. Kuvatova, E. A., "Experimental investigation of difference-frequency fluctuations in a ring laser emitting at $\lambda = 1.15$ μm," Sov. J. Quant. Electron. 6, pp. 373-374, 1976.

11. Siegman, A. E., Daino, B., and Manes, K. R., "Preliminary measurements of laser short-term frequency fluctuations," IEEE J. Qu. El. QE-3, pp. 180-189, 1967.

12. Vanier, J., "The active hydrogen maser: State of the art and forecast," Metrologia 18, pp. 173-186, 1982.

13. Simpson, J. H., "A fundamental noise limit to RLG performance," 1980 NAECON (IEEE, New York), Vol. 1, pp. 80-83; Klimontovich, Y. L., Kovalev, A. S., and Landa, P. S., "Natural fluctuations in lasers," Sov. Phys. Usph. 15, pp. 95-113, 1972; Yariv, A., Introduction to optical electronics, Holt, Rinehart and Winston, Inc. 1971, Sec. 10.6; Gordon, E. I., "Optical maser oscillators and noise," Bell Syst. Techn. J. 43, pp. 507-539, 1964; Scully, M., and Sanders, V., "Quantum noise and ultimate performance," SPIE, this issue.

14. Dorschner, T. A., Haus, H. A., Holz, M., Smith, I. W., and Statz, H., "Laser gyro at quantum limit," IEEE J. Quant. El. QE-16, pp. 1376-1379, 1980.

15. Hammons, B. W., and Ashby, V. J., "Mechanically dithered RLG at the quantum limit," 1982 NAECON (IEEE, New York), pp. 388-392.

16. Gagnepain, J. J., Uebersfeld, J., Goujon, G., and Handel, P., "Relation between 1/f noise and Q-factor in quartz resonators at room and low temperatures, first theoretical interpretation," Proc. 35th Ann. Freq. Contr. Symp., pp. 476-483, 1981.

17. Handel, P. H., "Quantum theory of 1/f noise," Phys. Lett. 53A, pp. 438-440, 1975.

II. A. 2 Flicker noise in frequency fluctuations of lasers (ref. 8)

A survey of some experimental data on fluctuations at low Fourier frequencies suggests a Q^{-4} dependence of the 1/f-noise on the quality factor Q of the passive cavity. We consider this a major information for designers of ringlaser gyros about long-term noise of such a device.

Flicker Noise in Frequency Fluctuations of Lasers

M. R. Sayeh and H. R. Bilger
School of Electrical and
Computer Engineering
Oklahoma State University
Stillwater, Oklahoma 74078

Measured power density spectra $S_{\delta f}$ of frequency fluctuations $\delta f(t)$ in ringlasers show $S_{\delta f} \propto 1/\nu$ at low Fourier frequencies ν, while quantum noise prevails at higher frequencies. $S_{\delta f}=(Af_o^2/Q^4)(1/\nu)$ has been found for the dependence of this $1/\nu$ noise (Flicker noise) on the quality factor Q, with $A\approx 4$ (f_o=laser frequency). The Q^{-4} dependence is readily explained by loss (or gain) fluctuations, using a Van der Pol oscillator.

PACS numbers: 05.40.+j, 06.30.Ft, 42.60.Da, 78.90.+t

Flicker Noise in Frequency Fluctuations of Lasers

M. R. Sayeh and H. R. Bilger
School of Electrical and
Computer Engineering
Oklahoma State University
Stillwater, Oklahoma 74078

Noise in lasers has been a subject of research for the last two decades [1]. The simple equation is

$$S_{\delta f}(\nu) = \frac{h f_o^3}{Q^2 P} \tag{1}$$

(h is Planck's constant, $f_o=\omega_o/2\pi$ is the resonance frequency, Q is the quality factor of the passive cavity, and P is the power loss per mode) for the one-sided power spectral density (PSD) $S_{\delta f}$ per mode versus the Fourier frequency ν. Here the frequency fluctuation $\delta f(t)$ due to quantum noise gives an approximate white-noise level which has been verified by experiment [2,9]. Eq. (1) was generalized by Haken [3].

Let us consider a noise-driven Van der Pol oscillator as a model for a laser oscillator [4].

$$\ddot{x} + [r - (g - \gamma x^2)]\dot{x} + \omega_o^2 x = N(t) , \tag{2}$$

where x is the mode amplitude, r is energy decay rate, g is the unsaturated gain, γ is the saturation parameter, and N(t) is the noise source due to the spontaneous emission processes.

From this model one can find the PSD of the frequency fluctuations as [4]

$$S_{\delta f}(\nu) = \frac{\gamma r h f_o}{8\pi^2 (g-r)} \left[\frac{N_2}{N_2 - N_1(g_2/g_1)} \cdot \frac{g(\nu+f_o)}{g(f_o)} + n_{th} \right] , \qquad (3)$$

where N_1 and N_2 are the populations of the lower and upper laser levels respectively, g_1 and g_2 are the level degeneracies, $g(f)$ is the transition lineshape, and n_{th} is the number of thermally emitted photons. Under limiting conditions ($N_2 \gg N_1$, $\nu \ll f_o/Q$, $hf_o/kT \gg 1$), Eq. (3) converges to Eq. (1).

To realize that noises with Fourier frequency dependent PSD, e.g. $S_{\delta f}(\nu) \propto 1/\nu$ (Flicker noise) exist, we consider a noise mechanism from a different source. Let us assume that there exist fluctuations in the loss, r, independent of the existence of white noise, i.e. for the purpose of this derivation N(t) in Eq. (2) is set to zero. Now we try to find the PSD of the frequency fluctations due to loss fluctuations.

We first establish an approximate solution to Eq. (2) up to first order in μ=g-r [5]:

$$x(t) \simeq \sqrt{\left(\frac{\mu}{\gamma}\right)} \quad 2 \cos (\xi \omega_o t) , \qquad (4)$$

where $\xi = 1 - \mu^2/16\omega_o^2$, and $\mu = g-r$. The resonance frequency $\omega = \xi\omega_o$ therefore depends on the loss r, viz.

$$\omega = \omega_o - \frac{(g-r)^2}{16\omega_o} . \qquad (5)$$

By making use of g≃r in a laser in steady-state operation, we find the fluctuation δf with respect to the fluctuation δr as

$$\frac{\delta f}{f} = \frac{1}{2Q^2} \frac{\delta r}{r} , \tag{6}$$

where $Q = \omega_o/r$.

The PSD of the fractional frequency fluctuation can be related to the PSD of the fractional loss fluctuation by using Eq. (7) as follows

$$S_{\delta f/f}(\nu) = \frac{1}{64Q^4} S_{\delta r/r}(\nu) \quad . \tag{7}$$

The PSD of $\delta f/f$ is related to the PSD of $\delta r/r$ by the Q^{-4} law. This has been observed experimentally in quartz oscillators over six decades of PSD [6]. The proportionality to Q^{-4} thus is independent of the specific assumptions on the type of loss fluctuations.

Using Handel's quantum theory of $1/\nu$ noise [7], one would expect loss fluctuations to originate from loss processes inside the cavity whose elementary cross sections of interaction with the electromagnetic field fluctuate with a $1/\nu$ spectrum [8]. In this case we expect

$$S_{\delta r/r}(\nu) = \frac{A}{\nu} , \tag{8}$$

where A is a constant depending on the nature of the interaction. Therefore the PSD of the frequency fluctuation per mode can then be written as

$$S_{\delta f}(\nu) = \frac{A f_o^2}{64Q^4} \frac{1}{\nu} . \tag{9}$$

A ring laser gyro (RLG) can be used to study the frequency fluctuations in lasers [9]. Fig. (1) shows a measured PSD of a four-mode RLG versus Fourier frequency (the RLG was placed in a thermostat with 100 μK temperature deviation). The white noise dominates down to

6×10^{-4} Hz, Flicker noise ($1/\nu$ noise) is from 6×10^{-4} Hz to 4×10^{-5} Hz, and $1/\nu^2$ noise predominates at frequencies less than 4×10^{-5} Hz. Generally it has been observed that the PSD of frequency fluctuations of ringlasers obeys the following relation [10]

$$S_{\delta f}(\nu) = h_{-2}\,\nu^{-2} + h_{-1}\nu^{-1} + h_0 \,. \tag{10}$$

We have collected data from different types of RLG, including fig. 1 and we verified that $1/\nu$ noise is commonly occurring in most cases. The white noise level, h_0 in Eq. (11), was ascertained [9].

Fig. (2) shows the measured values of h_{-1}, per mode, versus the quality factor Q. The least square fitted line in Fig. (2) gives a value 256 for the constant A in Eq. (10).

The experimental evidence therefore suggests for the $1/\nu$ noise

$$S_{\delta f}(\nu) \approx 4\,\frac{f_0^2}{Q^4}\,\frac{1}{\nu} \tag{11}$$

The 1/f noise in laser systems is thus to be considered as a fundamental process which affects the output frequency of a laser. 1/f noise in this model is linked to laser loss mechanisms which are inflicted upon the photon field. In this sense, it is an even more basic noise process than white noise. Of course, if in the absence of loss the quality factor goes to infinity, there are no fluctuation effects and correspondingly there would not be any 1/f noise. (There would also be no white noise but for different reasons). We note also, that the quality factor enters the formula for white noise, Eq. (1), only indirectly because spontaneous emission is at the origin of white noise.

This irreducible 1/f noise is of great practical importance, since averaging of data containing 1/f noise does not significantly reduce the noise level whereas averaging of data containing white noise over a time T reduces the noise level with $1/\sqrt{T}$. The 1/f noise is thus a measure of the ultimate stability of a laser oscillator, as is evidenced by a plot of the Allan variance of any oscillator [8], where the 1/f noise constitutes the flicker floor.

References

[1] See for example T. J. Jaseja, A. Javan, and C. H. Townes, "Frequency Stability of He-Ne Masers and Measurements of Length," Phys. Rev. Lett. 10, pp. 165-167, 1963; see also Refs. [2-3].

[2] See for example K. R. Manes, and A. E. Siegman, "Observations of quantum phase fluctuations in infrared gas lasers," Phys. Rev. 4, pp. 373-386, 1971.

[3] H. Haken, in: Encyclopedia of Physics, Vol. XXV/2c (ed. S. Fluegge, Springer-Verlag, Berlin-Heidelberg, New York, 1970).

[4] A. Yariv, "Quantum *electronics*," John Wiley & Sons, Inc. New York, 1975, Chpt. XIII.

[5] A. A. Andronov, A. A. Vitt, and S. E. Khaikin, "Theory of Oscillators," Addison-Wesley Publishing Company, Inc., Massachusetts, 1966.

[6] J. J. Gagnepain, J. Uebersfeld, G. Goujon, and P. H. Handel, "Relation between 1/f noise and Q-factor in quartz resonators at room and low temperatures, first theoretical interpretation," Proc. 35th Ann. Freq. Cont. Symp., pp. 476-483, 1981.

Figure Captions

Figure 1: Typical power spectral density of the frequency fluctuation $\delta f(t)$ versus Fourier frequency ν. There are three distinct regimes where $S \propto \nu^0$ (white noise), $S \propto \nu^{-1}$ (Flicker noise), $S \propto \nu^{-2}$

The error bars indicate the statistical accuracy of the data. This noise spectrum was obtained on ringlaser #2 from a 5-day run with frequency measurements taken every 100 s.

Figure 2: Summary of $1/\nu$-amplitudes versus cavity quality factor Q obtained in three ringlasers, with the best-fitted line $\propto Q^{-2}$

All ringlasers use HeNe and operate at f_o= 474 THz (λ=633nm). The error bars of RLG#1 are of the same size as the circles.

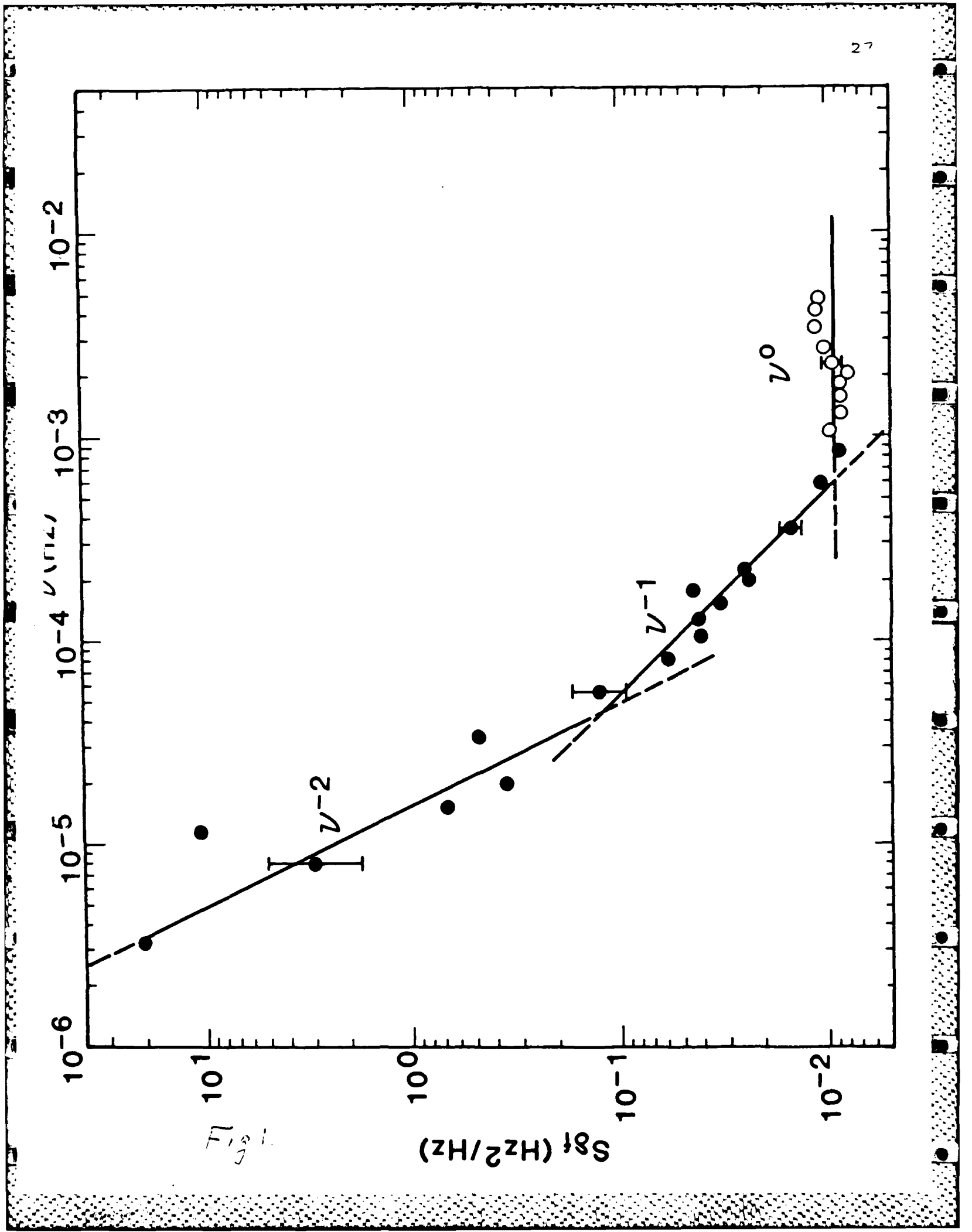

Fig 1.

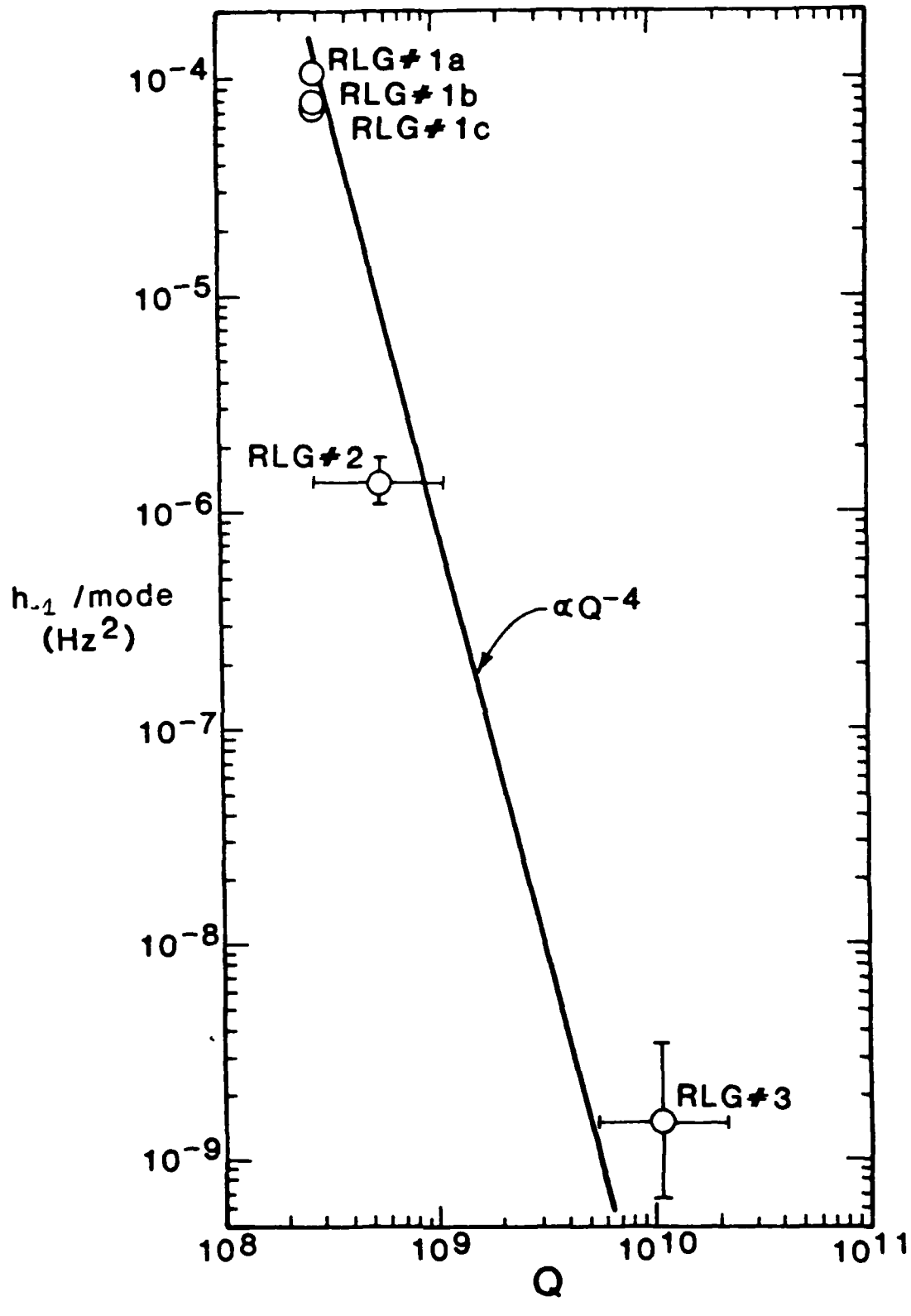
RLG#1a
RLG#1b
RLG#1c
RLG#2
RLG#3
$\propto Q^{-4}$
h_{-1} /mode
(Hz^2)
10^{-4}
10^{-5}
10^{-6}
10^{-7}
10^{-8}
10^{-9}
10^8
10^9
10^{10}
10^{11}
Q

Fig 2.

II. B. Astigmatic Gaussian beam in plane ring: Stability, curvature radius of beam, location and size of waist(s)

The fundamental Gaussian beam is the basic signal in optical circuits, as is the sinusoidal voltage in low-frequency circuits. The following section reviews application of ray matrices to a closed optical circuit (plane quadrangle) with the purpose of establishing a unique complex curvature q along the ring. Radii of curvature and spot sizes are derived, as well as locations and sizes of waists; the results are applied to an example (published by the Seiler group) of mode matching. In the latter case, perfect alignment is presupposed. Various checks have been built in to improve the reliability of the calculations. The latter make this section a proper base for a computer program.

Plane Four-Mirror Ring Cavity:

Waists (Location, Size), Curvature Radii,

Mode Matching

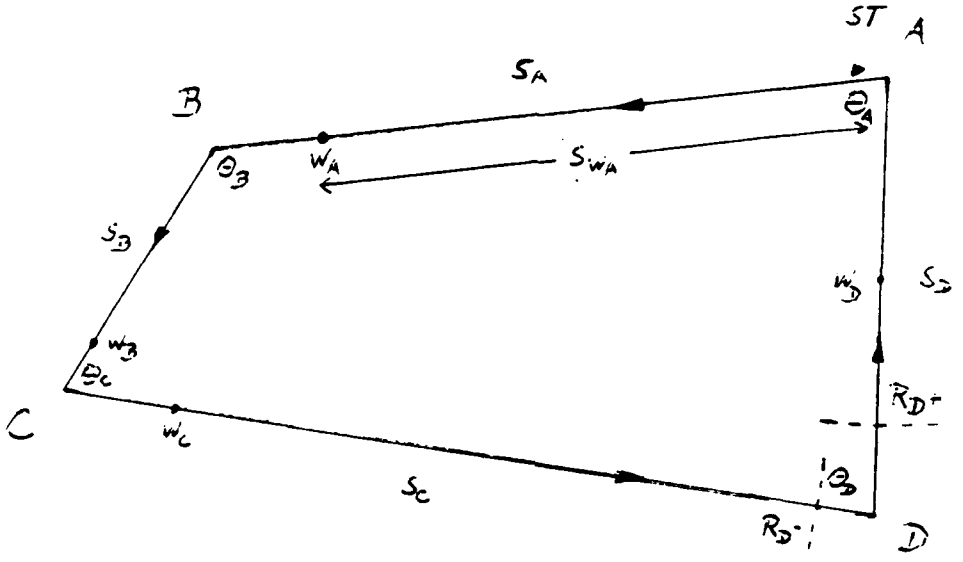

Definitions: Beam travels counterclockwise, CCW. Radius of curvature of mirror or beam is called positive if concave in the direction of the beam.

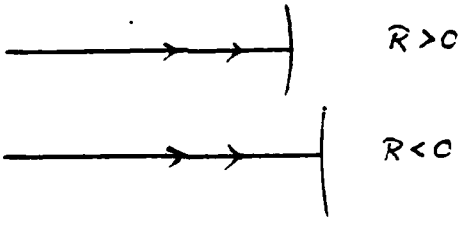

Waist in branch AB: location S_{WA} (off mirror A), size w_A., etc.

Radius of curvature of beam entering at A: R_{A-}

Radius of curvature of beam leaving A: R_{A+}, etc.

There are at most four waists in the ring, and either zero or one waist in each branch. The length of the branch following A is S_A (positive),

etc. The angle between entering and leaving beam at A is θ_A etc. Note that the ring is plane.

Procedure: Use ray-matrices throughout, and the law of propagation of the complex curvature q:

$$q_{out} = (A\, q_{in} + B)/(C\, q_{in} + D) \ .$$

The circuit consists of straight sections and mirrors. For oblique incidence, a curved mirror is astigmatic, i.e. it has a different focal length for sheaths of rays in the plane of the ring (x) and normal to the plane of the ring (y).

Straight section of length S

$$\begin{pmatrix} 1 & S \\ 0 & 1 \end{pmatrix}$$

Mirror with focal length f

$$\begin{pmatrix} 1 & 0 \\ -1/f & 1 \end{pmatrix}$$

One leg, including first a straight section, and then a mirror:

$$\begin{pmatrix} 1 & 0 \\ -1/f & 1 \end{pmatrix} \begin{pmatrix} 1 & S \\ 0 & 1 \end{pmatrix} = \begin{pmatrix} 1 & S \\ -1/f & 1-S/f \end{pmatrix} .$$

Applying four legs to a ring, starting CCW from ST, at A^+:

$$M_{A+} = \begin{pmatrix} A & B \\ C & D \end{pmatrix}_{A^+} = \begin{pmatrix} 1 & S_A \\ -f_B^{-1} & 1-S_A/f_B \end{pmatrix} \begin{pmatrix} 1 & S_B \\ -f_C^{-1} & 1-S_B/f_C \end{pmatrix} \begin{pmatrix} 1 & S_C \\ -f_D^{-1} & 1-S_C/f_D \end{pmatrix} \begin{pmatrix} 1 & S_D \\ -f_A^{-1} & 1-S_D/f_A \end{pmatrix}$$

Check whether determinant is 1:

$$\begin{vmatrix} A & B \\ C & D \end{vmatrix} = 1 = AD - BC .$$

This is a necessary condition in a round trip.

Check whether ring is stable: $0 \leq 1 - (A + D)^2/4 \leq 1$

This is required for the uniqueness of the gaussian eigenmode.

Complex curvature q at A^+:

From the condition that q is uniquely specified at any point, we get

$$q_{A+} = (A\ q_{A+} + B)/(C\ q_{A+} + D) \text{ , or}$$

$$q_{A+} = -(D - A)/2C + [B/C + (D - A)^2/4\ C^2)]^{1/2}$$

(the positive root has to be chosen) .

The root is imaginary, if the ring is stable. Proof:

Because of $AD - BD = 1$, $C = (AD - 1)/B$, we get

$$q_{A+} = (A - D)/2C + (|B|/|AD - 1|)[-(1 - (A + D)^2/4)]^{1/2}.$$

Also

$$q_{A+}^{-1} = (D - A)/2B - j[1 - (A + D)^2/4]^{1/2}/\ B \cong R_A^{-1} - j(\lambda/\pi w_{A+}^2).$$

Location of waist: At the waist the curvature radius of the beam becomes infinity, $R_w \to \infty$, i.e. $q_w = j(\pi w_A^2/\lambda)$.

By adding a straight section S_{wA} to A, we arrive at the waist, where

$$q_{SwA} = q_{A+} + S_{wA} = q_w = j(\pi w_A^2/\lambda)$$

or $Re(q_{A+} + S_{wA}) = 0$, or $S_{wA} = (D - A)/2C = - Re(q_{A+})$

Check: a) if $S_{wA} > S_A$, there is no waist in S_A

b) if $S_{wA} < 0$, there is no waist in S_A.

Size of waist: Translation from A to the location of the waist does not change the imaginary part of q, therefore

$$\pi w_A^2/\lambda = Im(q_{A+}) = [-B/C - (D - A)^2/4C^2]^{1/2}.$$

Radius of curvature at mirror A (before and after reflection)

From above, we get for the radius just after reflection at A:

$$\mathrm{Re}(q_{A+}^{-1}) = R_{A+}^{-1} = (D - A)/2B, \text{ or } R_{A+} = 2B/(D - A) = [\mathrm{Re}(q_{A+}^{-1})]^{-1}$$

This can be positive or negative.

Radius of curvature just before reflection at A:

Use A B C D - law:

$$q_{A+} = (1\ q_{A-} + 0)/(-f_A^{-1}\ q_{A-} + 1), \text{ or } q_{A-}^{-1} = R_{A-}^{-1} - j(\lambda/\pi w_{A-}^2)$$

$$= q_{A+}^{-1} + f_A^{-1}$$

or

$$R_{A-} = [f_A^{-1} + (D - A)/2B]^{-1} = [f_A^{-1} + \mathrm{Re}(q_{A+}^{-1})]^{-1} = [1/R_{A+} + 1/f_A]^{-1}$$

Check: Given waist (size and location) and the distance, the following is true for one branch:

$$q_{A+} + S_{wA} = q_w = j(\pi w_A^2/\lambda)$$

or

$$[R_{A+}^{-1} - j(\lambda/\pi w_{A+}^2)]^{-1} = j(\pi w_A^2/\lambda) - S_{wA}.$$

Equating real and imaginary parts, we get

$$R_{A+} = -[S_{wA} + S_{wA}^{-1}(\pi w_A^2/\lambda)^2], \text{ or generally } R(z) = \pm z(1 + z_R^2/z^2)$$

$$w_{A+}^2 = w_A^2 + S_{wA}^2/(\pi w_A/\lambda)^2, \text{ or generally } w^2(z) = w_0^2\ (1 + z^2/z_R^2).$$

Here, R and w are the curvature radius and the spot size at a distance z from the waist, z_R is the Rayleigh range, $z_R = \pi w_0^2/\lambda$, with w_0 being the waist size.

Spot size at A:

Since $q_{A+}^{-1} = R_{A+}^{-1} - j\,(\lambda/\pi w_{A+}^2)$, we get

$$w_{A+} = [(\lambda/\pi)/(-\ \mathrm{Im}(q_{A+}^{-1}))]^{1/2} = w_{A-}$$

Waists and radii in other branches:

Two procedures can be applied

1) Recalculate ABCD matrix starting CCW off B, then C, then D. All the equations above reapply, after all letters A are changed into B, C, D.

2) Calculate q_{B+} by transforming q_{A+} through one leg with matrix

$$\begin{pmatrix} 1 & S_A \\ -1/f_B & 1-S_A/f_B \end{pmatrix}, \text{ or}$$

$$q_{B+} = (q_{A+} + S_A)/(-f_B^{-1}\ q_{A+} + 1 - S_A/f_B);\quad \text{find } \mathrm{Re}(q_{B+}),\quad \mathrm{Im}(q_{B+}),$$
$$\mathrm{Re}(q_{B+}^{-1}),\ \mathrm{Im}(q_{B+}^{-1}),$$

from which all interesting quantities can be evaluated; then proceed to q_{C+}, and q_{D+}.

Check: Transforming q_{D+} to q_{A+} should result in the same quantities as before.

Application: Mode matching paper by Seiler group

(Appl. Opt. 22, pp. 2487-2491, 1983, ref. 9)

Given an almost square, presumably plane, ring with the four sides

S_A = 78.90 cm (use "cm" to strike a compromise

S_B = 78.74 cm in resolution between S and w)

S_C = 78.58 cm

S_D = 78.74 cm (use $\lambda = 632.8 \times 10^{-7}$ cm = HeNe wavelength in air)

Assume $\vartheta_A = 90^0$ exactly.

Find the rest of the geometry

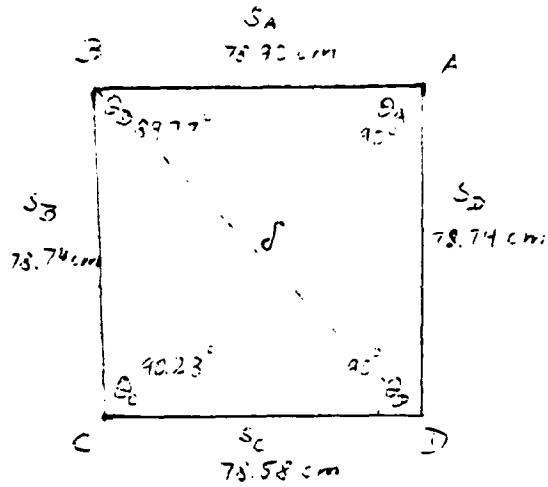

with $\delta = (S_A^2 + S_D^2)^{1/2}$ = 111.468 cm, calculate θ_C through cos-law

$\delta^2 = S_B^2 + S_C^2 - 2\, S_B\, S_C \cos\theta_C$, which gives

$\theta_C = 90.233^0$

Now, $\vartheta_B = \alpha + \alpha' = \tan^{-1} S_D/S_A + \cos^{-1} [(S_C^2 - S_B^2 - \delta^2)/(-2S_B\delta)]$,

which gives

$$\theta_B = 89.767^o.$$

Since it's a quadrangle, $\theta_D = 360^o - \theta_A - \theta_B - \theta_C = 89.999^o$.

The errors appear to be $\Delta S \sim 0.01$ cm, and the sides ~ 100 cm,

therefore, use rounded values $\theta_A = 90.00^o$

$\theta_B = 89.77^o$

$\theta_C = 90.23^o$

$\theta_D = 90.00^o$ (Trapeze)

Mirror radii (nominally):

$r_A = r_C = 600$ cm $\quad f_{Ax} = (r_A/2)\cos(\theta_A/2) = 212.132$ cm, $f_{Cx} = (r_C/2)\cos(\theta_C/2) = 211.706$ cm

$r_B = r_D =$ $\quad f_{Ay} = (r_A/2)/\cos(\theta_A/2) = 424.264$ cm, $f_{Cy} = (r_C/2)/\cos(\theta_C/2) = 425.118$ cm

Round-trip matrix at A:

$$M_{A+} = \begin{pmatrix} 1-(S_C+S_D)/f_C & (S_A+S_B)(1-(S_C+S_D)/f_C)+S_C+S_D \\ -(1-(S_C+S_D)/f_C)/f_A-1/f_C & (1-(S_C+S_D)/f_C)(1-(S_A+S_B)/f_A)-(S_A+S_B)/f_A \end{pmatrix} = \begin{pmatrix} A & B \\ C & D \end{pmatrix}_{A+}$$

In x-plane in y-plane

$$M_{A+,x} = \begin{pmatrix} +0.2569 & +197.817 \\ -0.00593 & -0.67713 \end{pmatrix} \qquad M_{A+,y} = \begin{pmatrix} +0.6299 & +256.623 \\ -0.003837 & +0.02432 \end{pmatrix}$$

Checks: $|M_{A+,x}| = 1 = |M_{A+,y}|$

$S_x = 1 - ((A + D)^2/4) = 0.96$, $S_y = 0.89.$

Stable, however, close to limit given by 4 flat mirrors: ($S \approx 1$).

Calculate $q_{A+,x}$, $q_{A+,y}$, and their reciprocals

$q_{A+,x} = -78.694 + j\ 164.743$ $\qquad$ $q_{A+,y} = -78.917 + j\ 246.277$

$q_{A+,x}^{-1} = -0.002361 - 0.004942$ $\qquad$ $q_{A+,y}^{-1} = -0.001180 - j\ 0.003682,$

from which the locations and the sites of the waists are:

$S_{wA,x} = -\mathrm{Re}(q_{A+,x}) = 78.694$ cm $\qquad$ $S_{wA,y} = +78.917$ cm

$w_{A,x} = [(\lambda/\pi)\mathrm{Im}(q_{A+,x})]^{1/2} = 0.05761$ cm $\qquad$ $w_{A,y} = 0.07043$ cm.

Curvature at A:

$R_{A-,x} = +424.95$ cm $= [f_{A,x}^{-1} + \mathrm{Re}(q_{A+,x}^{-1})]^{-1}$, $R_{A-,y} = +849.59$ cm

$R_{A+,x} = -423.58$ cm $= [\mathrm{Re}\ (q_{A+,x}^{-1})]^{-1}$, $R_{A+,y} = -847.47$ cm.

Spot at A

$w_{A+,x}$ = 0.06384 cm , $w_{A+,y}$ = 0.07396 cm.

Round-trip at C

(since the mirrors at B and D are flat, there can be two waists only)

Exchange $S_C \leftrightarrows S_A$, $S_B \leftrightarrows S_D$, $f_A \leftrightarrows f_C$, and feed in numbers

$$M_{C+,x} = \begin{pmatrix} +0.2569 & +198.052 \\ -0.005927 & -0.67712 \end{pmatrix} \qquad M_{C+,y} = \begin{pmatrix} +0.6284 & +256.506 \\ -0.003835 & +0.02582 \end{pmatrix}$$

Checks: $|M_{C+,x}| = 1$ $|M_{C+,y}| = 1$

S_x = 0.96 , S_y = 0.89 as above.

$q_{C+,x} = -78.786 + j\ 164.941$ $q_{C+,y} = -78.563 + j\ 246.390$

$q^{-1}_{C+,x} = -0.002358 - j\ 0.004936$ $q^{-1}_{C+,y} = -0.001175 - j\ 0.003684$

$S_{wC,x}$ = 78.79 cm $S_{wC,y}$ = +78.56 cm

$w_{C,x}$ = 0.05764 cm $w_{C,y}$ = 0.07045 cm

$R_{C-,x}$ = + 422.73 cm $R_{C-,y}$ =+849.18 cm

$R_{C+,x}$ = - 424.10 cm $R_{C+,y}$ = -851.30 cm

$w_{C+,x}$ = 0.06388 cm $w_{C+,y}$ = 0.07394 cm

Note that $S_{wC,x} > S_C$, i.e. there is no waist in the branch C, but in branch D: $S_{wC,x} + S_{wD,x} = S_{wC,x} - S_C$ = (78.79 - 78.58) cm = 0.21 cm. On the other hand, $S_{wC,y} < S_C$, but actually right at the mirror D. Generally, the tangential and the sagittal waists are not at the same locations.

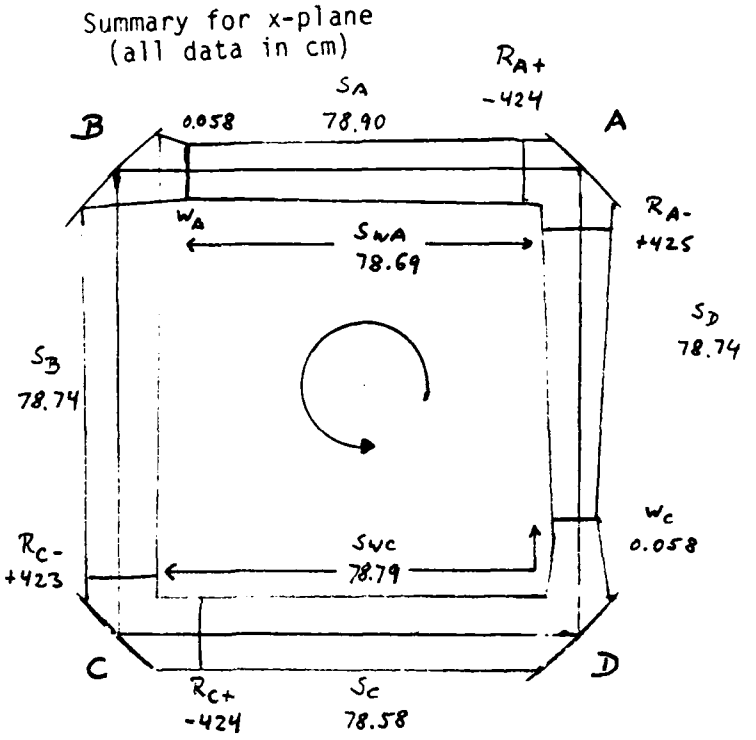

Corresponding y-values

Waist in branch A: S_{w_A} = 78.92 cm (about at mirror B), w_A = 0.0704 cm

Waist in branch C: S_{wC} = 78.56 cm (about at mirror D), w_C = 0.0704 cm

at mirror A: R_{A-} = +850 cm, R_{A+} = -847 cm, $w_{A+}=w_{A-}$ = 0.0740 cm

at mirror C: R_{C-} = +849 cm, R_{C+} =-851 cm, $w_{C+}=w_{C-}$ = 0.0739 cm

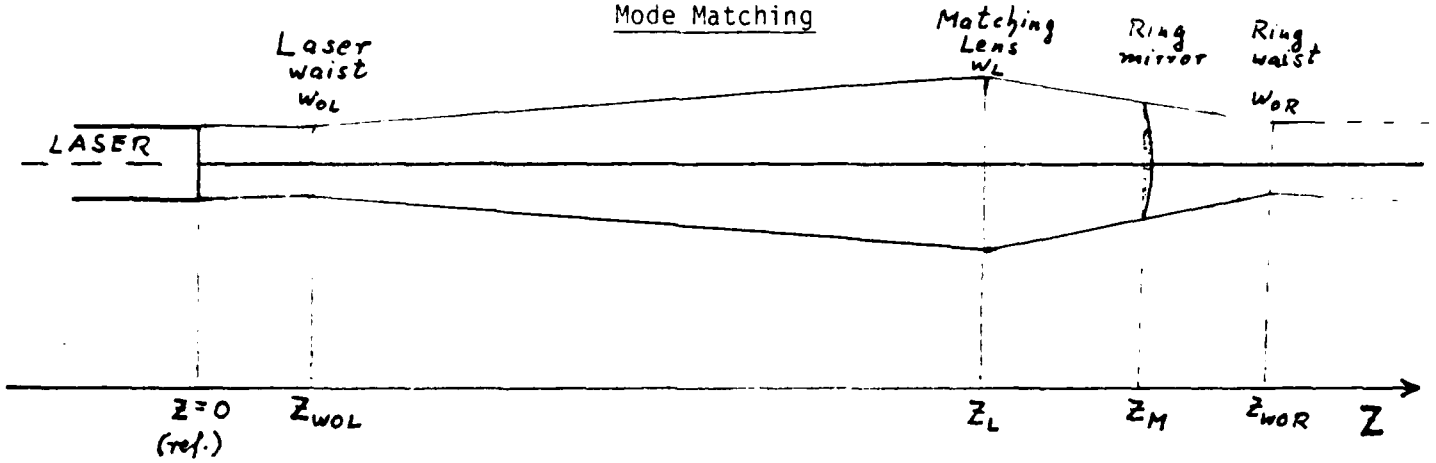

Z_{WOL} = 4.34 cm W_{OL} = 0.03014 cm x = 126.76 cm $Z_{WOR}-Z_M$=0.29 cm

$Z_M = Z_{WOL} + x - (Z_{WOR} - Z_M) = 4.34\text{ cm} + 126.76\text{ cm} - (0.29\text{ cm}) = 130.81\text{ cm}$

$Z_{WORx} = x + Z_{WOL} + 126.76\text{ cm} + 4.34\text{ cm} = 131.10\text{ cm}$

$W_{OR} = 0.05764$ cm

(Z_{WOL} is evaluated [p. 2488], Z_M is measured, $Z_{WOR} - Z_M$ is evaluated)

To find Z_L = Lens spot, where the spot sizes, extrapolated from either side, are equal (note that Z_{WOL}, Z_M, Z_{WOR} are fixed)

$$W_L^2 = W_{OL}^2 + (\lambda/\pi W_{OL})^2 (Z_L - Z_{WOL})^2 = W_{OL}^2 + (\lambda/\pi W_{OL})^2 Z_L'^2 \quad , (Z_L' = Z_L - Z_{WOL})$$

and

$$W_L^2 = W_{OR}^2 + (\lambda/\pi W_{OR})^2 (Z_{WOR} - Z_L)^2 = W_{OR}^2 + (\lambda/\pi W_{OR})^2 (x - Z_L')^2,$$

from which, by subtraction

$$W_{OL}^2 - W_{OR}^2 = (\lambda/\pi)^2[(x - Z_L')^2/W_{OR}^2 - (Z_L'^2/W_{OL}^2)],$$

or

$$W_{OL}^2 W_{OR}^2(W_{OL}^2 - W_{OR}^2) = (\lambda/\pi)^2[W_{OL}^2(x - Z_L')^2 - W_{OR}^2 Z_L'^2]$$

or

$$(W_{OL}^2-W_{OR}^2) Z_L'^2-2xW_{OL}^2 Z_L'+[x^2 W_{OL}^2+(\lambda/\pi)^2(W_{OL} W_{OR})^2 (W_{OR}^2 -W_{OL}^2)]=0,$$

which is a quadratic equation for Z_L'.

(Note: Z_L' = "Z" in manuscript; two typos in eq. 2)

Solution of quadratic equation = position of lens with respect to laser waist.

$$Z_L' = Z_L - Z_{WOL} = - x W_{OL}^2/(W_{OR}^2 - W_{OL}^2) + [x^2 W_{OL}^2/(W_{OR}^2 - W_{OL}^2) + (\pi/\lambda)^2 W_{OL}^2 W_{OR}^2 + x^2 W_{OL}^4/(W_{OR}^2 - W_{OL}^2)^2]^{1/2}$$

Horizontal case:

With x = 126.76 cm, (note: all in cm)

W_{ORx} = 0.05764 cm,

W_{OL} = 0.03014 cm,

$$\lambda = 632.8 \times 10^{-7} \text{ cm},$$

We get $Z'_{L,x} = Z_{Lx} = Z_{WOL} = 77.82$ cm

or $Z_{Lx} = 77.82 + 4.34 = 82.16$ cm

Vertical case:

From above, the vertical waist is located $S_{WA} = 78.92$ cm CCW from A (mirror r_2), which makes it appear in branch B (S_4), at $S_A - S_{WA} = (78.90 - 78.92)$ cm = (-) 0.02 cm, off mirror B (r_1). Projecting this waist to the left of mirror B by 0.02 cm, we get

$x = (Z_M - 0.02 - 4.34)$cm = 126.45 cm, $Z_{WOR,y} = x + Z_{WOL} = 130.79$ cm,

$W_{ORY} = 0.07043$ cm

$Z'_{LY} = 96.13$ cm, or $Z_{LY} = (96.13 + 4.34) = 100.47$ cm.

(If the paper's number $S_A - S_{WA} = 0.21$ cm is used, one gets $Z'_{L'Y} = 96.11$ cm or $Z_{L,Y} = 100.45$ cm, essentially no difference.)

The cylindrical lenses for the mode matching are spaced (100.45 - 82.16)cm = 18.29 cm = $Z_{L,Y} - Z_{L,X}$.

Curvature radii of matching lenses:

$f_x^{-1} = R^{-1}$(from laser) - R^{-1}(from ring, x), with

$R(\text{from laser}) = Z'_{L,x}\,[1 + (\pi W_{0L}^2/\lambda Z'_{L,x})^2] = 103.96$ cm.

$R(\text{from ring, x}) = -(Z_{WOR,x} - Z_{L,x})(1 + (\pi W_{OR,x}^2/\lambda(Z_{OR,x} - Z_{L,x}))^2) = -604.84$ cm,

or $f_x = +88.71$ cm.

$f_y^{-1} = R^{-1}(\text{from laser}) - R^{-1}(\text{from ring, y})$, with

$R(\text{from laser}) = Z'_{L,y}[1 + (\pi W_{0L}^2/\lambda Z'_{L,y})^2] = 117.29$ cm.

$R(\text{from ring, y}) = -(Z_{WOR,y} - Z_{L,y})(1 + (\pi W_{OR,y}^2/\lambda(Z_{WOR,y} - Z_{L,y})^2) = -2030.50$ cm,

or $f_y = +110.88$ cm

The data agree with those given in Appl. Opt. (paper by Seiler group)

Different approach to mode matching

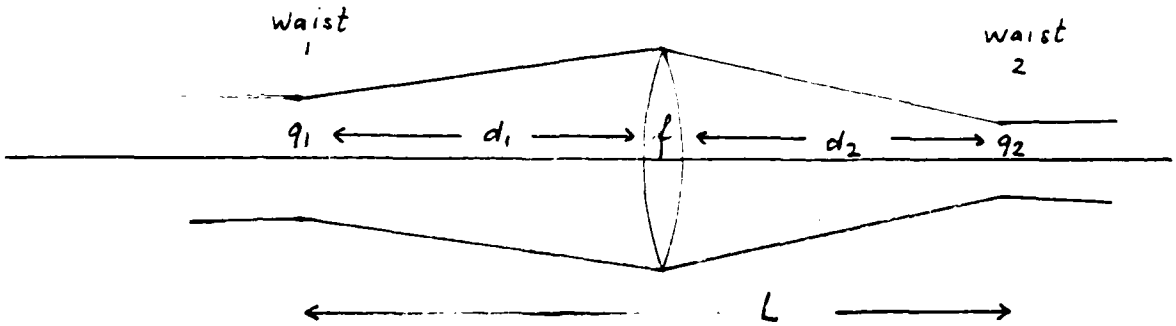

Given the distance between two waists, and their sizes, calculate d_1, d_2, f → focus length and location of matching lens. Since the curvature radius of the beam at a waist is ∞,

$$q_1 = j\frac{\pi w_1^2}{\lambda} \quad , \quad q_2 = j\frac{\pi w_2^2}{\lambda} \quad .$$

The matrix between q_1 and q_2 is

$$\begin{pmatrix} A & B \\ C & D \end{pmatrix} = \begin{pmatrix} 1 & d_2 \\ 0 & 1 \end{pmatrix}\begin{pmatrix} 1 & 0 \\ -1/f & 1 \end{pmatrix}\begin{pmatrix} 1 & d_1 \\ 0 & 1 \end{pmatrix} = \begin{pmatrix} 1-d_2/f & d_1+d_2(1-d_1/f) \\ -1/f & 1-d_1/f \end{pmatrix}$$

and

$$q_2 = \frac{Aq_1 + B}{Cq_1 + D} = \frac{(1 - \frac{d_2}{f})q_1 + d_1 + d_2(1 - \frac{d_1}{f})}{-\frac{1}{f}q_1 + 1 - \frac{d_1}{f}} \quad .$$

or

$$-\frac{1}{f}(q_1 q_2) + (1 - \frac{d_1}{f})q_2 = (1 - \frac{d_2}{f})q_1 + d_1 + d_2(1 - \frac{d_1}{f})$$

Using the fact the q_1, q_2 are imaginary, we compare real and imaginary parts

Real parts $-\frac{1}{f}(-\frac{\pi^2}{\lambda^2} w_1^2 w_2^2) = d_1 + d_2(1 - \frac{d_1}{f})$ to determine f and d_1;

Imaginary parts $(1 - \frac{d_1}{f})\frac{\pi w_2^2}{\lambda} = (1 - \frac{d_2}{f})\frac{\pi}{\lambda} w_1^2$

From the latter equation $\frac{1}{f}(-d_1w_2^2 + d_2w_1^2) = w_1^2 - w_2^2$

$$\text{or } f = \frac{d_2w_1^2 - d_1w_2^2}{w_1^2 - w_2^2} .$$

Substituting into real part

$$\frac{\pi^2}{\lambda^2} w_1^2w_2^2 \frac{w_1^2 - w_2^2}{d_2^2w_1^2 - d_1^2w_2^2} = d_1 + d_2 - \frac{w_1^2 - w_2^2}{d_2^2w_1^2 - d_1^2w_2^2} d_1 d_2$$

$$\text{or } \frac{\pi^2}{\lambda^2} w_1^2w_2^2(w_1^2 - w_2^2) = L(d_2w_1^2 - d_1w_2^2) - d_1d_2(w_1^2 - w_2^2) ,$$

$(L = d_1 + d_2)$

$$\text{or } L[(L - d_1)w_1^2 - d_1w_2^2] - d_1(L - d_1)(w_1^2 - w_2^2) = \frac{\pi^2}{\lambda^2} w_1^2w_2^2(w_1^2 - w_2^2)$$

$$d_1^2[w_1^2 - w_2^2] + d_1[-Lw_1^2 - Lw_2^2 - Lw_1^2 + Lw_2^2] = \frac{\pi^2}{\lambda^2} w_1^2w_2^2(w_1^2 - w_2^2) - L^2w_1^2,$$

$$\text{or } (w_1^2 - w_2^2)d_1^2 - 2Lw_1^2 + [L^2w_1^2 + (w_2^2 - w_1^2)(\frac{\pi}{\lambda})^2 w_1^2w_2^2] = 0 ,$$

Which is identical to the equation above, except for notations.

Note: The material in the section above has not been submitted for publication, as no originality is claimed. However, we consider the inclusion of the many checks above a considerable improvement over the published papers in ref. 9, and rather simple for programming.

II. C. Ray matrix approach to square, plane ring with equal mirror radii: Stability, waist sizes, spot sizes on mirrors, design for minimum spot sizes on mirrors (minimum diffraction, smallest mirror size), design for circular spot size on mirrors (near-confocal cavity for best mode-matching).

The results of the previous section are applied to a highly symmetric configuration. A square ring has certain advantages: It is easier to survey than a general ring, the waists are in the center of the branches (if four equal mirror radii are employed); there are no "holes" in the stability vs mirror radius; manufacturing of four equal mirrors is easier; due to the symmetry, the sagittal and tangential waists are coincident in the center of each branch; there is also the possibility to produce a circular spot size on each mirror: Since the injection of an external beam will take place at a mirror, mode-matching is particularly facilitated in this case by making the backside of the mirror into a cylinder lens. The beam will then be strictly stigmatic outside the cavity.

Ray matrix approach to square, plane ring with equal mirror radii: Stability, waist size, spot sizes or mirror, design for minimum Spot size on mirrors (minimum diffraction, smallest mirror size), design for circular spot size on mirrors (near-confocal cavity for best mode-matching).

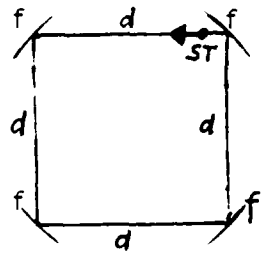

Relation between f and R:

In plane of ring (p-plane):

$f_p = (R/2) \cos 45^0 = (R/4)\sqrt{2}$

Perpendicular to plane of ring (s-plane):

$f_s = R/(2 \cos 45^0) = (R/2)\sqrt{2}$

One loop, starting CCW at st:

$$\begin{pmatrix} A & B \\ C & D \end{pmatrix} = \begin{pmatrix} 1 & 0 \\ -f^{-1} & 1 \end{pmatrix}\begin{pmatrix} 1 & d \\ 0 & 1 \end{pmatrix}\begin{pmatrix} 1 & 0 \\ -f^{-1} & 1 \end{pmatrix}\begin{pmatrix} 1 & d \\ 0 & 1 \end{pmatrix}\begin{pmatrix} 1 & 0 \\ -f^{-1} & 1 \end{pmatrix}\begin{pmatrix} 1 & d \\ 0 & 1 \end{pmatrix}\begin{pmatrix} 1 & 0 \\ -f^{-1} & 1 \end{pmatrix}\begin{pmatrix} 1 & d \\ 0 & 1 \end{pmatrix},$$

with $x = d/f$, we get

$$\begin{pmatrix} A & B \\ C & D \end{pmatrix} = \begin{pmatrix} 1 - 6x + 5x^2 - x^3 & d(4 - 10x + 6x^2 - x^3) \\ d^{-1}(-4x + 10x^2 - 6x^3 + x^4) & 1 - 10x + 15x^2 - 7x^3 + x^4 \end{pmatrix}$$

Since the beam "exits" where it enters,

$$\begin{vmatrix} A & B \\ C & D \end{vmatrix} = 1 \stackrel{?}{=} (1-6x+5x^2-x^3)(1-10x+15x^2-7x^3+x^4) - d(4-10x+6x^2-x^3)\, d^{-1}(-4x+10x^2-6x^3+x^4)$$

$$= x^0\,(1) + x^1\,(-10-6+16) + x^2\,(+15+60+5-40-40) + x^3\,(-7-90-50-1+24+100+24) + x^4\,(+1+42+75+10-4-60-60-4) + x^5\,(-6-35-15+10+36+10)$$

$$+ x^6 (+ 5 + 7 - 6 - 6)$$

$$+ x^7 (-1 + 1)$$

$$= 1$$

(This is a good check on numerical errors)
Note also, that in this case $B = - Cd^2/x$ (!)

Stability: (Verdeyen p. 33)

$$- 1 \leq (A+D)/2 \leq 1$$

or

$$0 \leq (A+D+2) \leq 4$$

So: $- 1 \leq (1/2)(A+D) = (2 - 16x + 20x^2 - 8x^3 + x^4)\ (1/2) \leq + 1$

Stability of square, symmetric ring

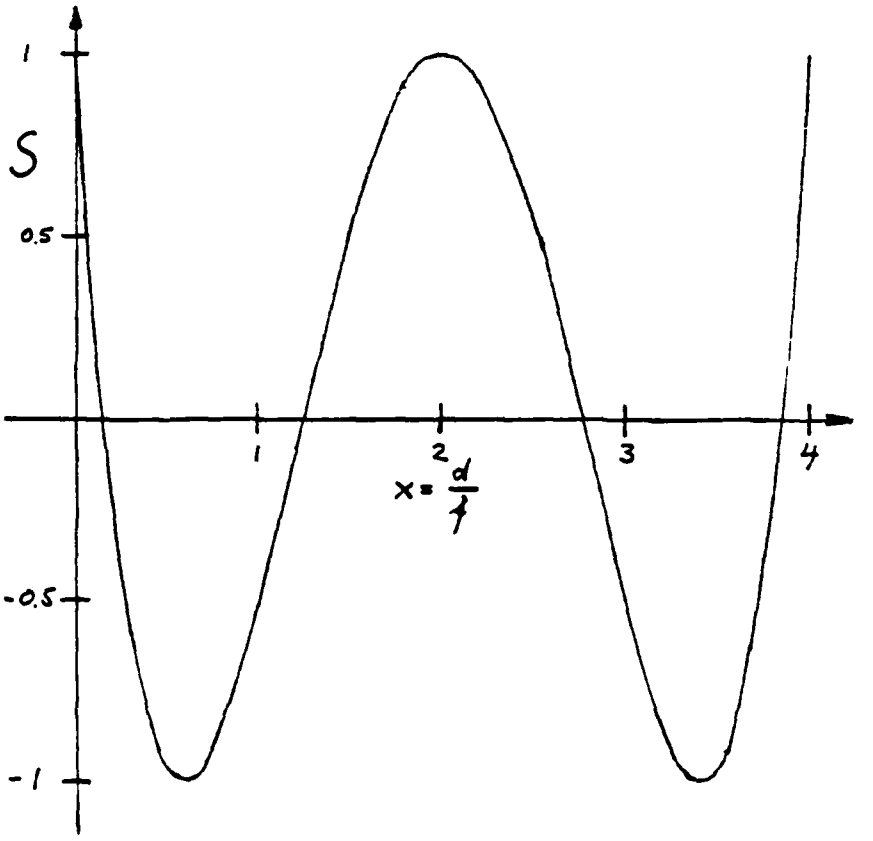

Also $- 1 \leq (A+D)/2 = [1 - x(x-2)^2 (4-x)/2] \leq + 1$

From this it is immediately clear that

$x \leq 4$ (otherwise $(A+D)/2 > 1$)

as well as $0 \leq x$.

To insure that inside the range $0 \leq x \leq 4$ there is stability for any x,

we determine the extrema.

$\partial[(A+D)/2]/\partial x = 0 = (1/2)(-16 + 40x - 24x^2 + 4x^3) = 2(-4 + 10x - 6x^2 + x^3)$

which gives extrema at $x = 2$: $(A+D)/2 = +1$

$x = 2 + \sqrt{2}$: $(A+D)/2 = -1$

$x = 2 - \sqrt{2}$: $(A+D)/2 = -1$ (marginal stability)

i.e. the cavity is stable everywhere in the range

$$0 \leq x = d/f \leq +4 \quad .$$

Smallest R, to have stability in p and s: $R_{min} = d/\sqrt{2}$ (7.6m/$\sqrt{2}$ = 5.4 m)

Waists: Because of symmetry, they should be in the center between

neighboring mirrors.

To find the round-trip matrix from center to center, do this:

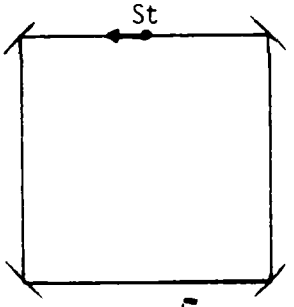

, and start at St

$$\begin{pmatrix} A' & B' \\ C' & D' \end{pmatrix} = \begin{pmatrix} 1 & d/2 \\ 0 & 1 \end{pmatrix} \begin{pmatrix} 1 & 0 \\ -f^{-1} & 1 \end{pmatrix} \left[\begin{pmatrix} 1 & d \\ 0 & 1 \end{pmatrix} \begin{pmatrix} 1 & 0 \\ -f^{-1} & 1 \end{pmatrix} \right]^3 \begin{pmatrix} 1 & d/2 \\ 0 & 1 \end{pmatrix} .$$

Again, with x = d/f, we get

$$\begin{pmatrix} A' & B' \\ C' & D' \end{pmatrix} = \begin{pmatrix} 1 - 8x + 10x^2 - 4x^3 + x^4/2 & (8 - 22x + 17x^2 - 5x^3 + x^4/2)(d/2) \\ d^{-1}(-4x + 10x^2 - 6x^3 + x^4) & 1 - 8x + 10x^2 - 4x^3 + x^4/2. \end{pmatrix} .$$

Here, A'=D'. Also note, that A' + D'=A + D (Stability!)

Check, whether A'D' - C'B' = 1:

$(1/2)\, x^0\, (2)$ $\quad + 1/2\, x^5\, (-8-80-80-8+2+50+102+22)$

$+ (1/2)\, x^1\, (-16-16+32)$ $\quad + 1/2\, x^6\, (+10+32+10-5-30-17)$

$+ (1/2)\ x^2\ (+20+128+20-88-80) \qquad + 1/2\ x^7\ (-4-4+3+5)$

$+ (1/2)\ x^3\ (-8-160-160-8+68+220+48) \qquad + 1/2\ x^8\ (+1/2 - 1/2)$

$+ (1/2)\ x^4\ (+1+64+200+64+1-20-170+132-8) \qquad = 1 \ .$

Waists at centers of each branch, w_0:

From previous section:

$R = -2B'/(A'-D')$; Since $A' = D'$ at each center, it follows that $R \to \infty$, which indicates a waist.

Size of waist:

$$(\pi/\lambda)\ w_0^2 = B'/\left[1 - (A'+D')^2/4\right]^{1/2} = B'/\left[1 - A'^2\right]^{1/2},$$

Since $A' + D' = 2A' = A + D$, independent of the starting point of the round trip. Incidentally, the condition $1 - A'^2 > 0$ recovers the stability condition.

At the center of each branch we get thus

$$(\pi/\lambda)\ w_0^2 = (d/2)(8-22x+17x^2-5x^3+x^4/2)/\left[1 - (1-8x+10x^2-4x^3+x^4/2)^2\right]^{1/2}$$

which can be factorized, with the result

$$4\pi\ w_0^2/\lambda\ d = (x-4)(x-2-\sqrt{2})(x-2)(x-2+\sqrt{2})/[(1/2)(x-2)(x-2-\sqrt{2})(x-2+\sqrt{2})\sqrt{x(4-x)}]$$

or

$$w_0^2 = (\lambda d/2\pi)\sqrt{(4-x)/x} \ .$$

Within the stability limits $0 < x < 4$, the waist w_0 decreases steadily, from $w_0\ (x \to 0) \to \infty$ (flat mirrors) to $w_0\ (x = 4) = 0$; See figure below.

Spot size at mirrors, w_M:

Again,

$$(\pi/\lambda)w_M^2 = B/\left[1-(A+D)^2/4\right]^{1/2} = 2d(4-10x+6x^2-x^3)/[(x-2)(x-2-\sqrt{2})(x-2+\sqrt{2})\sqrt{x(4-x)}].$$

Factorizing

$$w_M^2 = 2(\lambda d/\pi)/\sqrt{x(4-x)}$$

The spot size on the mirrors has a definite minimum versus $x = d/f$:

$(\partial/\partial x)[x(4-x)]^{-1/2} = 0$ gives $x = 2$, such that

$$w_{M,\ \text{minimum}} = \sqrt{\lambda d/\pi}\ .$$

The corresponding waist size at the center of each branch is

$$w_o = \sqrt{\lambda d/2} = (1/\sqrt{2})\sqrt{\lambda d/\pi}$$ for minimum spot size <u>at mirror</u>

Numerical example: $\lambda = 514.5$ nm, $d = 7.62$ m

$$\rightarrow w_o = 7.90 \times 10^{-4}\ \text{m} \simeq 0.8\ \text{mm}$$

$$\rightarrow w_M = 1.12 \times 10^{-3}\ \text{m} \simeq 1.1\ \text{mm};$$

relation to full width at half-power (see Verdeyen, p. 60)

$$w_{FWHM} = \sqrt{2\ln 2}\ w = 1.18\ w\ .$$

<u>Circular beam cross section at any mirror in square symmetric ring</u>:

First note that the mirror spot size is symmetric with respect to $x = 2$: Put $x' = x - 2$, and get

$$w^2 = w_M^2/(\lambda d/\pi) = [x(1-x/4)]^{-1/2} = (1-x'^2/4)^{-1/2}$$

i.e $w(-x') = w(+x')$.

Now, the ring is astigmatic, i.e. for a given mirror radius R, the focal length in the plane of the ring is different from the focal length normal to the plane.

From the above it is however possible to choose a mirror radius such that the spot size at the mirror is circular; simply choose

$$(d/f_p)-2 = 2-(d/f_s)$$

or

$$d/(R \cos 45^0/2)-2 = 2-d/(R/2 \cos 45^0) \ .$$

This results in

$$R = 3\sqrt{2}\ d/4 \simeq 1.06\ d \ . \qquad (d = 7.6\ m \rightarrow R = 8.06\ m)$$

To properly mode-match the injected beam, put a cylinder surface on input mirror and output mirror.

With the above choice of R/d, the spot sizes at the mirrors are w_M $= w_{M,p} = w_{M,s} = (\lambda d/\pi)^{1/2} \times 1.030$, (only 3% above the minimum spot size possible).

and

$$d/f_p = 2 + 2/3$$

$$d/f_s = 2 - 2/3 \ .$$

Note also that a problem of instability in near-confocal cavities (where $f_1 = (d/2) - \varepsilon$, but $f_2 = (d/2) + \varepsilon$, see Siegman", problem 7 in chpt. 8) does <u>not</u> appear here: Given the nominal mirror radii R, the actual focal lengths f_p and f_s are quite removed from f = d/2, viz.

$$f_p = (d/2)(3/4) \quad , \quad f_s = (d/2)(3/2),$$

due to astigmatism.

That means that the tolerances of the mirror radii have merely to be < 25%, to avoid near-confocal instability.

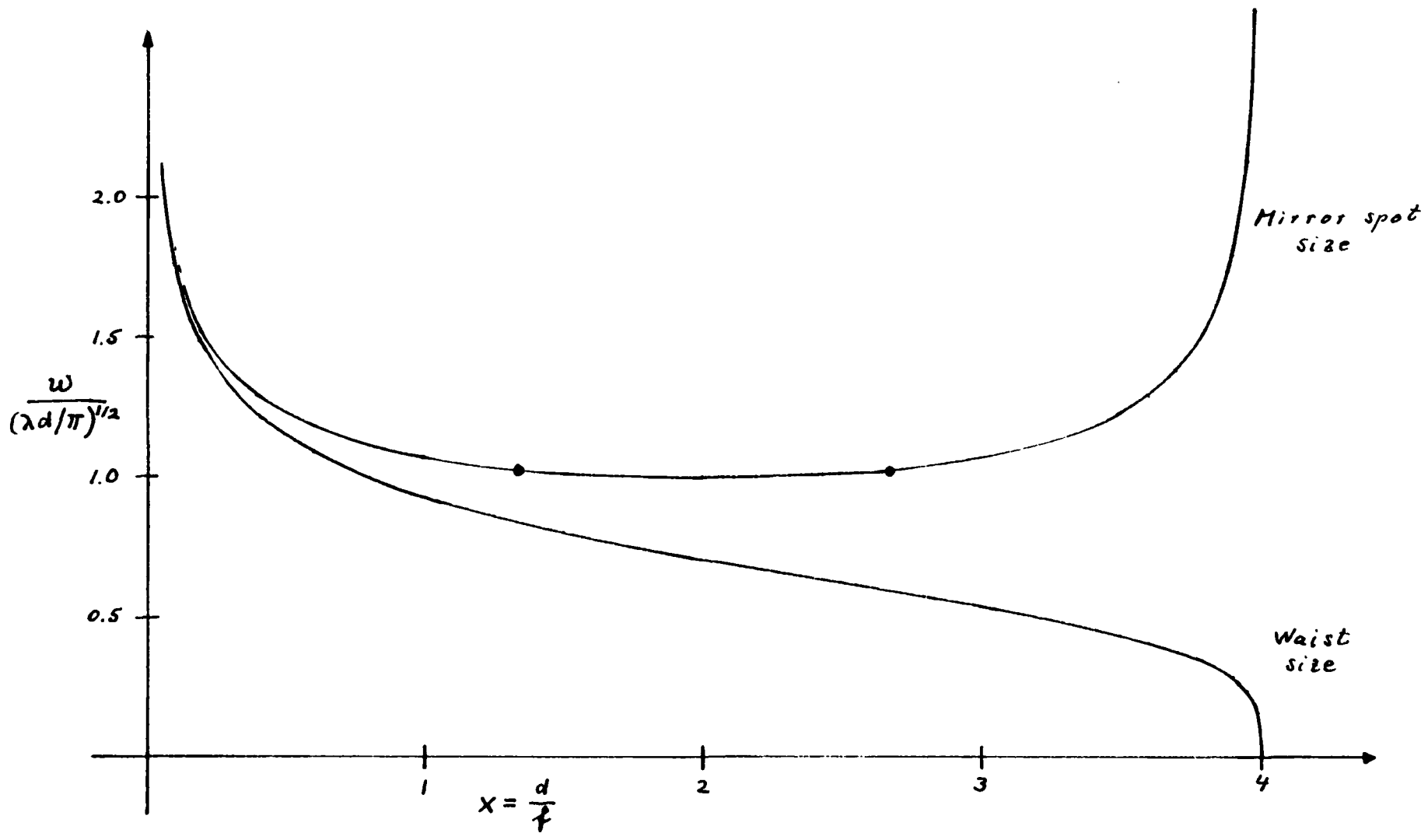

Example: $\lambda = 514.5\ nm$, $d = 7.6\ m$, $x = 2$ (confocal): $w_M = 1.12\ mm$, $w_0 = 0.79\ mm$

II. D. Injection errors: Response of ring to offset and tilt of injecting ray.

In this section, the excursion of a pencil ray off the optical axis due to tilting and/or offset of an injecting ray is investigated. The method is reminiscent of orbit calculations in synchrotrons, except that in this section no wave picture is employed. The solution of the standard difference equation for rays with such perturbations is simple. It gives however some insight into the "stability" of a given ring against injection errors.

II. D. Injection errors: Response of ring to offset and tilt of injecting ray.

(For analytical background see Verdeyen, Chap. 2)

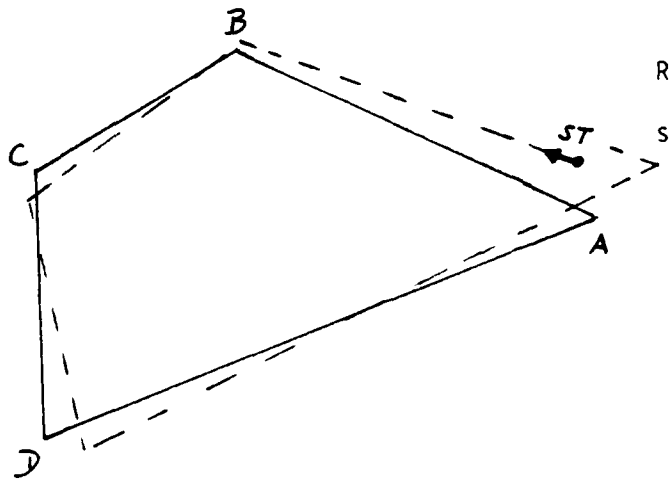

Ray matrix for round trip, starting at a point ST

$$\begin{pmatrix} A & B \\ C & D \end{pmatrix}$$

Assume an initial offset $r_0 = a$, and an initial slope $r_0' = m$ at ST.

The offset r at any point (off optical axis) on the ring is then given through a difference equation

$$r(s+2) - (A+D)\, r(s+1) + r(s) = 0,$$

where $r(s+\nu)$ = offset at ST after $s + \nu$ round trips. The offset anywhere in the ring is obtained by choosing a non-integer value for s.

Solution: $r(s) = r_{max} \sin(s\theta + \alpha)$

where r_{max} is the maximum offset in the ring,

$\cos\theta = (1/2)(A + D)$, and

$$\tan \alpha = [1-(A+D)^2/4]^{1/2}/[(A-D)/2+Br_0'/r_0].$$

From $r(s = 0) = r_0 = r_{max} \sin \alpha$, we determine r_{max} as

$$r_{max} = (1/S)\ [(1-AD)r_0^2 + B^2r_0'^2 + (A-D)B\ r_0\ r_0']^{1/2},$$

with S = stability condition = $[1 - (A+D)^2/4]^{1/2}$.

$$(0 < S < 1)$$

The maximum excursion is homogeneous in r_0 and r_0', as it should be. In the limit of stability, $S \to 0$, r_{max} diverges.

The same difference equation holds also true for the slopes, viz.

$$r'(s+2) - (A+D)\ r'(s+1) + r'(s) = 0$$

with the solution

$$r'(s) = r'_{max} \sin (s\theta + \alpha') \quad ,$$

$$\cos \theta = (1/2)\ (A+D)\ , \text{ and}$$

$$\tan \alpha' = [1-(A+D)^2/4]^{1/2}/[(D-A)/2+Cr_0/r_0'], \text{ so that}$$

$$r'_{max} = (1/S)\ [(1-AD)r_0'^2 + C^2r_0^2 + (D-A)C\ r_0r_0']^{1/2}.$$

Note that since α and α' and the roots are multivalued, there exist in principle solutions for α and α' in all four quadrants, given the initial conditions r_0 and r_0', and the ring matrix. In the following we will convene r_{max} and r'_{max} as positive, and α and α' shall be uniquely specified by choosing them such that $r(0) = r_0$, $r(1) = Ar_0 + Br_0'$, as well as $r'(0) = r_0'$, $r'(1) = Cr_0 + Dr_0'$.

Special cases:

a) No initial offset, no initial slope: <u>Proper operation</u>.

$r_0 = r_0' = 0$: $r_{max} = r'_{max} = 0$, the ray stays on the optical

axis.

b) No offset, but slope:

$$r_0 = 0,\ r_0' = m: \qquad r_{max} = (B/S)m, \qquad r'_{max} = [(-BC)^{1/2}/S]m$$

$$\alpha = 0 \text{ or } \pi\ ,\ \alpha' = \tan^{-1}(2S/(D-A)).$$

c) Offset, but no slope

$$r_0 = a,\ r_0' = 0: \qquad r_{max} = [(-BC)^{1/2}/S]a \qquad r'_{max} = (C/S)a$$

$$\alpha = \tan^{-1}\ (2S/(A-D)),\ \ \alpha' = 0 \text{ or } \pi\ .$$

Application to square, symmetric ring with four equal mirrors

Starting off one mirror, the matrix is, with $x = d/f$:

$$\begin{pmatrix} A & B \\ C & D \end{pmatrix} = \begin{pmatrix} 1-6x+5x^2-x^3 & d(4-10x+6x^2-x^3) \\ d^{-1}(-4x+10x^2-6x^3+x^4) & 1-10x+15x^2-7x^3+x^4 \end{pmatrix}$$

$$= \begin{pmatrix} 1-6x+5x^2-x^3 & d(2-x)(x-2+\sqrt{2})(x-2-\sqrt{2}) \\ -(x/d)(2-x)(x-2-\sqrt{2})(x-2+\sqrt{2}) & 1-10x+15x^2-7x^3+x^4 \end{pmatrix}$$

where $(B/d)x = -dC$,

$$S = (1/2)(x-2)(x-2-\sqrt{2})(x-2+\sqrt{2})\cdot[x(4-x)]^{1/2} = [1-(A+D)^2/4]^{1/2}$$

$$1-AD = -BC = x(2-x)^2(x-2-\sqrt{2})^2\ (x-2+\sqrt{2})^2$$

$$A - D = (x/d)B = -dC = x(2-x)(x-2-\sqrt{2})(x-2+\sqrt{2})$$

and, as before, $AD - BC = 1$, with the stability limits

$$0 \leq x \leq 4\ .$$

For the special cases above

$r_0 = 0,\ r_0' = m$, we get $\alpha = 0$ or π $\qquad r_{max} = 2dm/[x(4-x)]^{1/2}$

$\alpha' = \tan^{-1}\ [(4-x)/x]^{1/2}, \qquad r'_{max} = 2m/(4-x)^{1/2}$

$r_0 = a,\ r_0' = 0 \qquad \alpha = \tan^{-1}\ (4-x)^{1/2}, \qquad r_{max} = 2a/(4-x)^{1/2}$

$\alpha' = 0 \text{ or } \pi\ , \qquad r'_{max} = (2a/d)[x/(4-x)]^{1/2}.$

Generally, the square symmetric ring with equal mirror radii gives

$$r_{max} = 2(xr_0^2+d^2r_0'^2+dxr_0r_0')^{1/2}/[x(4-x)]^{1/2},\ \tan\alpha = [x(4-x)]^{1/2}(-r_0)/(xr_0+2dr_0')$$

$r'_{max} = 2[r'^2_o+(xr^2_o/d^2)+(r_o r'_o/d)]^{1/2}/(4-x)^{1/2}$, $\tan\alpha' = [(4-x)/x]^{1/2}\, r'_o/[r'_o+(r_o/d)]$.

The offset at a given mirror is given through the relation

$r(s) = r_{max} \sin(s\,\theta + \alpha)$, and the slope through

$r'(s) = r'_{max} \sin(s\,\theta + \alpha')$,

where now s has a fractional value. Suppose the matrix is evaluated starting off mirror A in CCW direction. Then

B ←A

$r_A = r_{max} \sin(0\,\theta + \alpha)$

C D $r_B = r_{max} \sin(\theta/4 + \alpha)$

$r_C = r_{max} \sin(\theta/2 + \alpha)$

$r_D = r_{max} \sin(3\theta/4 + \alpha)$,

during the first round trip. In the second round trip increase s by 1, etc. Equivalent relations give r'_A, etc. Three examples are worked out below. All results are verified by applying the matrix of one leg to the column vector, i.e.

$$\begin{pmatrix} r_{\nu+1} \\ r'_{\nu+1} \end{pmatrix} = \begin{pmatrix} 1 & 0 \\ -f^{-1} & 1 \end{pmatrix} \begin{pmatrix} 1 & d \\ 0 & 1 \end{pmatrix} \begin{pmatrix} r_\nu \\ r'_\nu \end{pmatrix}$$ where ν is the νth corner.

No initial offset is considered, i.e. with $r_o = 0$, $r'_o = m$, we have

$r_{max} = 2dm/[x(4-x)]^{1/2}$, $\tan\alpha = 0$ $(\alpha = 0 \text{ or } \pi)$

$r'_{max} = 2m/(4-x)^{1/2}$, $\tan\alpha' = [(4-x)/x]^{1/2}$

1. Closed path after <u>one</u> round trip: $\theta = 2\pi$ or $\cos\theta = 1 = (1/2)(A+D)$

$= (1/2)(2-16x+20x^2-8x^3+x^4)$ Solutions: $x = 0, 2, 2, 4$

Only $x = 2$ is inside the stability limit: confocal

$x = d/f = 2$ $\rightarrow r_{max} = dm$, $\alpha = 0$ or π

$\rightarrow r'_{max} = \sqrt{2}\,m$, $\alpha' = \tan^{-1}(\pm 1) = \pm\pi/4, \pm\pi/4 + \pi$

$r = dm \sin(s2\pi)$, $r' = \sqrt{2}\,m \sin(s2\pi + 3\pi/4)$

($\alpha' = 3\pi/4$, to get $r'_A = r_o = m$ and $r'_B = (1-x)m = -m$)

s	0	1/4	1/2	3/4	1	
mirror	A	B	C	D	A	
r/dm	0	1	0	-1	0	(repet.)
r'/m	1	-1	-1	1	1	

All the values have been checked directly.

Example: $d = 7.6$ m, $m = \tan 1' = 0.00029$

$r_A = r_C = 0$, $r_B = -r_D = 2.21 \times 10^{-3}$ meter.

2. Closed path after <u>two</u> round trips: $\theta = \pi$ or $\cos\theta = -1 = (A+D)/2$;

Solutions $x = 2+\sqrt{2}$, $2+\sqrt{2}$, $2-\sqrt{2}$, $2-\sqrt{2}$

$x = d/f = 2 - \sqrt{2}$ (the other solution corresponds actually to $\theta = 3\pi$)

$\rightarrow r_{max} = \sqrt{2}$ dm, $\alpha = 0$

$\rightarrow r_{max} = \sqrt{2}\sqrt{2-\sqrt{2}}$ m, $\alpha' = \tan^{-1}[\pm(1+\sqrt{2})]$

$= \pm 3\pi/8, \pm 3\pi/8 + \pi$

$r = \sqrt{2}$ dm $\sin(s\pi)$, $r' = \sqrt{2}\sqrt{2-\sqrt{2}}m \sin(s\pi + 5\pi/8)$

$(r_A = m, r_B = (1-x)m = (\sqrt{2}-1)m)$

S	0	1/4	2/4	3/4	4/4	5/4	6/4	7/4	8/4	
mirror	A	B	C	D	A	B	C	D	A	
r/dm	0	1	2	1	0	-1	$-\sqrt{2}$	-1	0	repet
r'/m	1	$\sqrt{2}-1$	$-(\sqrt{2}-1)$	-1	-1	$-(\sqrt{2}-1)$	$\sqrt{2}-1$	1	1	

The offsets are only slightly larger than in the confocal arrangement:

$r_{max} = (1.08)$ dm

3. Two round trips, but with $\theta = 3\pi$

$x = d/f = 2 + \sqrt{2}$ $\quad r_{max} = \sqrt{2}$ dm $\quad \alpha = 0$

$r'_{max} = \sqrt{2}\sqrt{2+\sqrt{2}}$ m $\quad \alpha' = \tan\pm(\sqrt{2}-1)$

$= \pm \pi/8, \pm \pi/8 + \pi$

$r = \sqrt{2}$ dm $\sin(s3\pi)$, $r' = \sqrt{2}\sqrt{2+\sqrt{2}}m \sin(s3\pi + 7\pi/8)$

S	0	1/4	2/4	3/4	4/4	5/4	6/4	7/4	8/4	
mirror	A	B	C	D	A	B	C	D	A	
r/dm	0	0	$-\sqrt{2}$	1	0	-1	$\sqrt{2}$	-1	0	repet
r'/m	1	$-(\sqrt{2}+1)$	$(\sqrt{2}+1)$	-1	-1	$\sqrt{2}+1$	$-(\sqrt{2}+1)$	1	1	

The stronger focussing makes again slightly larger offsets: $r_{max} = 1.41$ dm

Maximum offset in square symmetric ring due to injection errors: initial slope m, initial offset a

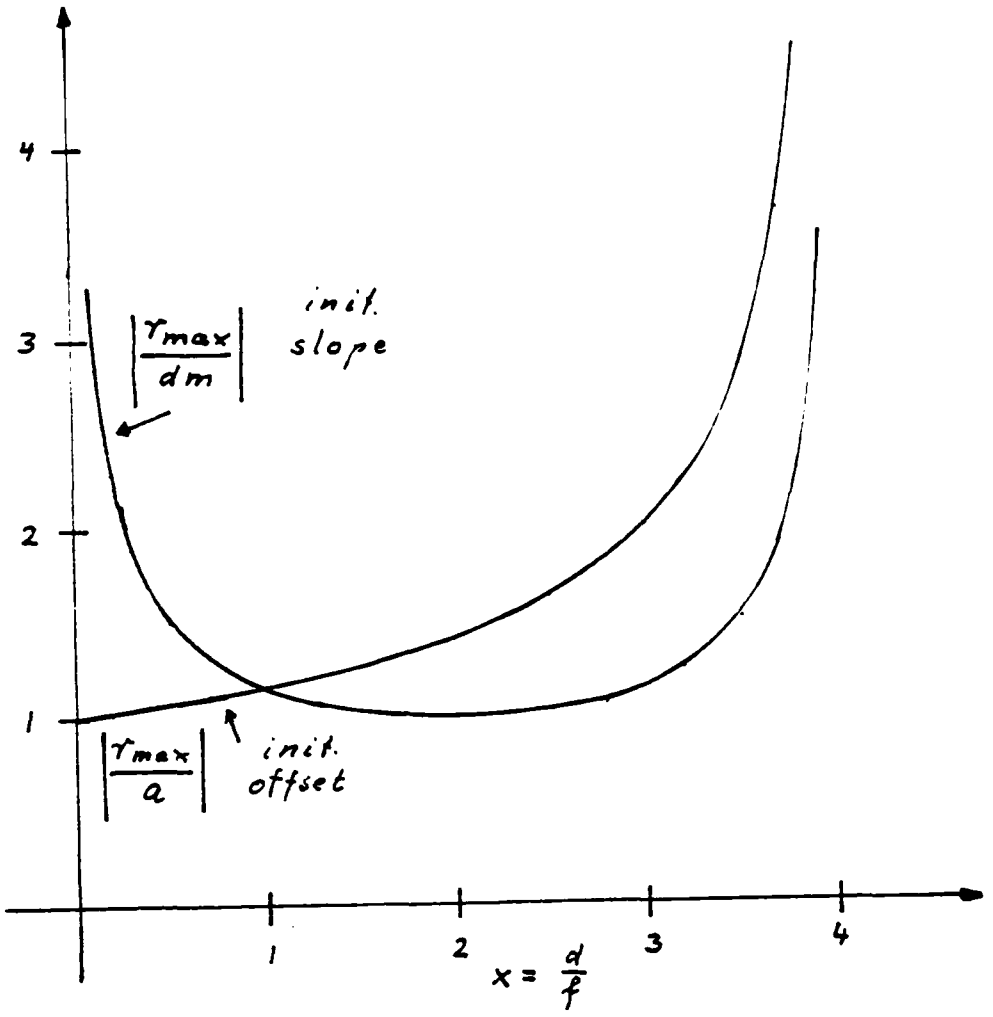

The figure gives an impression of the expected maximum excursion due to offset ($a \neq 0$, $m=0$) and due to tilt ($m \neq 0$, $a=0$): Going towards the strong focussing limit $x \to 4$, the excursions diverge. On the other side, for weak focussing ($x \to 0$), only a tilted ray diverges. It is quite obvious that from the point of view of minimizing effects of injection errors, intermediate stability figures are to be sought.

II. E. Resonant frequencies of Hermite-Gaussian modes in a ringlaser

Although the working modes in a ring laser gyro are fundamental Gaussians, a knowledge of the higher-order eigenmodes is important for design purposes. Imperfect injection into a ring excites higher-order modes (section II.F.); the resulting pulling effects depend on amplitude and frequency separation of these modes.

Collins' theory (ref. 10) is applied to a square-shaped ring with zero, one, two, four equally curved mirrors (in any one of these four cases, the other mirrors are plane). Simple formulas emerge which are useful for design.

Resonant frequencies of Hermite-Gaussian modes in a ringlaser

This section presents a general formula for the resonance frequencies of a given resonator with negligible apertures and symmetric focusing elements with respect to two normal planes. An astigmatic, plane, four mirror resonator with spherical mirrors falls in this category. The formula is derived in ref. 10. A configuration is sought where by proper choice of mirror radii the frequency difference of those modes to the fundamental mode is maximized, for minimum interaction.

The resonator mirrors may be replaced by thin lenses. The equivalent focal length of a thin lens depends on mirror curvature radius R and the incident angle of the beam. This is shown in Figure 1.

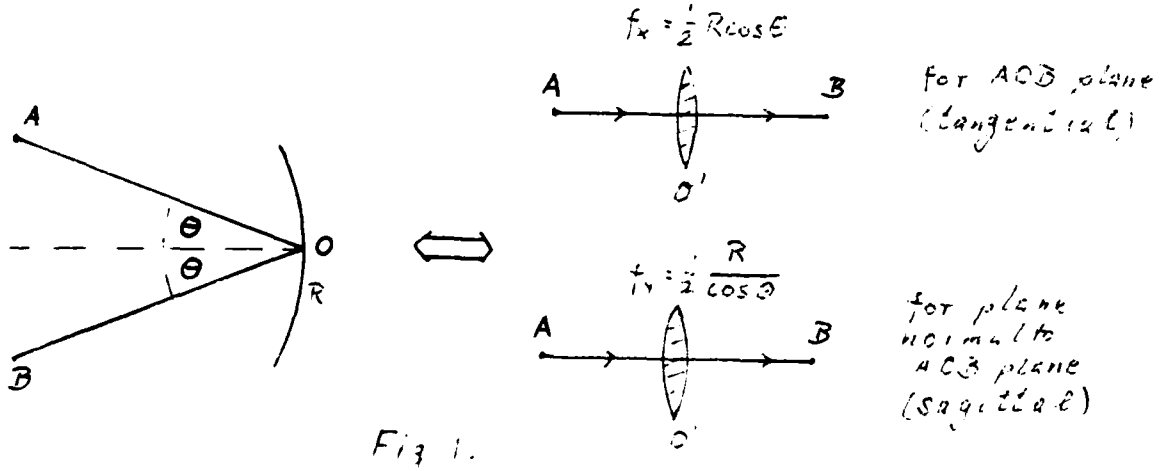

Fig 1.

For quadrangular resonators, the resonance frequencies are generally [10]

$$f_{qmn} = (c/L)[q + (m + 0.5)\alpha_x/2\pi + (n + 0.5)\alpha_y/2\pi] \qquad (1)$$

The parameters are

c = speed of light in vacuum (the resonator operates in vacuum)

L = optical distance coefficient (round-trip path length)

q = axial mode number, m, n = transverse mode numbers.

$$\alpha_\mu = \arccos\left(\sqrt{\frac{4\rho_{\mu 11}\rho_{\mu NN}}{\rho_{\mu 1N}^2}}\right)^{1/2} \quad (\mu = x \text{ or } y) \tag{2}$$

$$\rho_{\mu 11} = (1/2)(1/r_1 - |D_o, {}_o|/|D|), \tag{3}$$

$$\rho_{\mu NN} = (-1/2)(1/r_2 + |D_{N-1,N}|/|D|) \tag{4}$$

(N = number of mirrors, r_1, r_2 = radii of curvature of the reference surface.

$$\rho_{\mu 1N} = -(-1)^N |D_{o,N}|/|D|, \tag{5}$$

$$|D_{0,0}| = \begin{vmatrix} f_1+f_2-d & -f_2 & 0 & 0 & \cdot & \cdot & 0 \\ -f_2 & f_2+f_3-d_2 & -f_2 & 0 & \cdot & \cdot & 0 \\ 0 & -f_2 & \cdot & \cdot & \cdot & \cdot & 0 \\ \cdot & \cdot & \cdot & \cdot & \cdot & \cdot & \cdot \\ 0 & & & 0 & -f_{N-1} & f_{N-1}-d_{N-1} & \end{vmatrix} \tag{6}$$

f_i and d_i = shown in Figure 2-2.

$$|D_{N-1,N}| = \begin{vmatrix} f_1-d_0 & -f_1 & 0 & 0 & 0 \\ -f_1 & f_1+f_2-d_1 & -f_2 & \cdot & 0 \\ 0 & -f_1 & & \cdot & 0 \\ 0 & & & & -f_{N-2} \\ 0 & & & -f_{N-2} & f_{N-2}+f_{N-1}-d_{N-2} \end{vmatrix} \tag{7}$$

$$|D_{0,N}| = (-1)^{N-1} \prod_{p=1}^{N-1} f_p \tag{8}$$

$$|D| = \begin{vmatrix} f_1-d_0 & -f_1 & 0 & \cdot & 0 \\ -f_1 & f_1+f_2-d_1 & -f_2 & \cdot & 0 \\ 0 & & \cdot & 0 & -f_{N-1} \\ 0 & & \cdot & -f_{N-1} & f_{N-1}-d_{N-1} \end{vmatrix} \qquad (9)$$

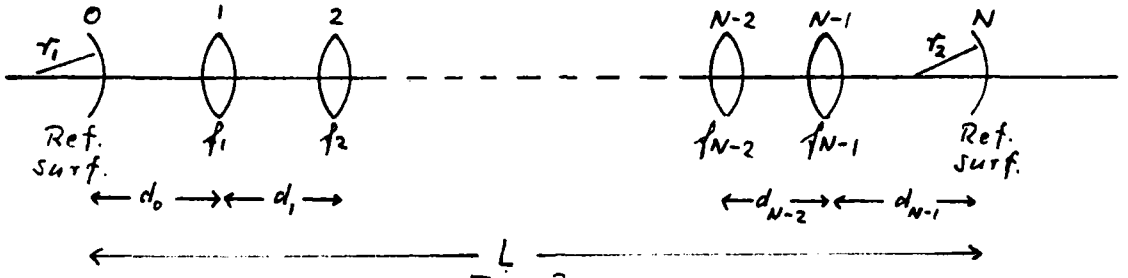

Fig. 2.

Now we make use of these equations to find the resonance frequencies for different square-shaped resonators.

Square ring with three flat mirrors and one curved mirror (see figure 3): The equivalent thin lens wave guide is shown in Figure 4.

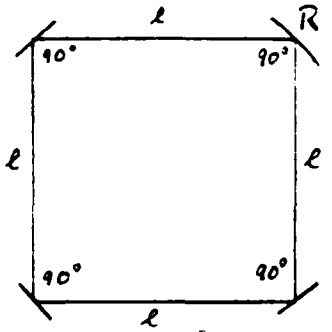

Fig 3

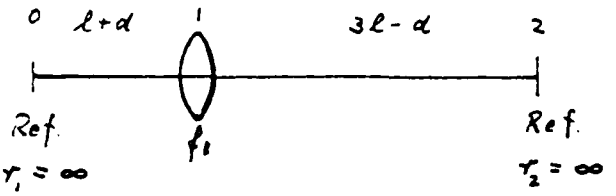

Fig 4

In the equivalent lens waveguide (Figure 4), the reference surface is tentatively placed in a leg which is not adjacent to the curved mirror. The equivalent focal lengths are

$f_{1x} = R\cos 45^0/2 = (\sqrt{2}/4)R$ (obliquity angles are all 45^0)

$f_{1y} = R/(2\cos 45^0) = (\sqrt{2}/2)R$

The curvature radii of the reference surface are $r_1 \to \infty$, $r_2 \to \infty$, and N=2.

The angles α_x and α_y are obtained from Eq. 2 after substituting eq's. (3), (4), and (5) as

$$\cos \alpha_\mu = \left[\frac{|D_{0,0}||D_{1,2}|}{|D_{0,2}|^2} \right]^{1/2}.$$

Now we need to calculate $|D_{0,0}|$, $|D_{1,2}|$, and $|D_{0,2}|$. These determinants are

$|D_{0,0}| = f_\mu - L/2$

$|D_{1,2}| = f_\mu - L/2$

$|D_{0,2}| = -f_\mu$.

Thus,

$\cos \alpha_\mu = 1 - L/2f_\mu$

Therefore the resonance frequencies are given as follows

$$f_{qmn} = (c/L)[q+(m+0.5)\arccos(1-L\sqrt{2}/R)/2\pi+(n+0.5)\arccos(1-L/\sqrt{2}R)/2\pi]. \quad (10)$$

The stability condition is given by

$-1 \leq \cos \alpha_\mu \leq 1$

or $(1/2) \leq R/L \leq \infty$ (the stronger focussing tangential plane dictates the lower limit for R).

Square ring with two diagonally opposite flat mirrors and two equally curved mirrors (figure 5).

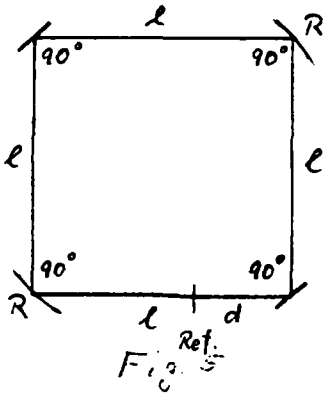

Fig. 5

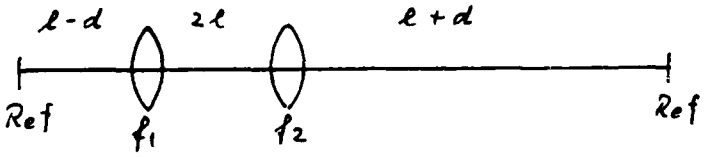

Fig. 6.

The equivalent lens wave guide for the square ring is shown in Figure 6. Here, again, $r_1 = r_2 \to \infty$, but N=3 (two curved mirrors).

The angles α_x and α_y are obtained by Eq. (2) as

$$\cos \alpha_\mu = \left[\frac{|D_{0,0}||D_{2,3}|}{|D_{0,3}|}\right]^{1/2},$$

where $|D_{0,0}|$, $|D_{2,3}|$, and $|D_{0,3}|$ are calculated as follows

$$|D_{0,0}| = \begin{vmatrix} 2f_\mu - 2\ell & -f_\mu \\ -f_\mu & f_\mu - \ell \end{vmatrix} = 2(f_\mu - \ell)^2 - f_\mu^2$$

$$|D_{0,3}| = f_\mu^2$$

$$|D_{2,3}| = \begin{vmatrix} f_\mu - \ell & -f_\mu \\ -f_\mu & 2f_\mu - 2\ell \end{vmatrix} = 2(f_\mu - \ell)^2 - f_\mu^2$$

Thus,

$$\cos \alpha_\mu = 2\left(1 - \frac{\ell}{f_\mu}\right) - 1 \text{ ,i.e } \cos\alpha_x = 2\left(1 - \frac{2\ell\sqrt{2}}{R}\right)^2 - 1, \text{ and } \cos\alpha_y = 2\left(1 - \frac{\ell\sqrt{2}}{R}\right)^2 - 1.$$

The resonance frequencies are

$$f_{qmn} = (c/L)[q+(m+0.5)\arccos(1-L/\sqrt{2}R)/\pi+(n+0.5)\arccos(1-L/2\sqrt{2}R)/\pi] \quad (11)$$

The stability condition is here

$$(1/2\sqrt{2}) < R/L > \infty$$

Square ring with four equally curved mirrors (see figure 7).

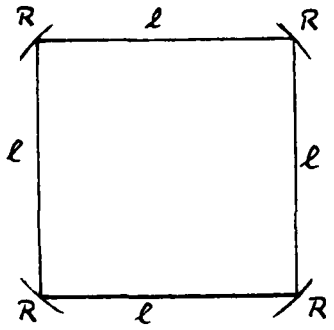

Fig. 7

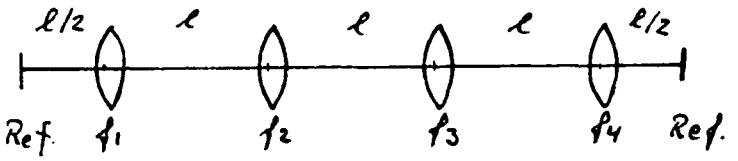

Fig. 8

The equivalent lens waveguide for the square ring is shown in Figure 8. This example shows an alternative way to find the resonance frequencies. It is assumed that the total phase shift due to one round trip around the resonator must be $2\pi q$ where q is an integer. Therefore we need to find the total round trip phase shift ϕ_{tr}.

The longitudinal phase shift is $\phi_d = kd_\mu$ (ref. 11) due to the distance $d_\mu = L/2$ between a lens and a; the transverse phase shift is

$$\phi_\mu = -(\mu + 0.5) \arctan (d_\mu / z_{0_\mu})$$

where μ = m or n.

Here, the Rayleigh-length is $z_{0\mu} = (L/8)[f_\mu(4-L/4f_\mu)/(L/4)]^{1/2}$.

The total phase shift is therefore

$$\phi_{tr}=4k\ell - (m + \tfrac{1}{2})\arctan[f_x(4-\ell/f_x)/\ell]^{-1/2}-(n + \tfrac{1}{2})\arctan[f_y(4-\ell/f_y)/\ell]^{1/2}.$$

We need to satisfy $\phi_{tr} = 2\pi q$; therefore the resonance frequency is

$$f_{qmn} =(c/L)[q+2(m+0.5)\arccos(1-L/2\sqrt{2}R)/\pi+2(n+0.5)\arccos(1-L/4\sqrt{2}R)/\pi] \quad (12)$$

Discussion:

The three types of square rings give surprisingly simple, and similar, results for the resonance frequencies. With a parameter δ, δ = 1,2,4 for rings with 1,2,4 (equal) mirror curvatures, respectively, the resonance frequencies (10, 11, 12) are given by the same equation for all three cases as:

$$f_{qmn} =(cq/L)+(c\delta/2\pi L)[(m+0.5)\arccos(1-\sqrt{2}L/\delta R)+(n+0.5)\arccos(1-L/\sqrt{2}\delta R)] .$$

A cavity with 4 flat mirrors is contained here is as a special case with δ=4, R$\to\infty$.

The spacing of the fundamental modes (m=n=0) is always as usual

Δf = (c/round trip path length)(Δq=1) = c/L (free spectral range)

This is true for any δ.

The arguments of the arccosines vary with R. To achieve a specific operation, given by a point in the stability diagram, $\delta R/\ell$ has to be chosen properly.

The two stability limits are, for any δ,

$\frac{\sqrt{2}}{\delta}\frac{L}{R} = 0$ ($R \to \infty$, all mirrors flat) , and $\frac{\sqrt{2}}{\delta}\frac{L}{R} = 2$ (mirrors with maximum curvature)

They provide us also with limiting frequency differences.

In the former case

$f^{*}_{q,m,n} = (c/L)q$ (all m,n modes resonate at the same frequency for a given q),

in the latter case

$$f^{*}_{q,m,n} = (c/L)q + (c/4L)\delta[2(m + 0.5) + (n + 0.5)]$$

such that all resonances are either 0, 1/4, 1/2, 3/4 or 1 free spectral range apart from the fundamental mode.

In the latter case, for example, *a (q, 0, 0) mode and a* (q-1, 1, 0) mode would have the same resonance frequency in a 2 curved mirror ring ($\delta = 2$).

The problem is therefore to find a ring configuration where the unwanted Hermite-Gaussian resonances are as far away as possible from the desired q00 resonances.

To facilitate the search for a ring configuration with well-spaced resonances we developed a graph, Fig. 9, that contains the relative spacing $(f_{q,m,n} - f_{q,0,0})/(f_{q+1,0,0})(2/\delta)$ (δ=number of equally curved mirrors) versus a parameter $C=2\sqrt{2}L/\delta R$ within the stability limits $0<C<1$.

It appears from these calculations, that not much, if anything, can be gained by avoiding these special symmetry cases, as indeed any frequency distribution pattern can be identically reproduced by a square resonator with 1, 2, 4 curved mirrors; all what needs to be done is to

RESONANCE FREQUENCIES OF HERMITE-GAUSSIANS IN SQUARE RING

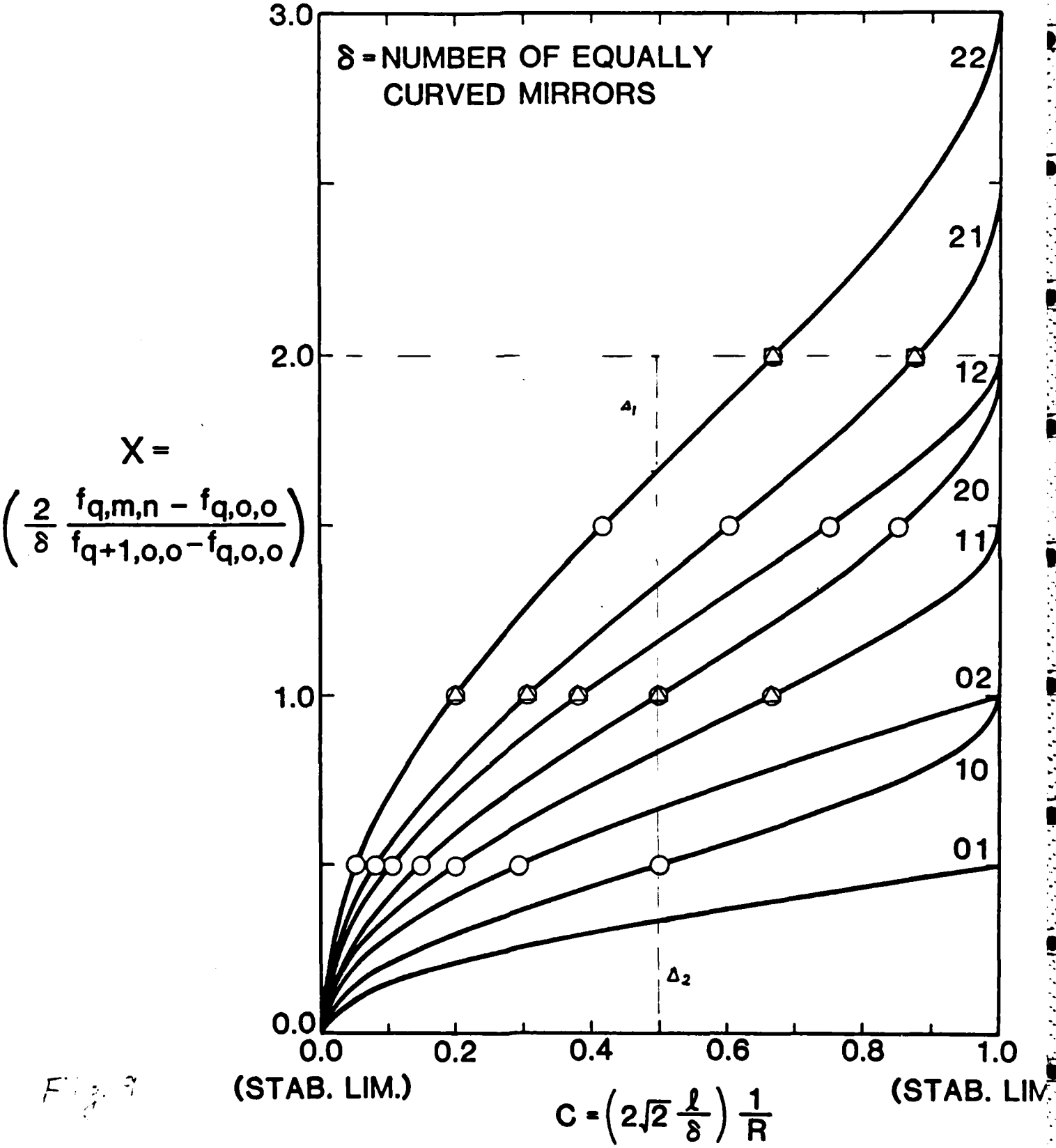

Fig. 9

Example:

1 curved + 3 flats ($\delta = 1$): $C_{opt} \simeq 0.50$ ($R = 5.66\,\ell$)

adjust the parameter ($L/\delta R$) to the same value.

After these results had been obtained, a scheme was developed where the ($L/\delta R$) was evaluated for optimum discrimination against Hermite-Gaussians. The results are found, but not included in this report. They show that the problem of pulling has a unique solution.

II. F.Injection errors: Misalignment and mismatching of an injected Gaussian beam. Effects of offset, tilt, mismatch by creating Hermite-Gaussian eigenmodes (H.-G.'s). Power loss and pulling of (fundamental) Gaussian.

A real ring has finite adjustment errors. Since H.-G.'s form a orthogonal and complete base, such errors can be expressed in an H.-G. expansion. In real life, a ring behaves indeed that way, as a proper interpretation of experimental data in ref. 12 shows. The latter was done, among other things, by us in ref. 13, and is summarized at the end of this section. We consider this section as a basic contribution to design of a large ring, and we intend to publish it.

The complexity of our approach is somewhere between our ray approach (section II.D.) and that of ref. 14, the latter using an expansion in elliptic wave functions. We treated, separately, three different adjustment errors: Offset, tilt, mismatch. Only the last type receives attention in the literature, although it is actually the most benign case, giving rise to rapidly decaying even-indexed H.-G.'s. The other types usually have all H.-G.'s in their expansion. The crucial parameter is the ratio of "misadjustment" to spot width.

We were able to quantitatively explain the data in ref. 12, where most H.-G.'s were indeed due to misalignment, contrary to the claim stated therein.

II. F. Injection errors: Misalignment and mismatching of an injecting Gaussian beam. Effects of offset, tilt, mismatch in creating Hermite-Gaussian eigenmodes. Power loss and pulling of (fundamental) Gaussian.

II. F. 1 Introduction

In order to obtain a detailed description of the optical modes in resonators, the diffration theory based on the Huygens-Fresnel's principle is used[11]. The fields across the reference surfaces are extended by means of the Fresnel-Kirchhoff integral in second order to give the fields everywhere inside and outside the resonator. This integral is of the form

$$u(x,y,z) = \frac{je^{-jkz}}{z\lambda} \int_S \int u_0(x_0,y_0) e^{-j(k/2z)[(x-x_0)^2+(y-y_0)^2]} dx_0 dy_0, \tag{1}$$

x,y,z = a rectangular coordinate system where the z axis is along the direction of the wave propagation, x_0, y_0 = coordinates on the surface of the reference surface mirror, at $z_0 = 0$.

The parameters are:

$u(x,y,z)$ = complex wave amplitude,

$u_0(x_0,y_0)$ = complex wave amplitude of input at mirror.

k = wave number = $2\pi/\lambda$,

S = reference surface,

In order to find a solution for the above integral, it is assumed that the resonator mirrors are circularly symmetric which basically

leads to Gaussian-Laguerre solutions, or they are rectangularly symmetric which leads to the Hermite-Gaussian solutions. As a practical matter, any slight misalignments or mirror imperfections may inhibit circular modes (Bessel modes),and the resonator may oscillate in H.-G.'s. Therefore, Hermite-Gaussian solutions are considered in this report exclusively.

The Hermite-Gaussian solutions for the amplitude u_{mn} are

$$u_{mn}(x,y,z)=\frac{C_{mn}}{(1+Z^2/Z_0^2)^{1/2}}\,\psi_m(\frac{\sqrt{2}x}{w})\psi_n(\frac{\sqrt{2}y}{w})\exp[-\frac{jk}{2R}(x^2+y^2)]\exp[j(m+n+1)\phi] \tag{2}$$

The parameters are defined as:

$$C_{mn} = \sqrt{[\frac{2}{w_0^2\pi\, 2^{m+n}m!n!}]},$$

w_0 = waist size, w = spot size, R = radius of curvature of beam phase

m = number of nodes along x axis

n = number of nodes along y axis

z_0 = Rayleigh length = $\pi w_0^2/\lambda$

ϕ = arctan (z/z_0)

$$\psi_\eta(\xi) = H_\eta(\xi)e^{-\xi^2/2}$$

$H_\eta(\xi)$ = Hermite polynomials of degree η, $H_\eta(\xi)\equiv(-1)^\eta e^{\xi^2}\frac{\partial^\eta}{\partial\xi^\eta}e^{-\xi^2}$.

An open optical resonator (e.g. Fabry-Perot resonator) is capable of oscillating with different axial and transverse modes. As Haus[15]

states, the electric field $\vec{E}_{mn}$ of a sperical Hermite-Gaussian wave propagating in the z-direction is,

$$\vec{E}_{mn}(x,y,z,t) = \sqrt{[2\eta P]}\ (\hat{x}u_{mn} - j\,\frac{\hat{z}}{k}\,\frac{\partial u_{mn}}{\partial x})e^{-jkz}e^{j\omega t}, \qquad (3)$$

with the major component of polarization assumed to be parallel to the x-axis.

The parameters are:

η = wave impedance

P = total power crossing an arbitrary z-plane

ω = angular frequency

$\hat{x}$ = unit vector in x-direction

$\hat{z}$ = unit vector in z-direction

Since the electric field waves are essentially monochromatic waves, $\vec{E}_{mn}(x,y,z,t)$ is written as

$$\vec{E}_{mn}(x,y,z,t) = \vec{E}_{mn}(x,y,z)e^{j\omega t}.$$

$\vec{E}_{mn}(x,y,z)$ only will be used in the following.

The z-component of the electric field is generally small with respect to the x-component, therefore it is omitted. The approximated electric field is then

$$\vec{E}_{mn} \approx \sqrt{[2\eta P]}\ \ u_{mn}e^{-jkz}\ \hat{x}\ . \qquad (4)$$

An open resonator can be excited by an external beam. The external source should satisfy the following conditions:

1. Its mode should be transferred into a fundamental gaussian ring mode as completely as possible.

2. It should have a frequency near the fundamental resonance frequencies of the resonator.

To fulfill the first requirement, the resonator has to be carefully aligned and matched. We will consider misalignment problems in the first section of the report.

Higher-order Gaussian beam modes are usually undesirable in resonator applications since a passive resonant ring laser gyroscope may give a false rotation signal due to the presence of the such modes. Irrespective of the amplitudes of such H.-G.'s one tries to design a resonator so that they appear as far away as possible from the fundamental mode. But since there is always a finite linewidth associated with the resonance frequencies, the tail of the resonance does pull the fundamental mode's frequency. Therefore the maximization of the frequency difference between the fundamental mode (TEM_{00}) and the next higher-order mode is needed.

II. F. 2) Misalignment

A resonator-source system can be misaligned in two ways:

a) The resonator becomes misaligned internally,

b) The external source is not aligned with the resonator.

The latter is dicussed throughout the report. The new optical axis of an internally misaligned resonator can be found by applying variational calculus (minimize pathlength). The external source can then be explained relative to this new base by the methods outlined below. It is assumed that the resonator fields are given by Eq. (4).

In this report, we consider the case where the injected beam is a TEM_{00} mode only. Three types of external misalignment are considered.

a) Offset source beam:

The center of the injected beam is not on the z-axis (optical axis) but the beam is parallel to the z-axis, with the same waist size as that of the resonator.

b) Tilted source beam:

The injected beam makes a finite angle with the z-axis (again, the waist size is the same as that of the resonator).

c) Mismatched source beam:

The waist size of the injected beam does not match the waist size of the resonator beam, but the beam shall not be off the z axis nor shall make an angle with z-axis.

The above types of misalignment are treated in detail in the following subsections.

II. F. 2. 1) Offset Source Beam

As it is shown in Figure 1, the external laser beam is a TEM_{00}-beam parallel to the z-axis but the center of the beam is off by ε.
The electric field of the injected beam can be written as

$$\vec{E}_0 = \sqrt{[2\eta P]}\ u'_{00}\, e^{-jkz}\, \hat{x} \tag{5}$$

where

$$u'_{00} = \sqrt{\frac{2}{w^2\pi}}\ \exp\left[-\frac{(x+\varepsilon)^2+y^2}{w^2}\right]\exp\left\{-\frac{jk}{2R}[(x+\varepsilon)^2+y^2]\right\}e^{j\phi}.$$

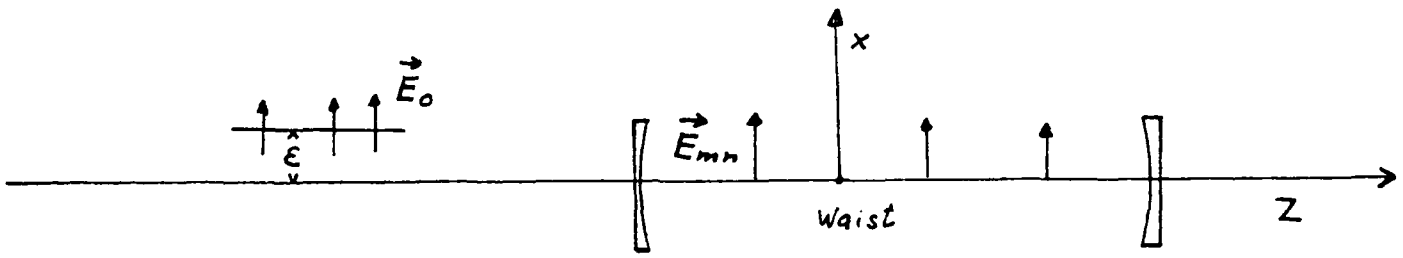

Fig 1.

It is easy to show that the functions $u_{mn}(m, n = 0, 1, 2, \ldots)$ form an orthogonal and complete set [15,16]. It is therefore possible to expand the injected beam in terms of this set, i.e.

$$E_0 = \sum_{m=0}^{\infty} \sum_{n=0}^{\infty} A_{mn} E_{mn} , \tag{6}$$

where

$$A_{mn} = \frac{\int_{-\infty}^{\infty} \int_{-\infty}^{\infty} E_{mn}^{*} E_0 \, dx \, dy}{\int_{-\infty}^{\infty} \int_{-\infty}^{\infty} E_{mn}^{*} E_{mn} \, dxdy} , \; E_{mn}^{*} \text{ is the conjugate complex of } E_{mn} .$$

To simplify the analysis, we expand the injected beam at the location of the waist of the proper resonator modes. It is assumed for this purpose that all H-G's of such a resonator have their waists at the same location at which the origin of our coordinate system is placed.

$$A_{mn} = \frac{\int_{-\infty}^{\infty} \int_{-\infty}^{\infty} (\sqrt{[2\eta P]} \; u_{mn}^{*} e^{jkz})(\sqrt{[2\eta P]} \; u'_{00} e^{-jkz}) dxdy}{\int_{-\infty}^{\infty} \int_{-\infty}^{\infty} (\sqrt{[2\eta P]} \; u_{mn}^{*} e^{jkz})(\sqrt{[2\eta P]} \; u_{mn} e^{-jkz}) dxdy} = \int_{-\infty}^{\infty} \int_{-\infty}^{\infty} u_{mn}^{*} u'_{00} dxdy$$

at $z = 0$ we have

$$A_{mn} = \int_{-\infty}^{\infty} \int_{-\infty}^{\infty} \{C_{mn} \psi_n(\frac{\sqrt{2}x}{w_0}) \psi_n(\frac{\sqrt{2}y}{w_0})\} \{\sqrt{\frac{2}{w_0^2 \pi}} \exp\left[-\frac{(x+\varepsilon)^2 + y^2}{w_0^2}\right]\} \, dxdy \tag{7}$$

where we use the fact that $R \to \infty$ and $\phi \to 0$ as $z \to 0$.

The double integral can be separated into two integrals over x and y, respectively. It may be written as

$$A_{mn} = C_{mn} \int_{-\infty}^{\infty} dx \{\psi_m(\frac{\sqrt{2}x}{w_0}) e^{-\frac{(x+\varepsilon)^2}{w_0^2}}\} \int_{-\infty}^{\infty} dy \{\psi_n(\frac{\sqrt{2}y}{w_0}) e^{-y^2/w_0^2} (\frac{2}{w_0^2 \pi})^{\frac{1}{2}}\} .$$

The second integral is unity for n = 0 and zero otherwise[17]. Thus,

$$A_{mn} = \begin{cases} C_{mo} \int_{-\infty}^{\infty} dx \{\psi_m(\frac{\sqrt{2}x}{w_0}) e^{-\frac{(x+\varepsilon)^2}{w_0^2}}\} & \text{for } n = 0 \\ 0 & \text{for } n \neq 0 . \end{cases} \quad (10)$$

The resulting expansion for an offset TEM_{00}-mode contains thus TEM_{m0}-modes only. The constants are

$$A_{m0} = e^{-\varepsilon^2/w_0^2} \left(\frac{2}{w_0 \pi 2^m m!}\right)^{\frac{1}{2}} \int_{-\infty}^{\infty} dx \{H_m(\frac{\sqrt{2}x}{w_0}) \exp[-2(x^2 + \varepsilon x)/w_0^2]\}. \quad (11)$$

This can be written as [18]

$$A_{mo} = \exp(-\varepsilon^2/2w_0^2)(-\varepsilon/w_0)^m/\sqrt{m!} \quad (14)$$

Now the injected electric field can be written as a single sum

$$\vec{E}_0 = \sum_{m=0}^{\infty} A_{m_0} \vec{E}_{m_0} \quad (15)$$

or

$$\vec{E}_0 = \sqrt{2\eta P} \sqrt{\frac{2}{\pi w^2}} e^{-\frac{\varepsilon^2}{2w_0^2}} e^{-\frac{x^2+y^2}{w_0^2}} \exp[-\frac{jk}{2R}(x^2+y^2)] \sum_{m=0}^{\infty} [(m!)^{-1}(-\frac{\varepsilon}{w_0})^m (2)^{-\frac{m}{2}}$$

$$\cdot H_m[(\frac{\sqrt{2}x}{w_0})]\hat{x} \quad (17)$$

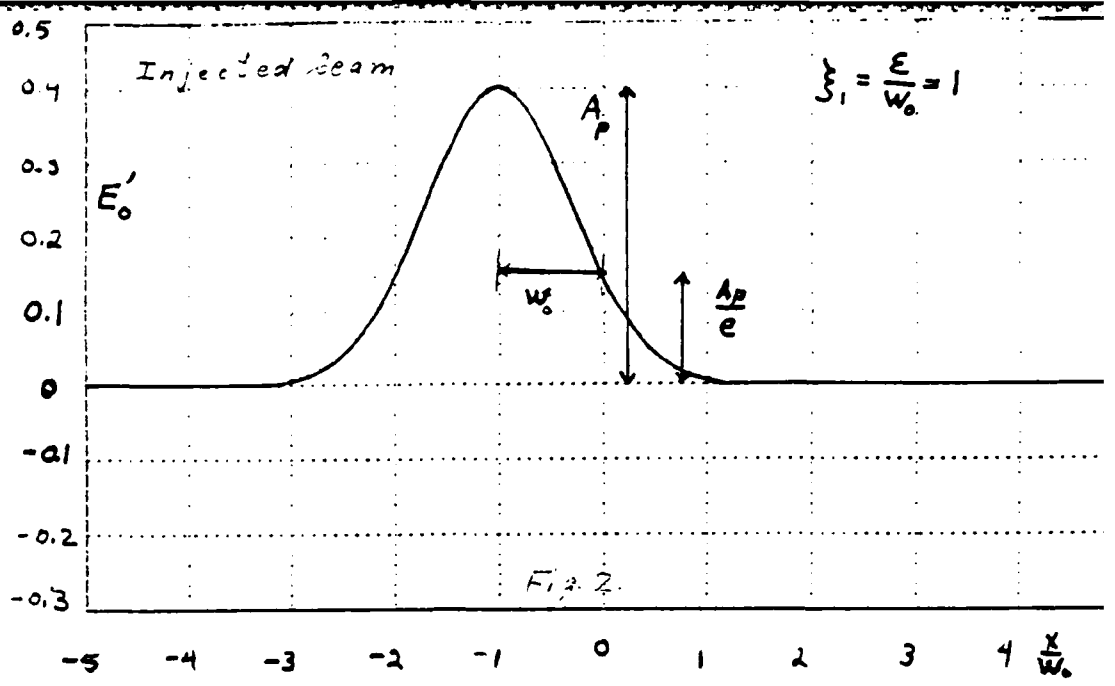

Fig. 2.

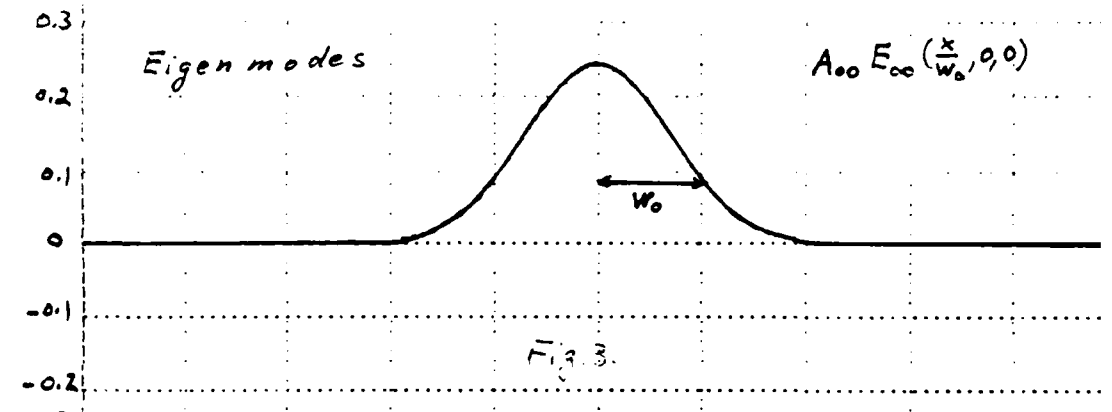

Fig. 3.

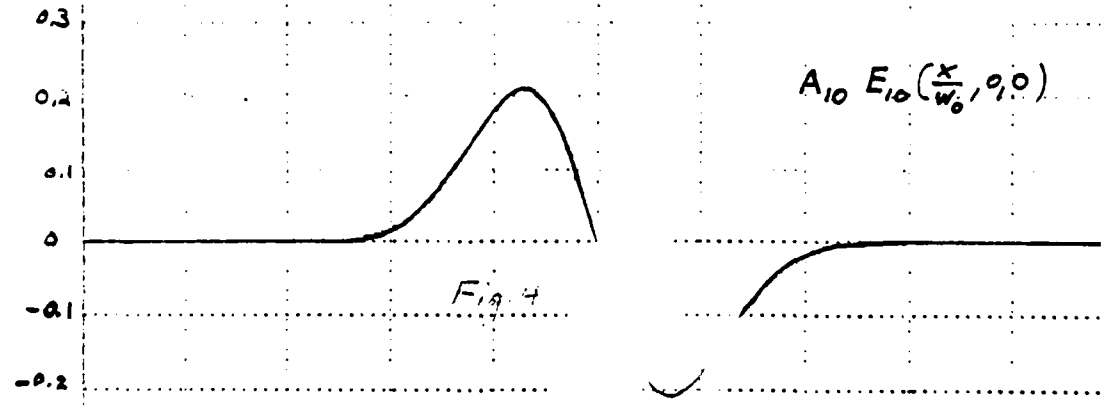

Fig. 4

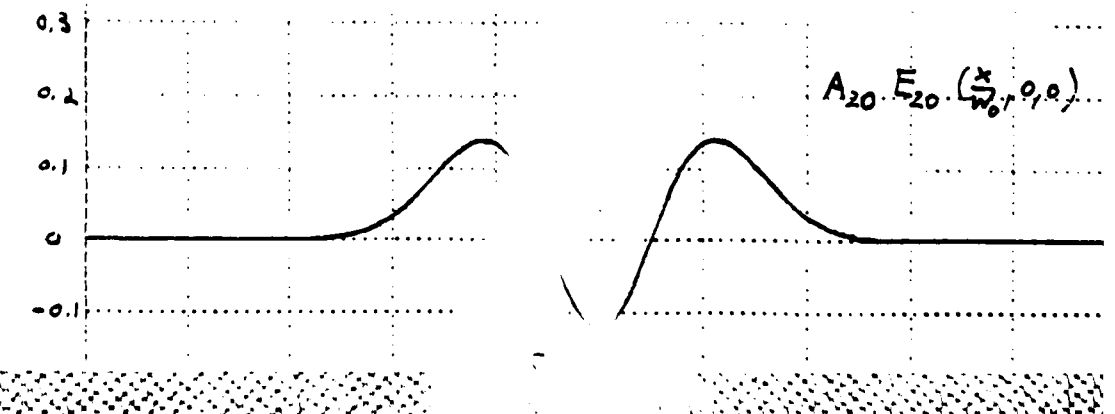

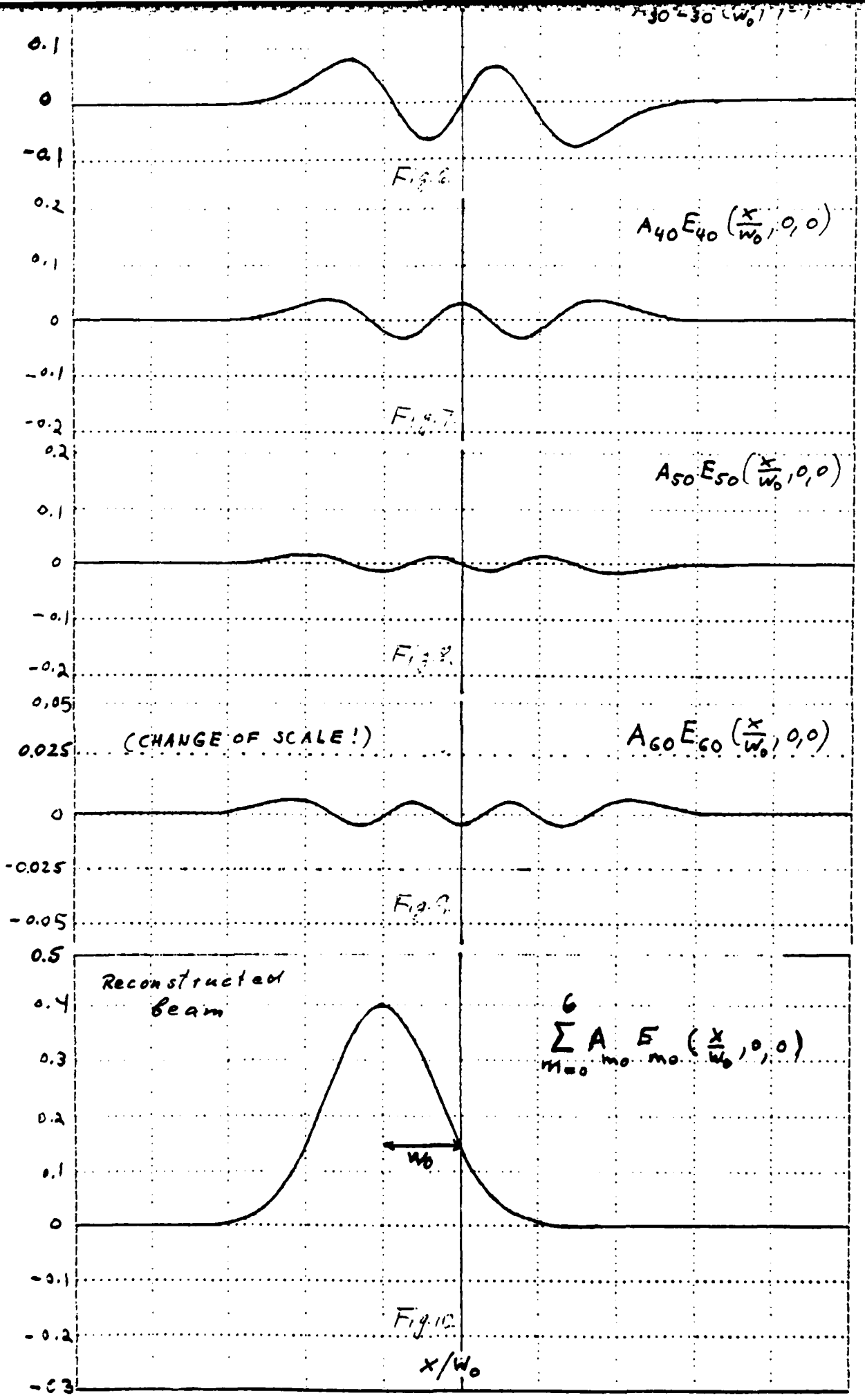
0.1
0
-0.1
$A_{30} E_{30} \left(\frac{x}{w_0}, 0, 0\right)$
Fig. 6
0.2
0.1
0
-0.1
-0.2
$A_{40} E_{40} \left(\frac{x}{w_0}, 0, 0\right)$
Fig. 7
0.2
0.1
0
-0.1
-0.2
$A_{50} E_{50} \left(\frac{x}{w_0}, 0, 0\right)$
Fig. 8
0.05
0.025
0
-0.025
-0.05
(CHANGE OF SCALE!)
$A_{60} E_{60} \left(\frac{x}{w_0}, 0, 0\right)$
Fig. 9
0.5
0.4
0.3
0.2
0.1
0
-0.1
-0.2
-0.3
Reconstructed beam
$\sum_{m=0}^{6} A_{m0} E_{m0} \left(\frac{x}{w_0}, 0, 0\right)$
w_0
Fig. 10
x/w_0

We plot equation (17) in the x plane, where in addition to z = 0, y is set to zero as well:

$$\vec{E}_0 = \sqrt{[2\eta P]}\ \sqrt{\frac{2}{w_0^2\,\pi}}\ e^{\frac{\varepsilon^2}{2w_0^2} - \frac{x^2}{w_0^2}} \sum_{m=0}^{\infty} \left[(m!)^{-1}\left(\frac{-\varepsilon}{\sqrt{2}\,w_0}\right)^m H_m\left(\frac{\sqrt{2}x}{w_0}\right)\right] \hat{x} \qquad (18)$$

An example of this expansion is given in Figure 2 through Figure 10. The dimensionless amplitude of the injected beam $E_0' = E_0(w_0^2/8\eta P)^{1/2}$ vs. (x/w_0), at y=0=z is given in Figure 2. The beam is offset by an amount ε which is set equal to its waist size w_0. The result of summation for the first seven terms is given in Figure 10. Figures 3 to 9 give an impression of the rate of convergence for this choice $\varepsilon = w_0$. This is an enormous misalignment. Introducing the offset parameter $\xi_1 = \frac{\varepsilon}{w_0}$, we may now evaluate the magnitude of the H-G's created by an offset TEM_{00}-mode as

$$A(\xi_1, m) = \frac{1}{\sqrt{[m!]}}(-\xi_1)^m\, e^{-\xi_1^2/2} \qquad (19)$$

II. F. 2. 2) Tilted Source Beam

The external beam crosses the resonator at its waist location under an angle α. This is shown in Figure 11.

Again, it is assumed that the injected beam is identical to the TEM_{00}-mode of the resonator except that it is rotated at the waist by an angle α. The electric field can be written as

$$\vec{E}_0 = \sqrt{[2\eta P]}\ \{u'_{00}\, e^{-jk(z\cos\alpha + x\sin\alpha)}\}(-\hat{z}\sin\alpha + \hat{x}\cos\alpha) \qquad (20)$$

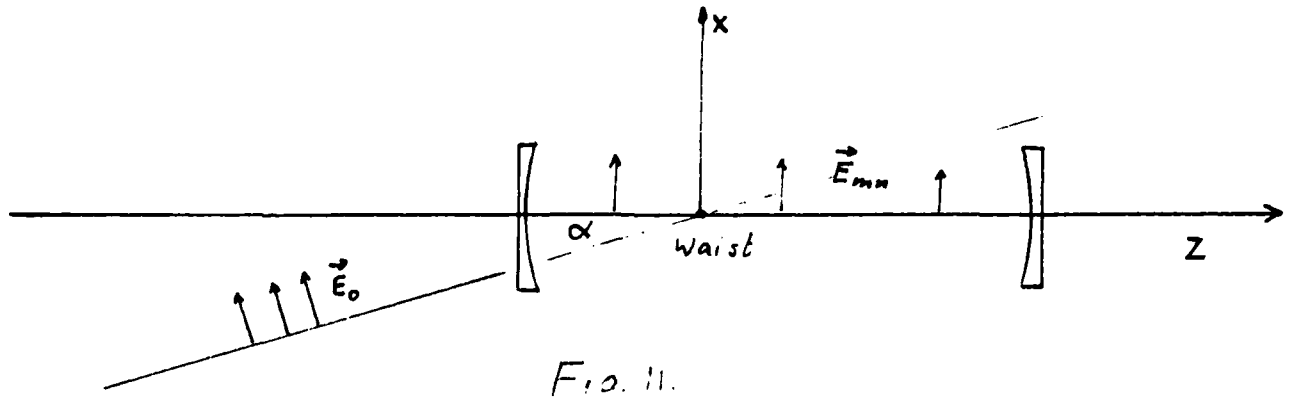

Fig. 11.

where

$$u'_{00} = \left\{\frac{2}{w_0^2\,\pi[1+(z\cos\alpha+x\sin\alpha)^2/z_0^2]}\right\}^{\frac{1}{2}} \exp\left[-\frac{(-z\sin\alpha+x\cos\alpha)^2+y^2}{w_0^2}\right]$$

$$\exp\left\{-\frac{jk}{2R}\left[(-z\sin\alpha + x\cos\alpha)^2 + y^2\right]\right\} e^{j\phi}.$$

The vector $\vec{E}_0$ can be written as follows.

$$\vec{E}_0 = E_{xo}\,\hat{x} + E_{zo}\,\hat{z} \tag{21}$$

where E_{xo} and E_{zo} are the x and z components of the vector $\vec{E}_0$ respectively. Since the resonator's eigenmodes have electric fields in the x-direction only, see Eq. (4), the injected electric field's x component only is able to excite the resonator modes. The y component would go through the resonator freely as there is no conceivable coupling of an orthogonal vector component in vacuum. We therefore expand the x component (i.e. E_{x0}) of the field $\vec{E}_0$ only:

$$E_{xo} = \sum_{m=o}^{\infty}\sum_{n=o}^{\infty} A_{mn}\,E_{mn} \tag{22}$$

where

$$A_{mn} = \frac{\int_{-\infty}^{\infty}\int_{-\infty}^{\infty} E_{mn}^{*}\,E_{xo}\,dxdy}{\int_{-\infty}^{\infty}\int_{-\infty}^{\infty} E_{mn}^{*}\,E_{mn}\,dxdy}\quad .$$

Now we calculate A_{mn} at z = 0 as before.

$$A_{mn} = \int_{-\infty}^{\infty}\int_{-\infty}^{\infty} dxdy\{C_{mn}\psi_m(\frac{\sqrt{2}x}{w_0})\ \psi_n(\frac{\sqrt{2}y}{w_0})\ \}\{(\frac{2}{w_0\pi[1+(\frac{x\sin\alpha}{z_0})^2]})^{\frac{1}{2}}$$

$$\cdot e^{-\frac{x^2\cos^2\alpha+y^2}{w_0^2}}\ \cos\alpha\ e^{(-jkx\sin\alpha)}\ . \qquad (23)$$

As before, it is possible to separate the double integral

$$A_{mn} = C_{mn}\cos\alpha\ .\ \int_{-\infty}^{\infty} dx\{\psi_m(\frac{\sqrt{2}x}{w_0})\ \frac{e^{-(\frac{x^2\cos^2\alpha}{w_0^2}+jkx\sin\alpha)}}{\sqrt{[1+(\frac{x\sin\alpha}{z_0})^2]}}\}$$

$$\cdot\int_{-\infty}^{\infty} dy\{\psi_n(\frac{\sqrt{2}y}{w_0})e^{-y^2/w_0^2}\ (\frac{2}{\pi w_0^2})^{\frac{1}{2}}\} \qquad (24)$$

The second integral is zero if $n \neq 0$ or it is unity otherwise. A_{mn} may be written as

$$A_{mn} = \begin{cases} C_{mo}\cos\alpha \int_{-\infty}^{\infty} dx\{\psi_m(\frac{\sqrt{2}x}{w_0})\ [1+(\frac{x\sin\alpha}{z_0})^2]^{-1/2}\exp(\frac{x^2\cos^2\alpha}{w_0^2} - jkx\sin\alpha)\} & n = 0 \\ 0 & n \neq 0 \end{cases}$$

$$A_{m0} = C_{m0}\cos\alpha\ (\frac{w_0}{\sqrt{2}})\ \int_{-\infty}^{\infty} d\xi\{H_m(\xi)\exp[-\frac{1}{2}(1+\cos^2\alpha)\xi^2 - (\frac{jkw_0}{\sqrt{2}}\sin\alpha)\xi]$$

$$(1+\frac{w_0^2\xi^2\sin^2\alpha}{2z_0^2})^{-1/2}\ \} \qquad (27)$$

A_{mo} may be approximated by

$$A_{mo} \simeq C_{mo} \cos\alpha \left(\frac{w_0}{\sqrt{2}}\right) \int_{-\infty}^{\infty} d\xi \{H_m(\xi)$$

$$\exp[-(1 + \cos^2\alpha)\xi^2/2 - jkw_0 \sin\alpha\, \xi/\sqrt{2}]\}. \qquad (28)$$

Let us calculate the integral and call it I.

$$I = \int_{-\infty}^{\infty} d\xi \{H_m(\xi) e^{-[\bar{a}^{-2}\xi^2 + j\bar{b}\xi]}\} \qquad (29)$$

where $\bar{a}^{-2} = \frac{1+\cos^2\alpha}{2}$, $\bar{b} = \frac{kw_0 \sin\alpha}{\sqrt{2}}$

By using Euler's formula, "I" can be written as

$$I = \int_{-\infty}^{\infty} d\xi [H_m(\xi) e^{-\bar{a}^{-2}\xi^2} \cos(\bar{b}\xi)] - j \int_{-\infty}^{\infty} d\xi [H_m(\xi) e^{-\bar{a}^{-2}\xi^2} \sin(\bar{b}\xi)] \qquad (30)$$

From Ref. [18], we have

$$I = \frac{\sqrt{\pi}}{\bar{a}} e^{-\frac{\bar{b}^2}{4\bar{a}^{-2}}} H_m\left[\frac{\bar{b}}{2\bar{a}^{-2}\left(\frac{1}{\bar{a}^{-2}} - 1\right)^{1/2}}\right] \left(1 - \frac{1}{\bar{a}^{-2}}\right)^{\frac{m}{2}} \qquad (31)$$

Now, we can substitute for a and b.

$$I = \sqrt{\left(\frac{2\pi}{1+\cos^2\alpha}\right)} \exp\left[-\frac{k^2 w_0^2 \sin^2\alpha}{4(1+\cos^2\alpha)}\right] \cdot H_m\left[\frac{kw_0}{\sqrt{2(1+\cos^2\alpha)}}\right] \left[-\frac{\sin^2\alpha}{1+\cos^2\alpha}\right]^{\frac{m}{2}} .$$

The real part of A_{m0} (i.e. $Re[A_{m0}]$) and the imaginary part of A_{m0} (i.e. $Im[A_{m0}]$) are written as

$$\mathrm{Re}[A_{m0}] = P_m \qquad \text{for even } m \tag{33}$$

and

$$I_m[A_{m0}] = -\,j\,P_m \qquad \text{for odd } m \tag{34}$$

where

$$P_m = j^m w_0\, C_{m0} \cos\alpha \sqrt{\frac{\pi}{1+\cos^2\alpha}} \exp\left[-\frac{k^2 w_0^2 \sin^2\alpha}{4(1+\cos^2\alpha)}\right] \cdot$$

$$\cdot H_m\left[\frac{kw_0\sqrt{1+\cos^2\alpha}}{\sqrt{2}(1+\cos^2\alpha)}\right]\left[\frac{\sin\alpha}{\sqrt{1+\cos^2\alpha}}\right]^m$$

where $C_{mo} = \sqrt{\dfrac{2}{w_0^2\,\pi 2^m m!}}$

Now we substitute for C_{m0} in I_m.

$$P_m = j^m \cos\alpha \sqrt{\frac{2}{(1+\cos^2\alpha)2^m m!}} \exp\left[-\frac{k^2 w_0^2 \sin^2\alpha}{4(1+\cos^2\alpha)}\right] \cdot$$

$$\cdot H_m\left[\frac{kw_0}{\sqrt{2}(1+\cos^2\alpha)}\right]\left[\frac{\sin\alpha}{\sqrt{1+\cos^2\alpha}}\right]^m \tag{35}$$

In order to plot these equations and make a numerical example, we would like to inspect the function vs x only at y = z = 0 (waist). The injected beam can be written as

$$\vec{E}_0 = \hat{x}\left(\sum_{m=0}^{\infty} P_m u_m\right) + \hat{z}\, E_{zo} \qquad \text{at } z=o \tag{36}$$

at z = 0

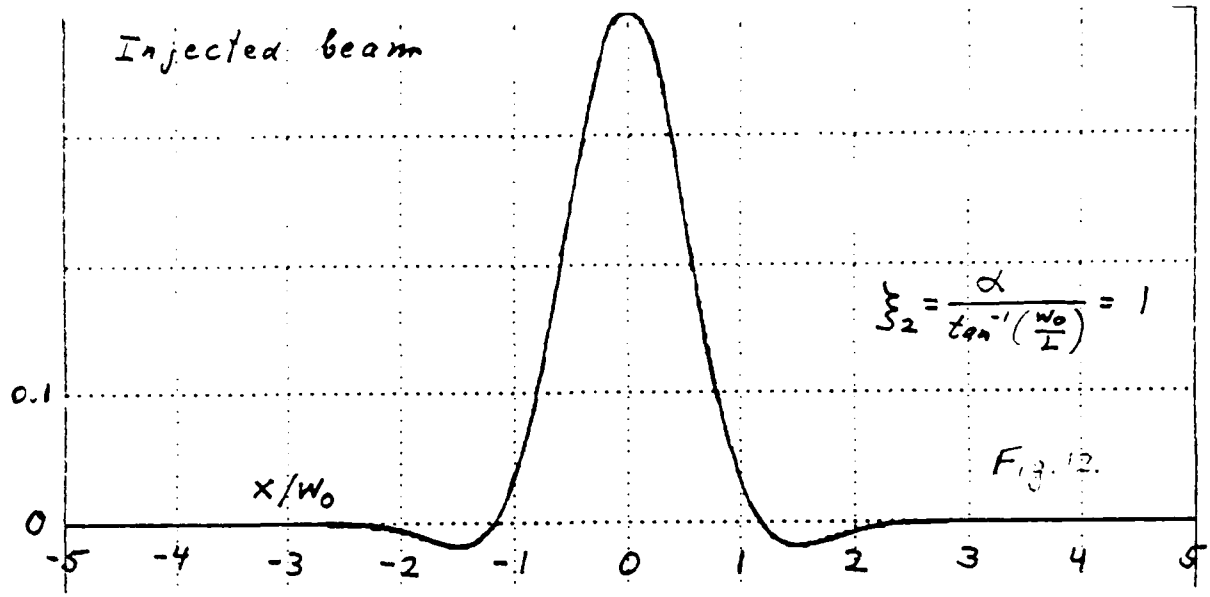

Fig. 12.

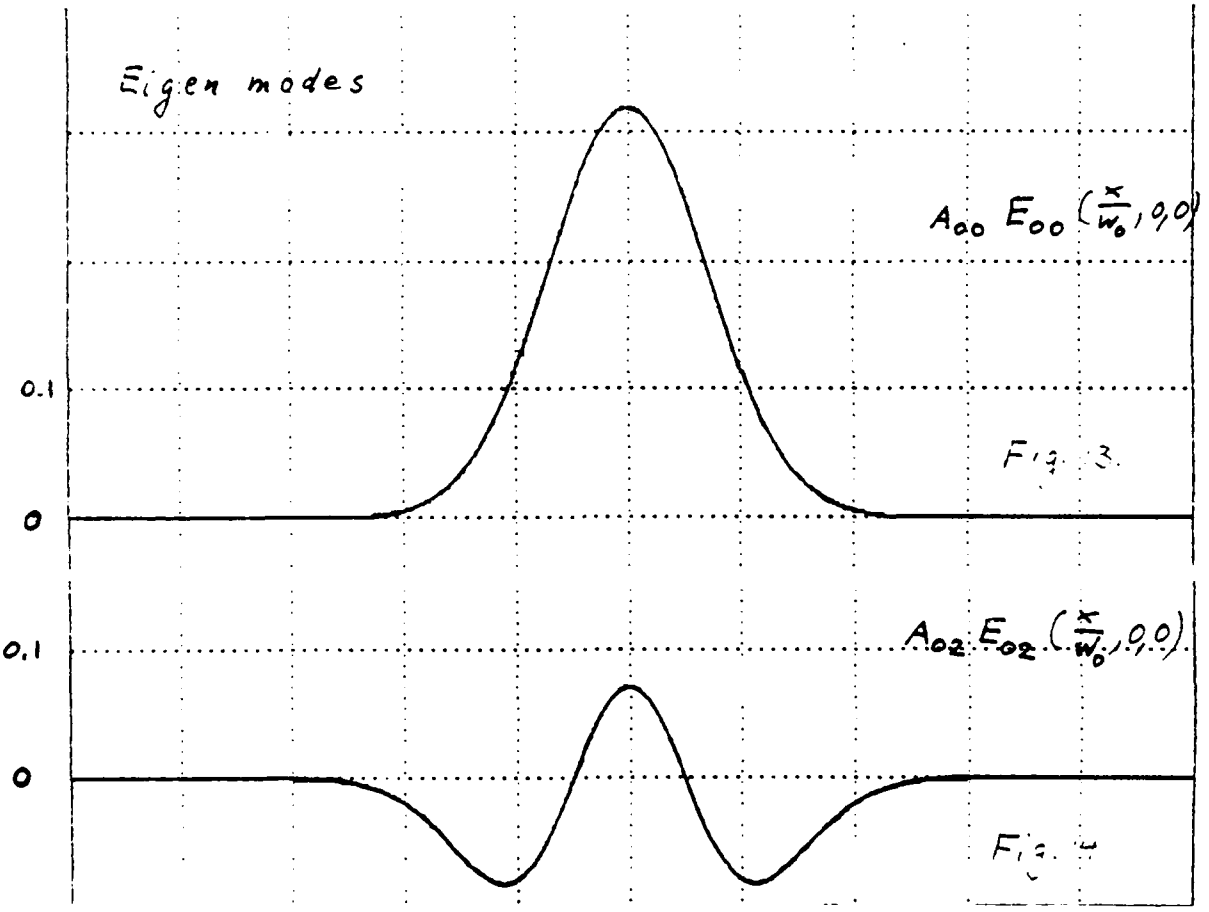

Fig. 13.

Fig. 14

AD-A158 293 MODELING A LARGE RING RESONATOR GYROSCOPE(U) OKLAHOMA 2/2
STATE UNIV STILLWATER SCHOOL OF ELECTRICAL AND COMPUTER
ENGINEERING H R BILGER 30 MAR 85 AFOSR-TR-85-0526
UNCLASSIFIED AFOSR-84-0058 F/G 3/1 NL

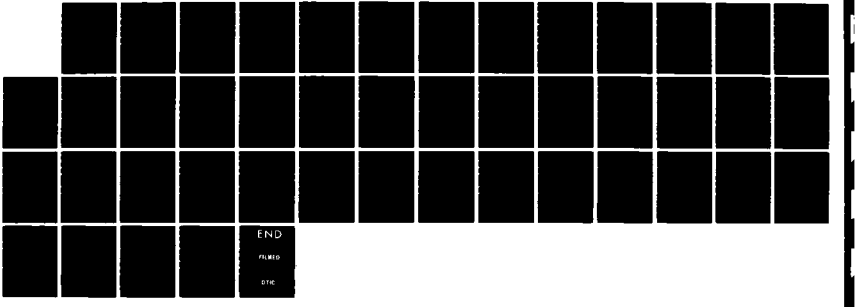

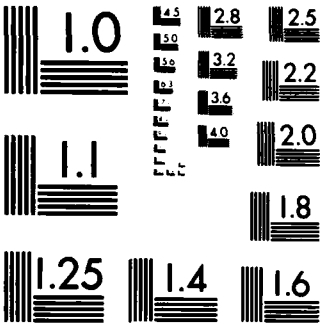

MICROCOPY RESOLUTION TEST CHART
NATIONAL BUREAU OF STANDARDS-1963-A

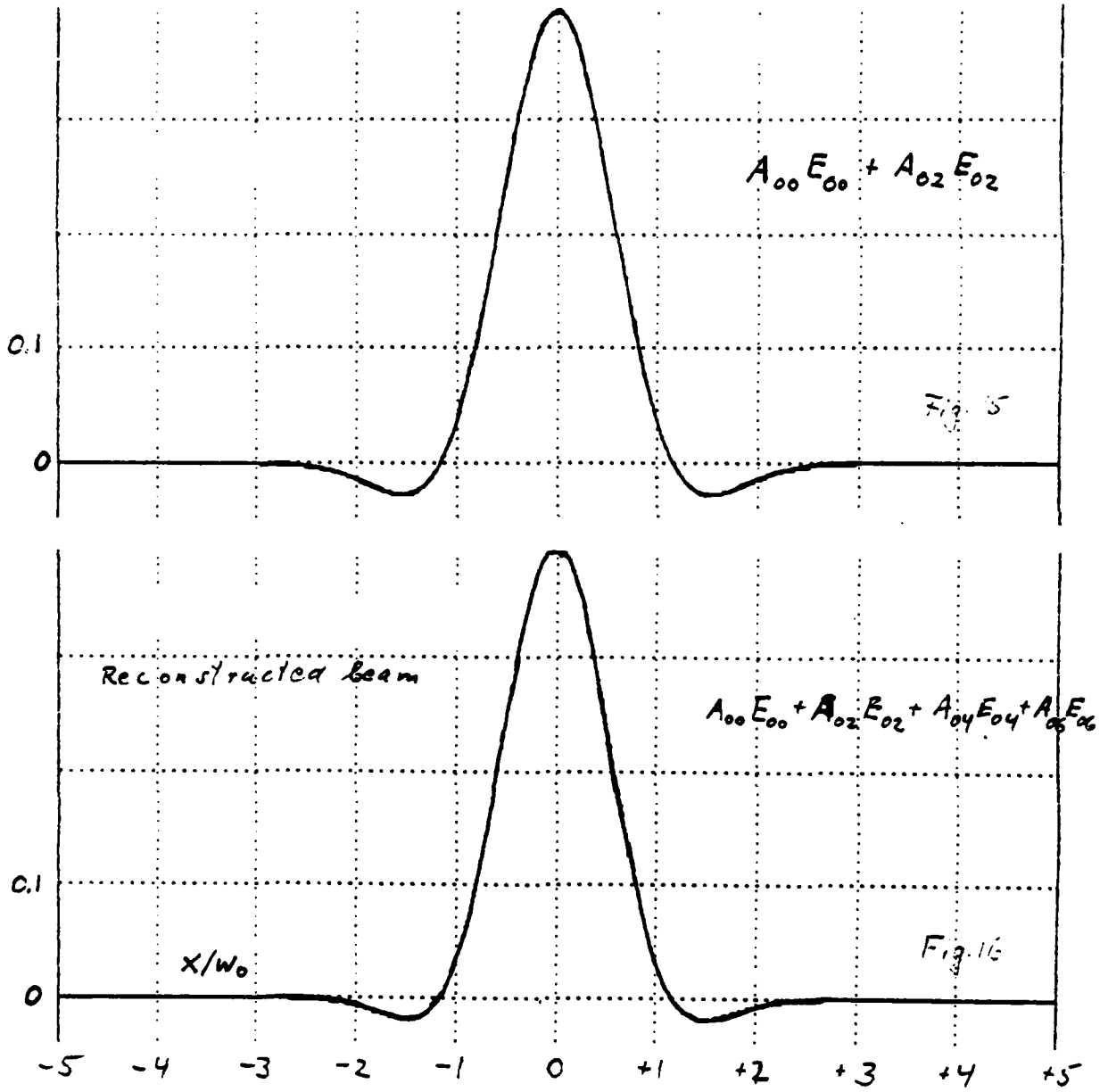
$A_{00}E_{00} + A_{02}E_{02}$
0.1
0
Fig. 15
Reconstructed beam
$A_{00}E_{00} + A_{02}E_{02} + A_{04}E_{04} + A_{06}E_{06}$
0.1
0
Fig. 16
x/w_0
-5
-4
-3
-2
-1
0
+1
+2
+3
+4
+5

Figure 12 shows the real part of the injected field, i.e.

$$\tilde{u}_{00} = u'_{00}(x, 0, 0) \cos(kx\sin\alpha) \cos\alpha \, . \tag{37}$$

A tilt given by

$$\xi_2 = \alpha/\tan^{-1}(w_0/L) = 1$$

is chosen (ξ_2 is the tilt angle measured in terms of the beam spread.) For a waist size of w_0 = 0.002m = 2mm, and a wave number k = $(2\pi/633 \times 10^{-9})m^{-1} = 9.93\times10^6$, this corresponds to a tilt angle of $\alpha=1.0\times10^{-4}$ rad = 21 arc second. Fig.'s 13 and 14 show two components.

In figure 15, the sum of the first two terms is shown. Comparing it to fig. 12, the quick convergence is evident. Figure 16, with four terms, is indistinguishable from fig. 12.

II. F. 2. 3) Mismatched Source Beam

The injected TEM_{00}-beam shall have a waist W. The resonator's eigenmodes shall be Hermite-Gaussian modes with waist size w_0. At z = 0, we expand the injected beam in terms of these Hermite-Gaussians, (see Figure 17).

The injected electric field is

$$\vec{E}_0 = \sqrt{2\eta P \cdot \frac{2}{\pi W^2}}\, e^{-\frac{x^2+y^2}{W^2}}\, e^{\frac{-jk}{2R}[x^2+y^2]}\, e^{j\phi}\, e^{-jkz}\, \hat{x} \, . \tag{39}$$

As before, we expand E_0 in the plane z = 0.

$$E_0 = \sqrt{2\eta P \cdot 2/\pi W_0^2}\, \exp[-(x^2 + y^2)/W_0^2]. \tag{40}$$

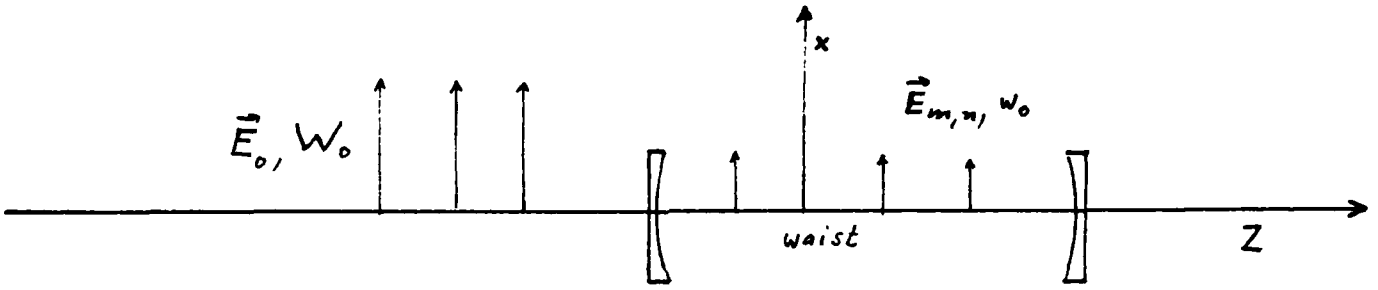

Fig. 17

$$= \sum_{m=0}^{\infty} \sum_{n=0}^{\infty} A_{mn} E_{mn} \tag{41}$$

where

$$A_{mn} = \frac{\int_{-\infty}^{\infty} \int_{-\infty}^{\infty} E_{mn}^{*} E_0 \, dxdy}{\int_{-\infty}^{\infty} \int_{-\infty}^{\infty} E_{mn}^{*} E_{mn} \, dxdy} .$$

After substituting for E_{mn} and E_0, we have

$$A_{mn} = \sqrt{\frac{2}{W_0^2 \pi}} C_{mn} \int_{-\infty}^{\infty} \{ e^{\frac{-x^2}{W_0^2}} H_m(\frac{\sqrt{2}x}{w_0}) e^{\frac{-x^2}{w_0^2}} dx \} \int_{-\infty}^{\infty} \psi_n(\frac{\sqrt{2}y}{w_0}) e^{\frac{-y^2}{W_0^2}} dy \tag{42}$$

Let $\xi = \frac{\sqrt{2}x}{w_0}$ and $\eta = \frac{\sqrt{2}y}{w_0}$, then

$$A_{mn} = \sqrt{\frac{2}{W_0^2 \pi}} C_{mn} \frac{w_0^2}{2} \{ \int_{-\infty}^{\infty} H_m(\xi) e^{-\frac{\xi^2}{2}[\frac{W_0^2 + w_0^2}{W_0^2}]} d\xi \}$$

$$\{ \int_{-\infty}^{\infty} H_n(\eta) e^{-\frac{\eta^2}{2}[\frac{W_0^2 + w_0^2}{W_0^2}]} d\eta \} \tag{43}$$

In order to make some simplifications, let $\beta^2 = \frac{W_0^2 + w_0^2}{2W_0^2}$, $t = \beta\xi$, and $t' = \beta\eta$, then

$$A_{mn} = \sqrt{\frac{2}{W_0^2 \pi}} C_{mn} \frac{w_0^2}{2} [\int_{-\infty}^{\infty} H_m(\frac{t}{\beta}) e^{-t^2} dt][\int_{-\infty}^{\infty} H_n(\frac{t'}{\beta}) e^{-t'^2} dt] \frac{1}{\beta^2} \tag{44}$$

From Ref. 18, we have

$$A_{mn} = \begin{cases} 0 & \text{for m, n odd} \\ 1 & \text{for } n = m = 0 \text{ and } w_0 = W_0 \\ \dfrac{2w_0W_0}{W_0^2 + w_0^2} \dfrac{\sqrt{n!m!}}{(\frac{n}{2})!(\frac{m}{2})!2^{m+n/2}} \left(\dfrac{W_0^2 - w_0^2}{W_0^2 + w_0^2}\right)^{\frac{m+n}{2}} & \text{otherwise.} \end{cases} \quad (45)$$

Finally the injected electric field can be written as the following summation.

$$\vec{E}_0 = \sqrt{2\eta P} \frac{\sqrt{8/\pi}\, W_0}{W_0^2 + W_0^2} e^{-\frac{x^2+y^2}{w_0^2}} \sum_{m=0,2,..}^{\infty} \sum_{n=0,2,..}^{\infty} \left\{ \frac{H_m(\frac{\sqrt{2}x}{w_0}) H_n(\frac{\sqrt{2}y}{w_0})}{\frac{n}{2}!\,\frac{m}{2}!\,2^{m+n}} \left(\frac{W_0^2 - w_0^2}{W_0^2 + w_0^2}\right)^{\frac{m+n}{2}} \right\} \hat{x} \quad (46)$$

A numerical example is given in Figures 18-24. In mismatching problems as given above, we may define a mismatch parameter

$$\xi_3 = \sqrt{\frac{W_0^2 - w_0^2}{W_0^2 + w_0^2}}.$$

In Figure 18, the injected beam amplitude is shown, in arb. units. It has a mismatch $\xi_3 = 0.77$ ($W_0 = 2w_0$).

Figures 19 to 22 show U_{00}, U_{02}, U_{20} and U_{22} respectively.

In figure 23, the summation of the first 2x2 terms is shown:

$U_{00} A_{00} + U_{02} A_{20} + U_{20} A_{20} + U_{22} A_{22}$

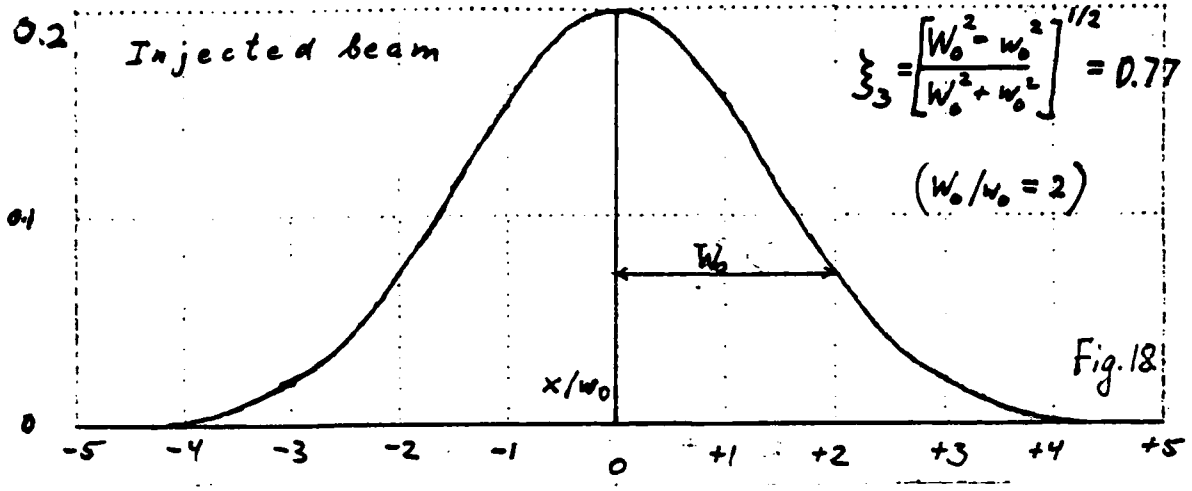

Fig. 18

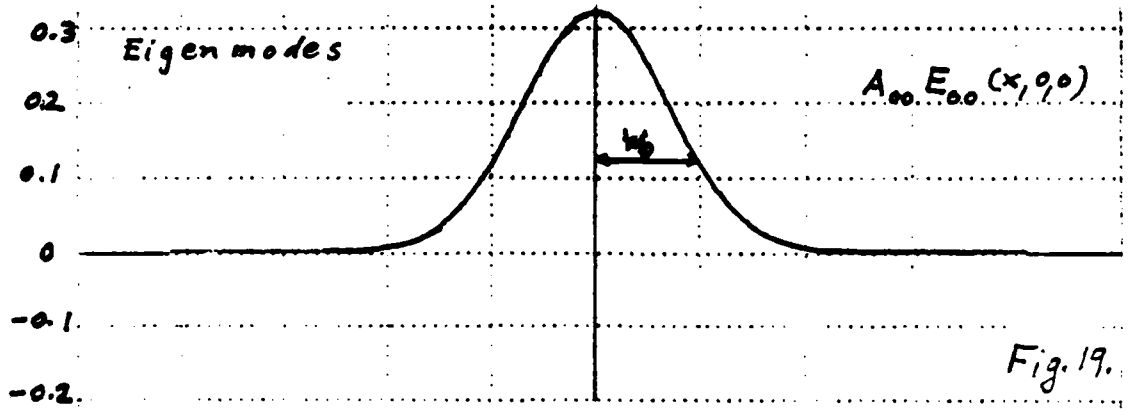

Fig. 19.

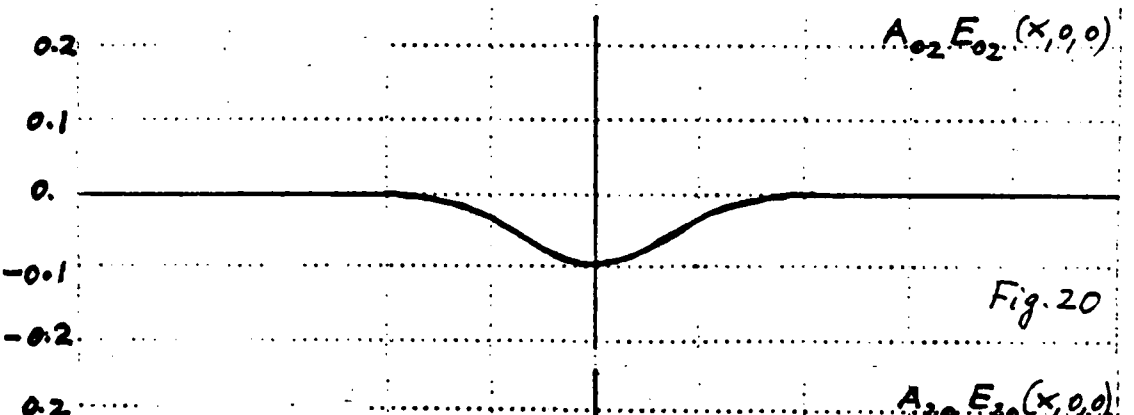

Fig. 20

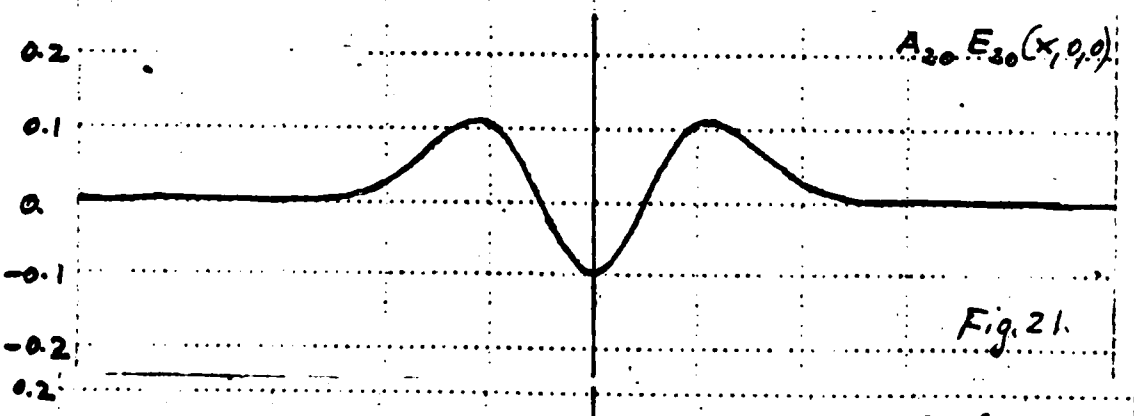

Fig. 21.

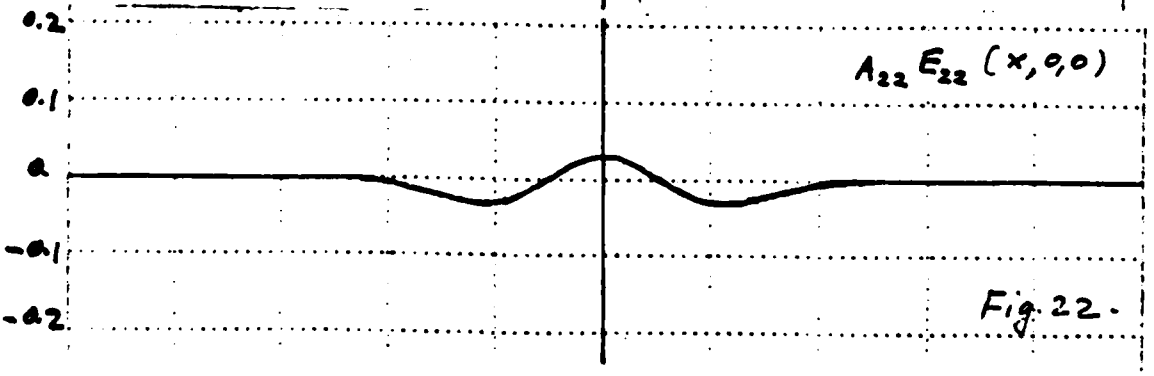

Fig. 22.

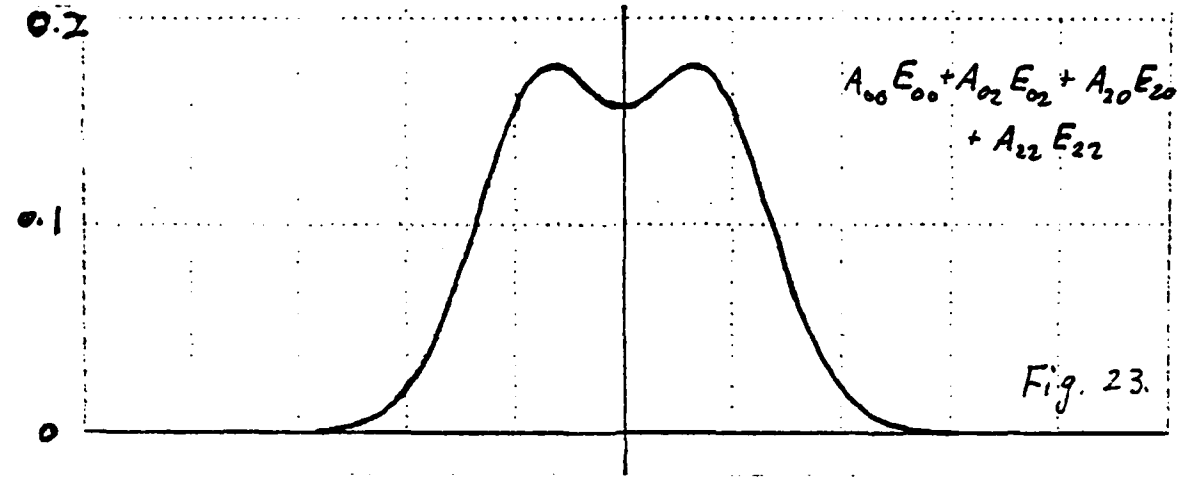
0.2
0.1
0
$A_{00}E_{00}+A_{02}E_{02}+A_{20}E_{20}$
$+A_{22}E_{22}$

Fig. 23.

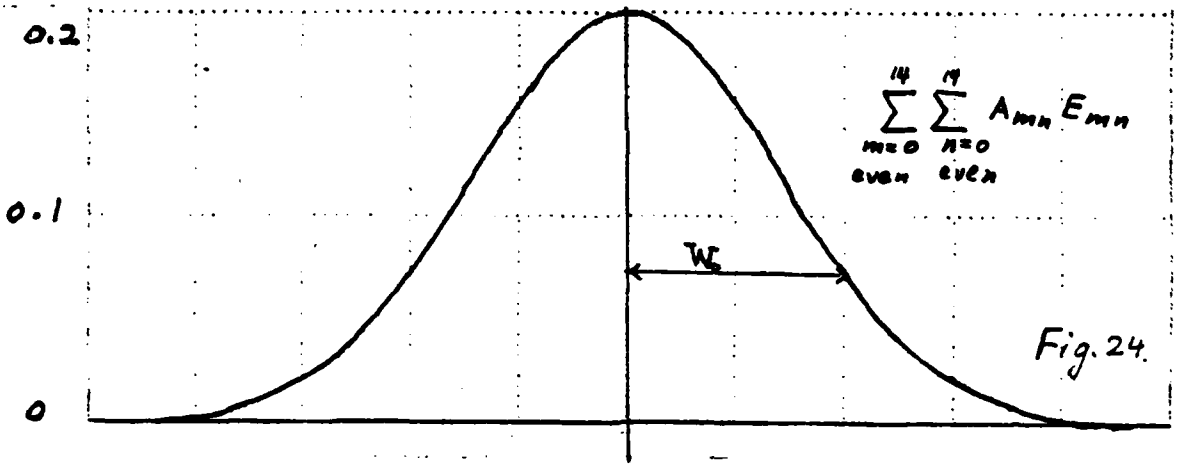
0.2
0.1
0
$\sum_{\substack{m=0 \\ \text{even}}}^{14}\sum_{\substack{n=0 \\ \text{even}}}^{14} A_{mn}E_{mn}$
W

Fig. 24.

Figure 23 shows a kurtosis. In Figure 24, the summation of the first 8 x 8 terms is shown.

$$\sum_{m=0,2,..}^{14} \sum_{n=0,2,..}^{14} A_{mn}\, u_{mn}$$

The peak of this partial sum is within 99% of the peak of the original curve.

II. F. 3. Application of the results of section II. F. to ringlasers

The misadjustment of an external stigmatic gaussian beam to a ring gives rise to Hermite-Gaussian eigenmodes in addition to excitation of the ring in the proper Gaussian mode. An added complication is the presence of astigmatism of the ring modes. The latter can be expressed by the presence of an elliptic ring waist with the two waist sizes w_{ox} and w_{oy}.

A misalignment, in two dimensions, is then expressed by the offsets ε_x and ε_y, and the tilt angles α_x and α_y, see figure 25. A slight generalization of the previous section gives then the misalignment parameters

$$\xi_x = \varepsilon_x/w_{ox} + (q_{ox}/w_{ox})\alpha_x$$

$$\xi_y = \varepsilon_y/w_{oy} + (q_{oy}/w_{oy})\alpha_y \ ,$$

where q_{ox}, q_{oy} are the <u>complex</u> curvatures of the ring modes at the waists. This simple set of equations is proper, since the propagation characteristics of the beam in the two orthogonal planes are not coupled.

MISALIGNED

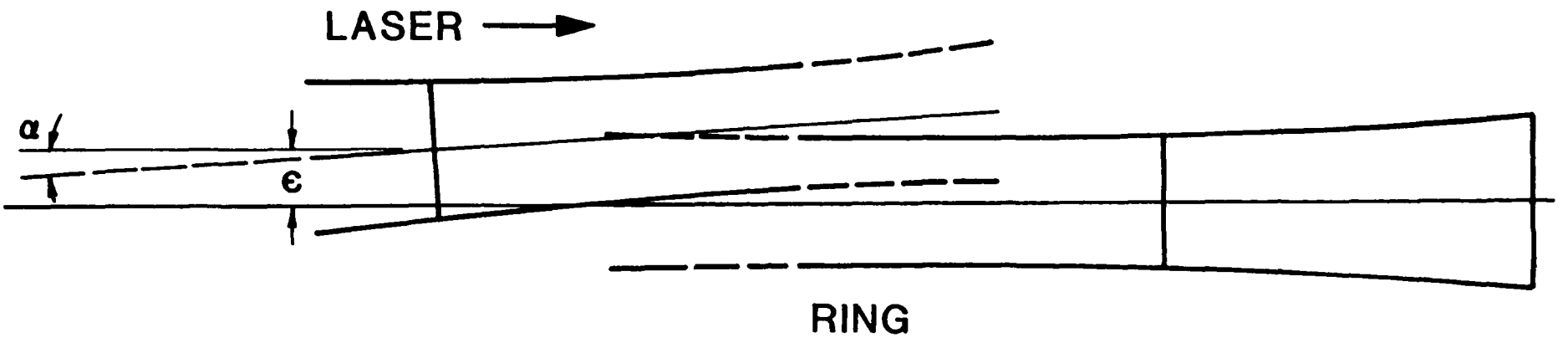

MISALIGNMENT PARAMETERS

$$\xi_x = \frac{\epsilon_x}{w_{ox}} + \frac{q_o}{w_{ox}} \alpha_x$$

$$\xi_y = \frac{\epsilon_y}{w_{oy}} + \frac{q_o}{w_{oy}} \alpha_y$$

Fig. 25

Furthermore, a mismatch, see figure 26, is given by the mismatch parameters

$$O_x = \left(\frac{W_0^2 - w_{ox}^2}{W_0^2 + w_{ox}^2}\right)^{1/2}, \qquad O_y = \left(\frac{W_0^2 - w_{oy}^2}{W_0^2 + w_{oy}^2}\right)^{1/2}$$

Note that for perfect adjustment, all parameters are zero.

The power ratio of a H.-G., P_{mn}/P_{00} to the power of the Gaussian in the ring can then be expressed as

$$P_{mn}/P_{00} = F_m(\xi_x, O_x) \cdot F_n(\xi_y, O_y),$$

where

$$F_m(\xi_x, O_x) = (2^m m!)^{-1} |O_x|^{2m} \left|H_m[j(1-O_x^2)\xi_x / \sqrt{2}O_x]\right|^2,$$

$$F_n(\xi_y, O_y) = (2^n n!)^{-1} |O_y|^{2n} \left|H_n[j(1-O_y^2)\xi_y / \sqrt{2}O_y]\right|^2,$$

judiciously exploiting the previous sections. These equations are useful to estimate the amount of pulling due to offset, misalignment, and mismatch.

The power transfer from a misadjusted Gaussian to the ring's Gaussian is, of course, of interest as well: For pure mismatch, with coinciding waists, it is simply

$$P_{00}/P_L = 1 - O^4 \qquad (O \to O_x \text{ or } O_y,\ P_L = \text{Power of injecting laser}).$$

For pure offset,

$$P_{00}/P_L = \exp(-\varepsilon^2/w_0^2) = \exp[-(Re\xi)^2]$$

The figure 27 shows a plot of the latter two equations. They show that alignment is to be treated more carefully than matching.

MISMATCH

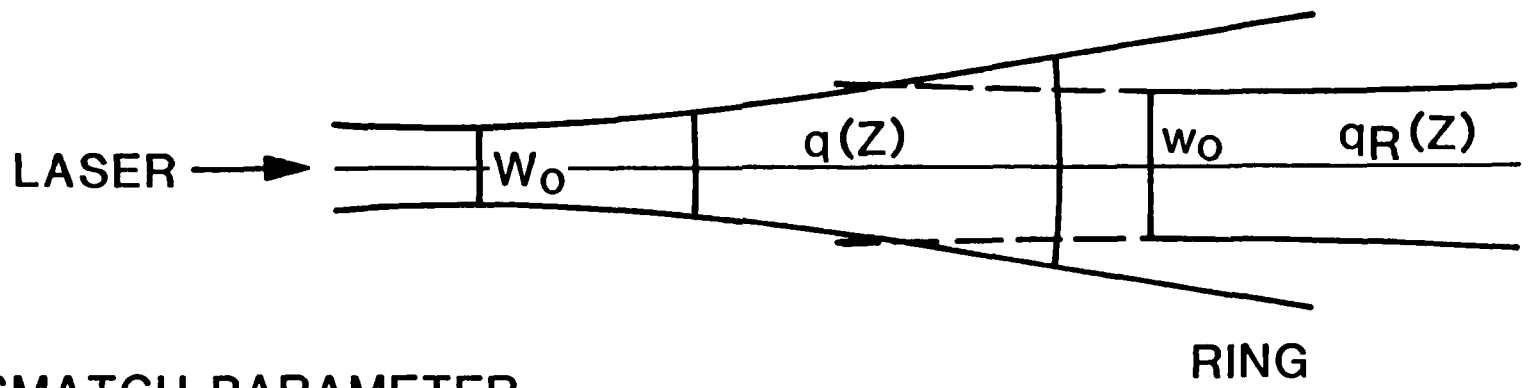

MISMATCH PARAMETER

$$O_x = \sqrt{\frac{q - q_{Rx}}{q + q_{Rx}}} \rightarrow \sqrt{\frac{W_o^2 - w_{ox}^2}{W_o^2 + w_{ox}^2}}$$

$$O_y = \sqrt{\frac{q - q_{Ry}}{q + q_{Ry}}} \rightarrow \sqrt{\frac{W_o^2 - w_{oy}^2}{W_o^2 + w_{oy}^2}}$$

Fig. 26

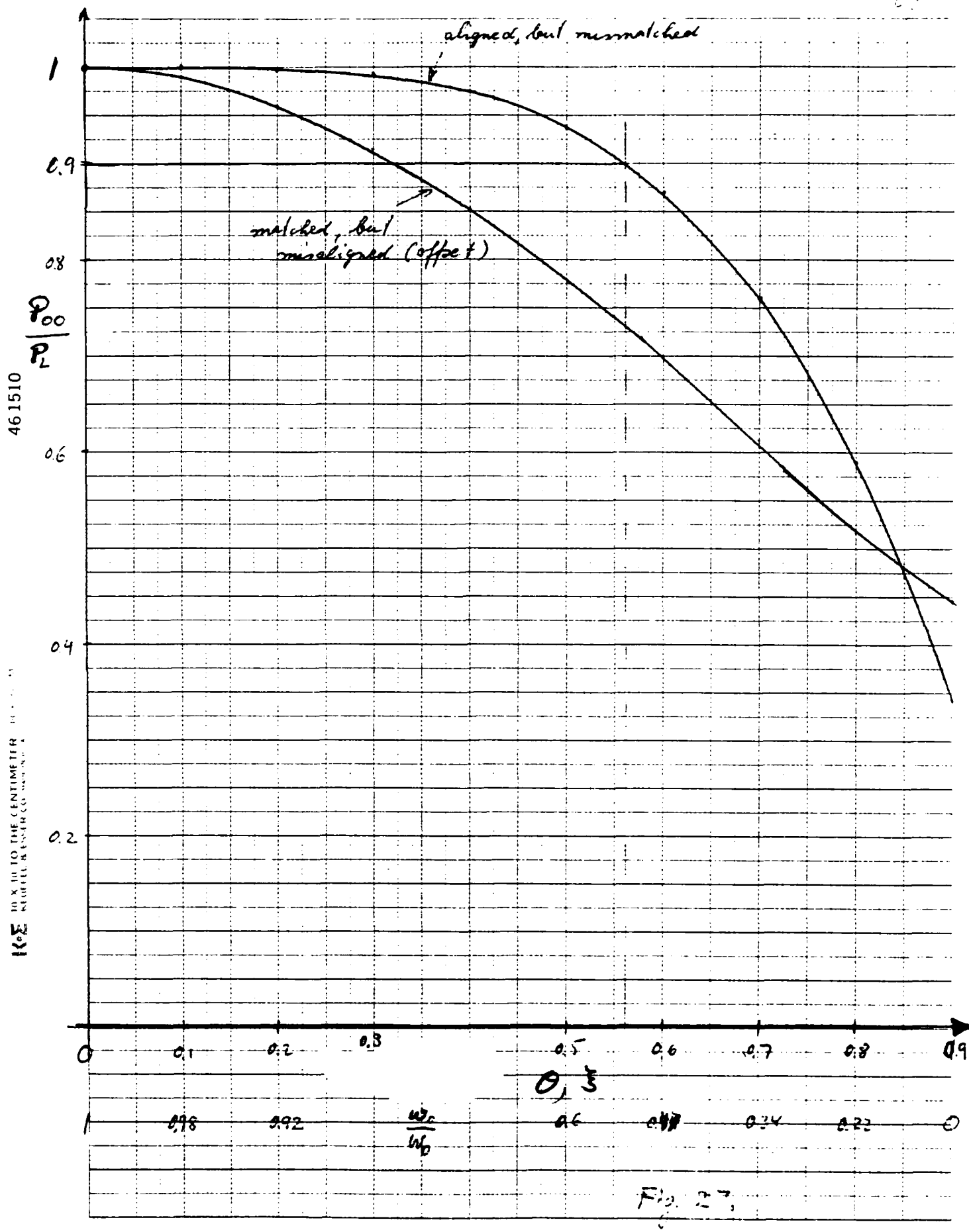

Fig. 27.

46 1510
10 X 10 TO THE CENTIMETER

II. F. 4 Experimental test of misalignment and mismatch.

The previous notions were put to the test by applying them to experimental results obtained by the Seiler group (ref. 12).

In a ring injected by a presumably stigmatic Gaussian beam with no matching circuit, the scanning analysis produced figure 28. The two largest spikes were identified as q,0,0 and q+1,0,0 modes, the rest were labelled "higher-order modes". An analysis of the frequencies involved verified that they are all H.-G.'s, with indices as given in the figure. 15 such modes were identified.

The fact that one of the most prominent H.-G. was q01 indicated serious misalignment, as mismatch produces even-indexed modes only.

The fact that the q10 mode is not visible indicates alignment in the plane of the ring.

The fact that the q02 mode and the q04 mode were almost equally strong indicates misalignment in the y-direction in general and no major mismatch.

On the other hand, the presence of the q20 and the q22 modes allows an estimate of the mismatch in the x-direction.

Given the optical circuit, the mismatch parameters are

$O_x = -0.53 \pm j0.66$, $O_y = -0.40 \pm j0.76$

with $|O_x| = 0.84$, $|O_y| = 0.87$

The misalignment parameter in the x-direction is negligible (good alignment in the plane of the ring), but in the y-direction it is

$\xi_y = 0.255 - j0.153$

as obtained from a least-squares fit of the H.-G. powers of lines q01 through q012 to the equation for misalignment (The fit was good to 2.4%).

MISALIGNED AND MISMATCHED

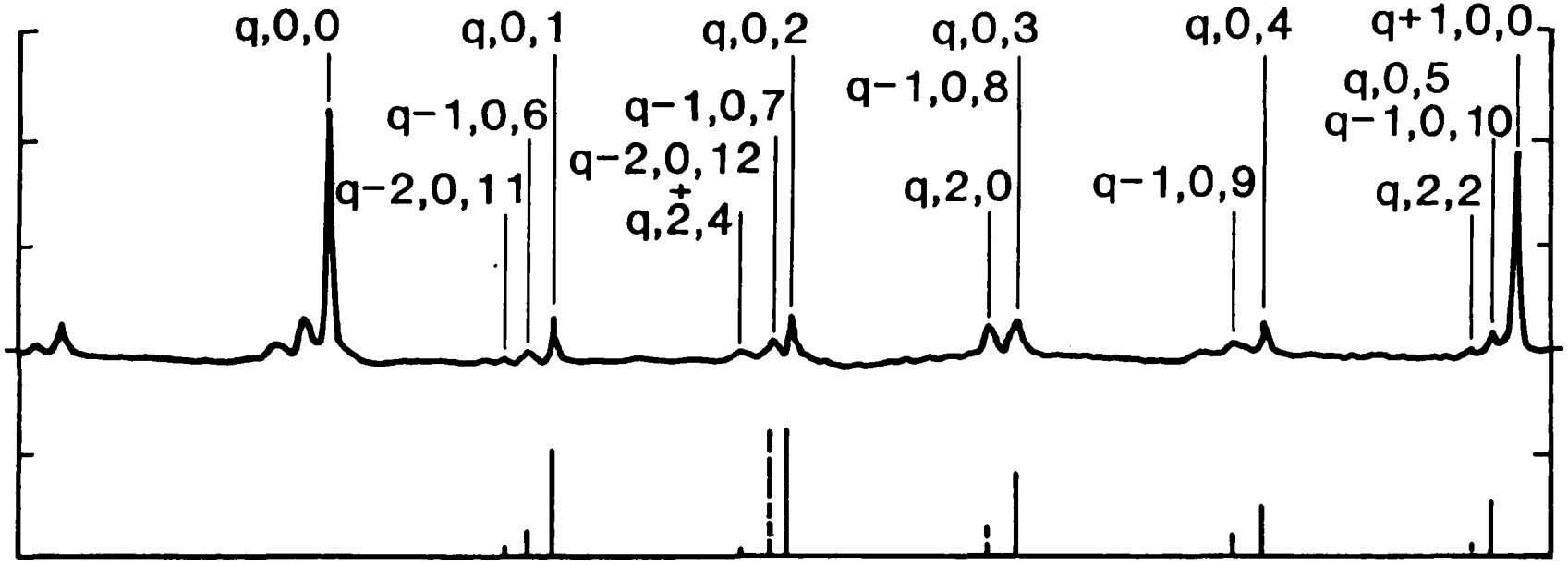

$|\xi_y| = 0.297$ $O_y = 0.40 - j.0.76$ $\epsilon_x = \alpha_x = 0$

$|\xi_x| = 0$ $O_x = 0.53 - j.0.66$ $\epsilon_y = 180\ \mu m$

$\alpha_y = -49''$

Fig. 28

PARTLY ALIGNED AND MATCHED

$O_x = 0.328 + j0$ $\quad |\xi_x| = 0.16$

$O_y = 0 + j0.303$ $\quad |\xi_y| = 0.19$

Fig 24.

The above result says that the offset in the y-direction was ε_y=180μm, and the tilt in the y-direction was α_y = -49 arc second.

The same paper shows a "partly matched" beam, Fig. 29, where a spherical lens was placed in a compromise position. The pattern shows, besides the q02, q20, and q01 modes, a newly emerging q10 mode indicating that now there is also misalignment in the x-direction.

the parameters are

$O_x = 0.328 + j0$, $O_y = 0 + j0.303$, $|\xi_x|=0.16$, $|\xi_y|=0.19$

reflecting a bigger effort in alignment as well as match.

Finally, the "matched" (actually aligned) cavity shows the fundamental Gaussians only, figure 30.

For "tutorial" purposes, figure 31 shows the cross sections of an offset and mismatched beam and its expansion into all Hermite-Gaussian eigenmodes of the astigmatic resonator. The contours are all the same isophote. Also, the aligned laser is shown to produce only even-indexed H.-G.'s. Note that the width W_0 of the circular incoming beam is made equal to the horizontal width w_{ox} of the resonator.

These results suggest an interesting way to keep a large ring aligned via servos:

1. Pick off the q10 mode and control with it the horizontal injection.
2. Pick off the q01 mode and control with it the vertical injection.
3. Pick off the q02 mode and control with it the vertical complex curvature of the beam (y-zoom).
4. Pick off the q20 mode and control with it the horizontal complex curvature of the beam (x-zoom).

ALIGNED AND MATCHED

Fig. 3c.

MISALIGNED AND MISMATCHED BEAM

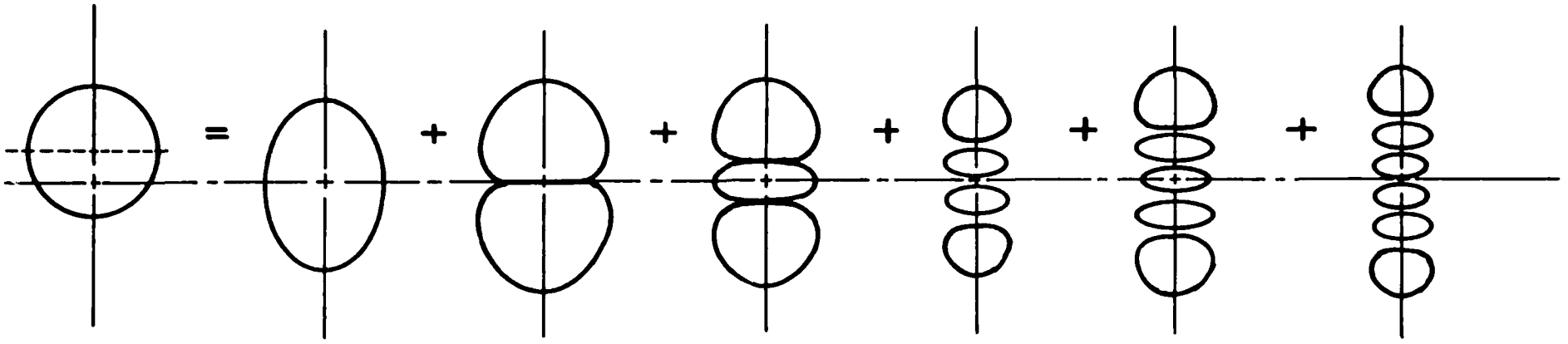

ALIGNED, BUT MISMATCHED BEAM

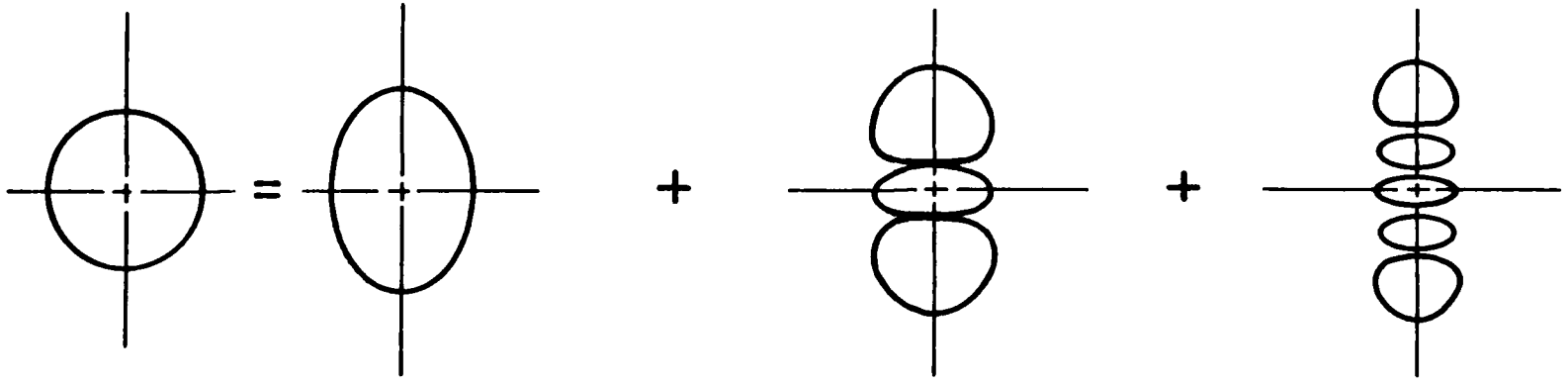

Fig. 31

III. Contributions to design of ringlaser

III. A. Scanning of an astigmatic beam, and beam evolution: New method to find beam and evolution parameters

This section contains the first experimental subject we were working on. It was motivated by the desire to establish experimentally the shape and size of an astigmatic beam spot. Scanning by a razor blade ("knife-edge") was recognized to deliver enough information to find the axes of an elliptical spot, and its inclination. The analysis proved to be surprisingly simple, and its results easily applicable. Data evaluation via non-linear least squares fitting is applied to find spot parameters as well as beam evolution. The programs are available upon request.

In the following, a reprint of a paper is given (ref. 19) which summarizes this work.

Knife-edge scanning of an astigmatic Gaussian beam

Hans R. Bilger and Taufiq Habib

The relations for position, spot size, and inclination of the major axis of an elliptical Gaussian beam to knife-edge scanning data are derived. A knife-edge whose scanning direction is adjustable to any angle has been employed to scan across a beam in at least three directions. Nonlinear least-squares fit programs have been developed to check whether a beam is Gaussian, and to evaluate the parameters, with errors, of such an elliptic spot. The evolution of an astigmatic beam in the tangential and sagittal plane is measured.

I. Introduction

Scanning of a Gaussian beam with circular cross section has been dealt with in several papers.[1] However, beams with different cross sections or power density distributions appear often in laser systems either as aberrations, e.g., through admixture of Hermite-Gaussian beams, or as an essential feature, as is the case in ring lasers. The extension reported here has several benefits in the laboratory:

(1) Quantitative determination of the degree to which a given spot deviates from a circular cross section.

(2) Determination of the parameters of an elliptical spot.

(3) Analytical (least-squares) evaluation of the spot, including an estimate of the errors of the evaluated parameters.

II. Scanning of a Gaussian Beam with Elliptical Cross Section

The spot size w shall be defined by the following distribution of the electric field amplitude E:

$$E(x,y) = E_0 \exp[-(x^2 + y^2)/w^2] \tag{1}$$

for a circular beam spot centered at $x = y = 0$; the beam propagates in the direction of the positive z axis.

Extending this to an elliptical cross section with arbitrary orientation (see Fig. 1) and using power density S (proportional to intensity I), we have

$$S(x',y') = \frac{2}{\pi}\frac{P_0}{w_a w_b} \exp(-2x'^2/w_a^2) \exp(-2y'^2/w_b^2), \tag{2}$$

where w_a, w_b are the spot sizes along the major and minor axes, respectively, P_0 is the total power in the beam, $2(P_0/\pi w_a w_b)$ is the power density in the beam center, and

$$x - x_0 = x' \cos\alpha_0 - y' \sin\alpha_0,$$
$$y - y_0 = x' \sin\alpha_0 + y' \cos\alpha_0. \tag{3}$$

Equations (3) include rotation by a tilt angle α_0 (measured from the positive x axis in the direction of the positive y axis) and translation of the beam center to x_0, y_0. A centered circular Gaussian beam [Eq. (1)] is included as a special case with $x_0 = y_0 = 0$ and $w_a = w_b = w$.

When a straightedge is placed at $x = x_s$ parallel to the y axis, obscuring the half-plane $x \leq x_s$, the power transmitted past the edge[2] is given by

$$P(x_s) = \int_{x=x_s}^{x=+\infty} \left[\int_{y=-\infty}^{y=+\infty} S(x,y)dy\right] dx. \tag{4}$$

This double integral can be expressed as a complementary error function of x_s,[3] namely,

$$P(x_s) = (P_0/2)\,\mathrm{erfc}(u), \qquad u = (\sqrt{2})(x_s - \bar{x}_s)/w(\alpha_0), \tag{5}$$

with $\mathrm{erfc}(u) = (2/\sqrt{\pi})\int_u^\infty \exp(-t^2)dt$, or as[4]

$$P(x_s)/P_0 = Q(v), \qquad v = [2/w(\alpha_0)](x_s - \bar{x}_s) = (\sqrt{2})u, \tag{6}$$

with

$$Q(v) = [1/\sqrt{(2\pi)}] \int_v^\infty \exp(-t^2/2)dt,$$

and

$$w^2(\alpha_0) = w_a^2 \cos^2\alpha_0 + w_b^2 \sin^2\alpha_0,$$
$$\bar{x}_s(\alpha_0) = x_0 \cos\alpha_0 + y_0 \sin\alpha_0 + x_{so} \tag{7}$$

(x_{so} is the offset of the translator micrometer).

The function $P(x_s)/P_0$ is drawn in Fig. 2 vs scanner position x_s for two widths, w_1 and w_2; the center of the beam is assumed to be at $x_s = 0$. Equation (7) contains the three parameters of interest w_a, w_b, and α_0. The apparent width $w(\alpha_0)$ is plotted in a polar plot in Fig.

The authors are with Oklahoma State University, School of Electrical & Computer Engineering, Stillwater, Oklahoma 74078.

Received 24 September 1984.
0003-6935/85/050686-05$02.00/0.

© 1985 Optical Society of America.

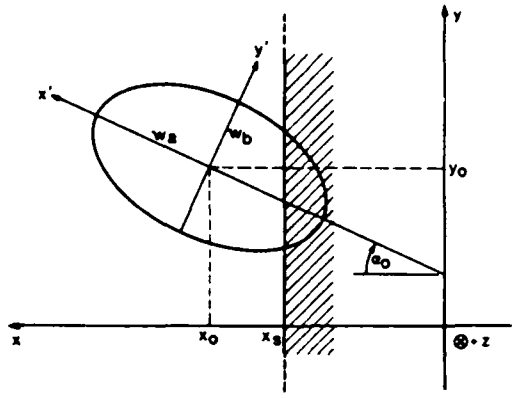

Fig. 1. Elliptical beam spot centered at x_0,y_0 with axes w_a and w_b tilted against the positive x axis (horizontal) by α_0. The beam goes into the paper plane (positive z axis). The scanning edge is placed at x_s.

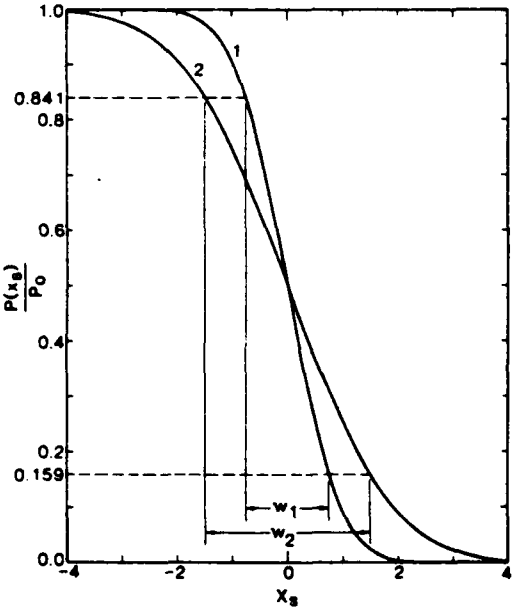

Fig. 2. Relative power $P(x_s)/P_0$ vs scanner position x_s for two spot sizes w_1 (= 1.5 units on the abscissa) and w_2 (= 3 units on the abscissa). The shapes of these curves are identical, except for a difference in w, for scanning of an arbitrarily placed elliptical beam. The beam centers are assumed to be at $x_s = 0$.

3 for three different ratios w_a/w_b, together with the actual spot shape (ellipse, dashed line) for $w_a/w_b = 2$. The measured widths $w(\alpha_0)$ agree with the widths of the ellipse at $\alpha = \alpha_0$ and $\alpha = \alpha_0 \pm 180°$ where $w(\alpha_0) = w_a$, and at $\alpha = \alpha_0 \pm 90°$ where $w(\alpha_0) = w_b$.

If the scanner is now rotated around the z axis by an angle α against the positive x axis, the equation for the resulting width is slightly generalized to

$$w^2(\alpha) = w_a^2 \cos^2(\alpha_0 - \alpha) + w_b^2 \sin^2(\alpha_0 - \alpha),$$
$$\bar{x}_s(\alpha) = x_0 \cos(\alpha_0 - \alpha) + y_0 \sin(\alpha_0 - \alpha) + x_s 0. \quad (8)$$

For a circular beam with $w_a = w_b = w$, the result is again $w(\alpha) = \text{const} = w$, as it should be.

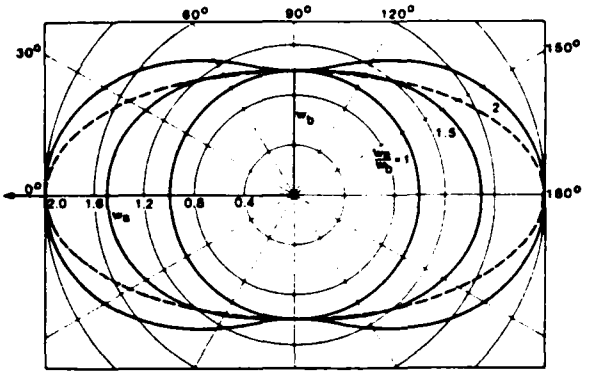

Fig. 3. Polar plot of widths vs scanning angle α for three different elliptical beam spots (solid curves). The spot for $w_a/w_b = 2$ is drawn as a dashed ellipse.

Three methods have been devised to evaluate $w(\alpha)$:

(a) Fractional power method: Noting that $Q(v_+ = 1) = 0.841 = P(x_s^+)/P_0$, and $Q(v_- = -1) = 0.159 = P(x_s^-)/P_0$ (see Fig. 2), we set the edge such that the relative power equals these fractions. The positions x_s^+ and x_s^- yield the width $w(\alpha)$ through

$$v_+ - v_- = 2 = [2/w(\alpha)](x_s^+ - \bar{x}_s) - [2/w(\alpha)](x_s^- - \bar{x}_s),$$

or

$$w(\alpha) = x_s^+ - x_s^-. \quad (9)$$

In principle, any pair v_+v_- can be chosen to evaluate w, but with a given absolute error in $P(v)$, it can be shown that the pair $v_\pm = \pm 1$ produces the width with minimum relative error. The center of the beam, $\bar{x}_s$, can be obtained by setting the scanner such that the transmitted power is halved, see Fig. 2.

(b) Graphical method: This method consists of plotting the relative power $P(x_s)/P_0$ vs x_s on error function paper.[5] A straight line on this paper indicates an error function, i.e., that the beam is indeed Gaussian. The points x_s^+ and x_s^- can then be used as above to find w. The center of the beam is again given by $P(\bar{x}_s)/P_0 = 1/2$. This method has the advantage over method (a) in that it makes use of all the measured scanning positions, that the latter do not have to be specifically chosen, and that the graph allows a check whether the beam is Gaussian. It also provides some estimate of measurement errors.

(c) Least-squares method: This third method consists of fitting the Q-function into the measured power vs x_s (see Fig. 2), by adjusting the three parameters P_0, w, and $\bar{x}_s$. This method does not require the data to be normalized with the power P_0 before analysis. It can furthermore accommodate a fluctuating total power and it reduces errors introduced by fluctuating power. The accuracy of the computer program is not limited to the usual ~1% of graphical methods. Any observer bias is eliminated. Finally the program also provides analytic estimates of the errors of the parameters by calculating the variance–covariance matrix.[6]

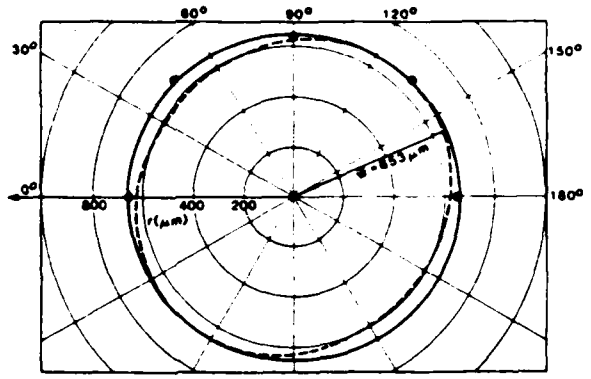

Fig. 4. Test of a spot at z = 90 cm off the laser without intervening optics at 5 angles, 0°, 45°, 90°, 135°, and 180°. The fit $w(\alpha)$ = const results in $w = (653 \pm 4)\ \mu$m. The sensitivity of the method to detect ellipticity is demonstrated by the dashed curve where tentatively $w_b/w_a = 0.9$ has been set.

Given the measured points $P(x_s)$, usually between five and twenty points covering the range from 0.9 P_0 to 0.1 P_0, the program fits the function

$$P(x) = a_1 Q[2(x - a_3)/a_2] \tag{6a}$$

into the points where $a_1 = P_0$, $a_2 = w(\alpha)$, $a_3 = \bar{x}_s$. An approximation for Q is chosen[4] which has a maximum error of $\pm 1 \times 10^{-5}$ over all arguments v:

$$Q(v) \simeq \tfrac{1}{2} + \mathrm{sgn}(v)\{[1/\sqrt{(2\pi)}] \times (a + bt + ct^2)t \exp(-v^2/2) - 1/2\},$$

$$t = 1/(1 + p|v|),$$

$$\mathrm{sgn}(v < 0) = -1, \quad \mathrm{sgn}(v = 0) = 0, \quad \mathrm{sgn}(v > 0) = +1,$$

$$p = 0.33267,\ a = 0.4361836,$$

$$b = -0.1201676,\ c = 0.9372980.$$

The program is iterative. It makes use of initial estimates for a_1, a_2, a_3 and refines these estimates until the sum of the residuals squared is satisfactorily close to the minimum. For a set of twenty points, the program takes ~800-msec CPU time on the VAX 11/750 for four iterations, which usually leads to convergence.[7]

III. Parameters of a Gaussian Beam with Elliptical Cross Section

One scan at an angle α gives $w(\alpha) = a_2$. We need at least three scans to calculate w_a, w_b, and α_0. In practice, scans at more than three angles are made. A separate least-squares fit program then determines the three parameters above through Eq. (8) or through

$$w(\alpha) = w_a\sqrt{[1 - \epsilon^2 \sin^2(\alpha_0 - \alpha)]}, \tag{8a}$$

with ϵ = numerical eccentricity = $\sqrt{(1 - w_b^2/w_a^2)}$.

IV. Establishment of an astigmatic Gaussian beam

A He–Ne laser (Oriel model 6697) was used to produce a well-behaved circular Gaussian beam. Its circularity was checked by scanning at several angles, see Fig. 4. A silicon detector (Optics Technology model 610) with a narrowband optical interference filter was used for detection with background light. The beam evolution was measured within the first 1.5 m off the laser front end. The spot size vs z was fitted by the equation

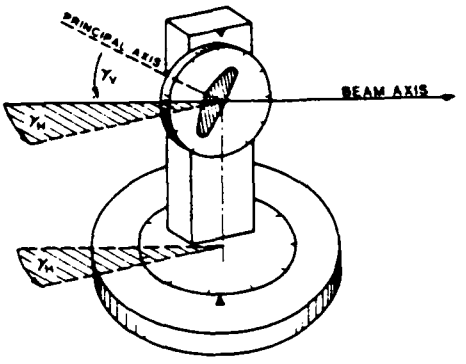

Fig. 5. Goniometer to adjust the obliquity angle of the lens. The reference position is given by retroreflection which originally aligns the principal axis of the lens with the beam axis = optical axis.

$$w(z) = w_0\sqrt{[1 + (z - z_w)^2/z_0^2]}, \tag{11}$$

with w_0 = waist size, located at $z = z_w$, and z_0 = Rayleigh length = $\pi w_0^2/\lambda$. The waist location z_w was found near the output mirror of the laser. The waist size was $w_0 = (316 \pm 5)\ \mu$m.

A plano-convex lens with focal length f_0 = 20 cm was then placed on a rudimentary goniometer (Fig. 5), which enabled us to rotate the lens around a vertical axis by an angle λ_h and also around a horizontal axis by an angle λ_v. The angle of obliquity[8] ϕ between the beam and the principal axis of the lens then becomes

$$\phi = \arccos(\cos\gamma_h \cos\gamma_v). \tag{12}$$

This angle lies in the tangential plane whose tilt against the horizontal plane (x-z plane) is given by

$$\alpha_0 = \arcsin(\sin\gamma_v/\sin\phi). \tag{13}$$

The tangential plane therefore contains one of the axes of the ellipse.

The lens was placed at $2f_0$ = 40 cm from the beam waist, with the two angles $\gamma_h = \gamma_v \approx 30°$, which results in the two focal lengths[9]: $f_{\text{tangential}}$ = 9.4 cm and f_{sagittal} = 16.8 cm. The beam, after traversing the lens, is expected to have a shape as given in Fig. 6, with the circle of least confusion[8,9] at $z \approx 15.5$ cm; before and after this point, the ellipse rotates by −90° (α_0 = 136.5° to α_0 = 46.5°). Since the input to the lens is a circular Gaussian beam, there will be a tangential waist and a sagittal waist placed approximately symmetrical to $z_{l,c}$. There are no focal lines in this case.

The propagation of the beam in the tangential plane is independent of that in the sagittal plane. Both are governed by Eq. (11), with two different sets of parameters: w_{0t}, z_{wt}, z_{0t}, and w_{0s}, z_{ws}, z_{0s}.

V. Experimental Evaluation of the Astigmatic Beam

The beam was probed at distances 12–60 cm after the lens. This range contains the interesting features (see Fig. 6): primary focus = waist in the tangential plane,

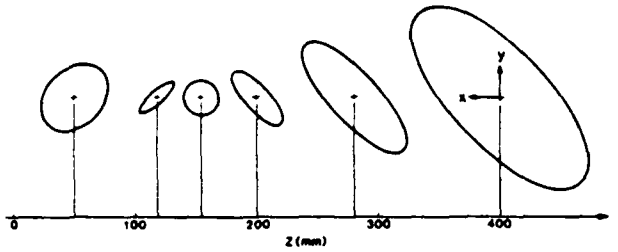

Fig. 6. Evolution of beam along the z axis. The circular Gaussian beam enters the lens at $z = 0$. The spots are shown as they appear in the x-y plane enlarged by ×100 relative to the z scale. Immediately to the left and right of the circle of least confusion, the tangential and sagittal waists are shown, respectively.

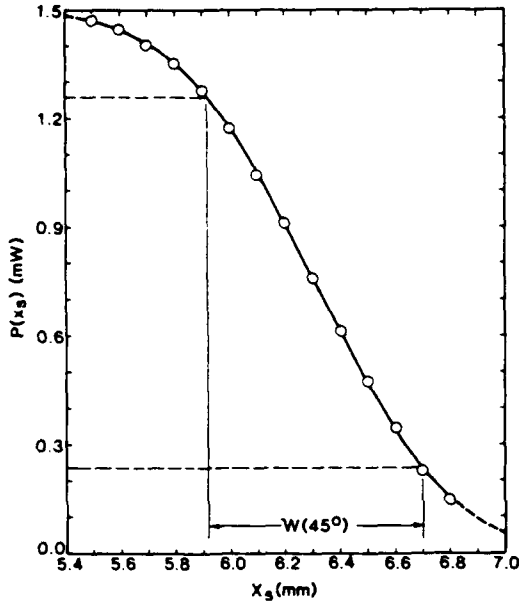

Fig. 7. Scan of astigmatic beam at $z = 60$ cm from the lens at $\alpha = 45°$. The least-squares fitted parameters are: total power $P_0 = (1.498 \pm 0.005)$ mW, center at $\bar{x}_s = (6.309 \pm 0.002)$ mm, spot size $w(45°) = (783 \pm 6)$ μm.

circle of least confusion, and secondary focus = waist in the sagittal plane.

Figure 7 shows a typical measurement of $P(x)$ at a distance $z = 60$ cm from the lens, at a scanning angle $\alpha = 45°$ with respect to the positive x axis. The least-squares fit of Eq. (6a) to the fourteen measured points gives $P_0 = (1.498 \pm 0.005)$ mW, $w(45°) = (783 \pm 6)$ μm, $\bar{x}_s = (6.309 \pm 0.002)$ mm. None of the individual residuals exceeded 8 μW; a translator with 10-μm resolution (smallest division) was used.

After at least four widths are evaluated for each spot, Eq. (8a) is fitted into the data $w(\alpha)$. Figure 8 shows a typical fit at $z = 35$ cm with the result $w_a = (801 \pm 3)$ μm, $\varepsilon = 0.920 \pm 0.003$, $\alpha_0 = (46.4 \pm 0.4)°$, which establishes the tilt and size of the ellipse at 35 cm together with the errors. The maximum deviation is 7.5 μm; the average deviation is 4 μm.

Finally, the evolution of the tangential spot sizes $w_t(z)$ and the sagittal spot sizes $w_s(z)$ is obtained (see

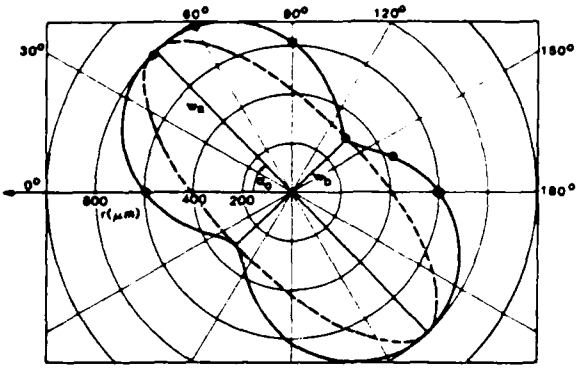

Fig. 8. Polar plot of spot sizes $w(\alpha)$, taken at $z = 35$ cm. The fit gives $w_a = (801 \pm 3)$ μm, $\varepsilon = 0.920 \pm 0.003$, $\alpha_0 = (46.4 \pm 0.4)°$. The rms deviation of the widths in this plot from the best-fitted solid curve is 4.5 μm. The resulting elliptical spot size is drawn as a dashed curve.

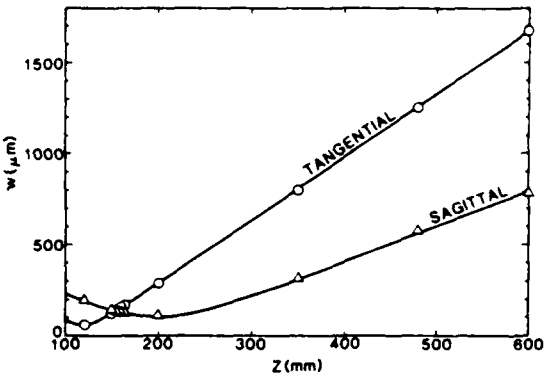

Fig. 9. Evolution of astigmatic beam vs z (see also Fig. 6). The waist sizes are $w_{0t} = (58.0 \pm 0.2)$ μm and $w_{0s} = (102.0 \pm 1.2)$ μm. They can be located with an accuracy of about ±2 mm.

Fig. 9) by least-square fitting Eq. (11) into the previously obtained results. The best-fitted parameters are

tangential waist $w_{0t} = (58.0 \pm 0.2)$ μm at $z_{wt} = (118.5 \pm 0.9)$ mm,

sagittal waist $w_{0s} = (102.0 \pm 1.2)$ μm at $z_{ws} = (201.3 \pm 2.5)$ mm.

The maximum deviation of any point was 8.5 μm for the tangential spot sizes and 14.6 μm for the sagittal spot sizes.

VI. Discussion of Results

The methods used here to scan an elliptical Gaussian beam with a straightedge (razor blade) are based on the result that the power spilling over the blade has the same dependence on the position of the blade as is the case in a circular Gaussian beam, except that the evaluated width is a simple function of position and size of the ellipse. At least three scans need to be done on each spot, with different angles α. If the position of the tangential plane (α_0) is known, two measurements would suffice, preferably taken at $\alpha = \alpha_0$ and $\alpha = \alpha_0 \pm 90°$.

Two methods were mainly used to obtain a width, namely, the fractional power method and the least-squares method. The latter established that the beam is indeed Gaussian, within the errors. However, subsequent measurements were usually done with the fractional power method, which is faster. Both methods yield typical errors of the order of one small division on the scanner (= 10 μm) or less. The data suggest indeed that translators with a resolution of 1 μm would produce yet smaller random errors.

To test the sensitivity of the methods to detect deviations from Gaussian profiles, a Hermite-Gaussian 1–0 mode of the same spot size[10] was evaluated. The calculated result of scanning along the x axis is

$$[P(x_s)/P_0]_{\mathrm{TEM}_{s10}} = (1/2)\,\mathrm{erfc}(u) + (u/\sqrt{\pi})\exp(-u^2),$$
$$u = (\sqrt{2})(x - \bar{x}_s)/w. \tag{14}$$

The major deviation from the error function occurs at $u_M = \pm 1/\sqrt{2}$ with an amount of $\sqrt{(2\pi e)} \approx 24\%$. This suggests that the detection of admixtures of such eigenmodes with a power of less than, say, 10% of the fundamental Gaussian has to make use of other methods, e.g., of Fabry-Perot scanning in the frequency domain.

It may be noted that by using the least-squares program above, an iteration of the type given in Ref. 11 can be avoided: The program finds directly one waist to satisfy both the asymptotic slope $1/z_0 = \lambda/\pi w_0^2$ as well as the minimum w_0 of the function $w(z) = w_0\sqrt{[1 + (z - z_w)^2/z_0^2]}$ with the criterion of minimizing random errors.

This paper is an outcome of research done under AFOSR grant 84-0058.

References

1. J. A. Arnaud, W. M. Hubbard, G. D. Mandeville, B. de la Claviere, E. A. Franke, and J. M. Franke, "Technique for Fast Measurement of Gaussian Laser Beam Parameters," Appl. Opt. **10**, 2775 (1971); Y. Suzaki and A. Tachibana, "Measurement of the μm Sized Radius of Gaussian Laser Beam Using the Scanning Knife-Edge," Appl. Opt. **14**, 2809 (1975); J. M. Khosrofian and B. A. Garetz, "Measurement of a Gaussian Laser Beam Diameter Through the Direct Inversion of Knife-Edge Data," Appl. Opt. **22**, 3406 (1983); M. Mauck, "Knife-Edge Profiling of Q-Switched Nd:YAG Laser Beam and Waist," Appl. Opt. **18**, 599 (1979).
2. The required size of the detector and its distance from the edge may be estimated as follows: An aperture of a diameter 4 w passes over 99.9% of a circular Gaussian beam of spot size w. As far as diffraction effects due to the edge are concerned, the power of the cylindrical waves in the shadow region diminishes as $(kz)^{-1}$ [M. Born and E. Wolf, *Principles of Optics* (Pergamon, New York, 1975), Chap. 11], which amounts to $\sim 10^{-5}$ for $\lambda = 633$ nm at $r = 1$ cm off the edge: with a detector placed more than 1 cm behind the edge we can safely disregard diffraction effects.
3. M. Abramowitz and I. A. Stegun, Eds., *Handbook of Mathematical Functions* (Dover, New York, 1972), Chap. 7.
4. Ref. 3, Chap. 26. The approximation 26.2.16 therein is over 2 orders of magnitude more accurate than that used by Khosrofian and Garetz (see Ref. 1); however the following approximation, which is similar to the latter in structure is also accurate to $\pm 1 \times 10^{-5}$ for $-\infty \leq x \leq +\infty$:
   $Q(x) \simeq [1 + \exp[f(x)]]^{-1}$, $f(x) = a_1 x + a_2 x^3 + a_3 x^5 + a_4 x^7$,
   $a_1 = 1.595700$, $a_2 = 0.072953$, $a_3 = -0.000324$,
   $a_4 = -0.0000350$.
5. Error function paper is available as graph paper no. 46800 from Keuffel & Esser, covering relative magnitudes from 0.01 to 99.99; a better-suited variant of it, covering 0.15–0.85, was devised by D. Preonas, Dayton Research Institute, in 1980. This latter graph paper makes use of the central portion of the Gaussian only, thus avoiding errors due to deviations of the beam from Gaussian shape in the tails.
6. W. C. Hamilton, *Statistics in Physical Science* (Ronald Press, New York, 1964), Chaps. 4 and 5.
7. The program is available on request.
8. F. A. Jenkins and H. E. White, *Fundamentals of Optics* (McGraw-Hill, New York, 1976), Sec. 9.9.
9. Ref. 8, p. 169, Eq. (9q).
10. This situation prevails in eigenmodes of a ring laser.
11. T. D. Baxter, T. T. Saito, G. L. Shaw, R. T. Evans, and R. A. Motes, "Mode Matching for a Passive Resonant Ring Laser Gyroscope," Appl. Opt. **22**, 2487 (1983).

III. B. Vacuum in ring: Residual Fresnel drag

A passive ring can be evacuated. What is the required residual pressure? We investigated two effects on the output, here we report on Fresnel drag (section III. C. shows calculations on quality factor).

A portion of this section is published (ref.'s 20, 21).

Vacuum in ring: Residual Fresnel drag

Light drag is a surprisingly simple means to introduce an anisotropy in the ring. Experimentally, some drag equations have been verified to the level of 0.1%.[22]

For a homogeneous velocity field $\vec{v}$ of a gas parallel to the light beam over a distance d, the beat frequency in a ringlaser is to a good approximation given by

$$\Delta f = (4/\lambda L)\ (n-1)\ vd, \tag{1}$$

where n = index in refraction. For helium this approximation is good to 1%. The quantity (n-1) is proportional to the gas pressure. For an ideal gas

$$(n-1)_{T,p,\lambda} = (T_0/T)\ (p/p_0)\ (n-1)_{T_0,p_0,\lambda} \tag{2}$$

T = absolute temperature of flowing gas, p = pressure of flowing gas, T_0, p_0 = standard conditions. For stationary mass flow, the flow rate

$$M = d(pV)/dt = q(vp) = kT\ dN/dt = \text{constant} \tag{3}$$

(q = tube cross section, V = volume of gas, N = number of gas molecules, k = Boltzmann constant). It follows for the beat frequency due to light drag

$$\Delta f = (4/\lambda L)\ (d/q)\ (n-1)_{T_0,p_0,\lambda}(T_0/Tp_0)M \tag{4}$$

The beat frequency is therefore determined by the mass flow rate. The velocity vs length is arbitrary and need not be known; the drag is independent of pressure and pressure gradients along the path, as long as M is constant and the flow is stationary.

Vacuum Requirement. Inadvertent drag due to moving residual gas has to be avoided. From the foregoing we can estimate upper limits of mass flow sources for negligible drag. To push drag effects below 10^{-7} Hz

generally we require the sources (inadvertent leaks, outgassing, etc.) to have flow rates below 10^{-9} Pa•m^3/s, which is equivalent to 10^{-8} torr ℓ/s.

However, typical information about vacuum is given through pressure, which in turn is related to flow via the pump resistance of the ring.

It turns out that with mass flow rates even as high as "100 micron cubic foot per hour" (10^{-4} Pam^3/s) we are already close to the high vacuum regime. In this regime, the pump resistance R (s/m^3) of a cylindrical tube of cross section q and length d, molecular weight m is [23]

$$R(s/m^3) = (3\pi/4)\ (m/2kT)^{1/2}\ d/q^{3/2} \qquad (5)$$

(m=mass of one molecule) and the pressure difference along such a tube is

$$P_2 - P_1 = MR\ . \qquad (6)$$

Assuming a worst case of "inadvertent" mass flow injection of M = 10^{-9} Pam^3/s farthest away from the pump, d = 7.6 m, and a tube with 1 cm diameter as above, we obtain

$$P_2 - P_1 \approx P_2 = 0.62\text{x}10^{-4}\ \text{Pa}\ (=4.7\text{x}10^{-7}\ \text{torr})$$

whereby the pressure P_1 at the input of a 75 1/s pump would be $1.3\text{x}10^{-8}$ Pa (= $1\text{x}10^{-10}$ torr), i.e., negligible. From this we conclude that reasonable high vacuum conditions have to prevail. They are achievable in a laboratory with modest cleaning and pumping.

It should be noted, that an "active" ringlaser requires by definition material in the light path, e.g. the HeNe gas for

amplification. Indeed much of the residual problems with small commercial, active, ringlasers are directly related to light drag from moving gas (Langmuir flow)[24]. The gas pressures needed to sustain the necessary amplification are so far above those calculated in this section, that it is considered impossible to render negligible any false signals (noise) due to Fresnel drag. We consider this true even if elaborate measures are used to balance mass flow etc, as it is done in small ring laser gyros.

III. C. Vacuum in ring: Effect on quality factor

Power loss of a beam due to scattering by a gas was recognized very early as a source of imperfection, but it was clearly considered negligible. After more important error sources had been eliminated, this effect got more into the forefront. In a large ringlaser, with very high sensitivity and quality factors of the order of 10^{12}, scattering becomes a substantial effect. Fortunately, as this section demonstrates, even modest pumping will render negligible its effect on the quality factor of even a large resonator. Rayleigh scattering off neutral atoms is treated as the only scattering mode. Born and Wolf[25] served as a basis of a classic (non-quantum) calculation in this section.

Vacuum in a ring: Effect on quality factor

The residual gas in an evacuated ring will cause scattering losses of the traversing beam.

The total scattered power P_{sc} is calculated, and the quality factor Q_{sc} is then obtained by

$$Q_{sc} = \omega_0 \frac{(W = \text{energy stored})}{(P_{sc} = \text{scattered power})} . \tag{1}$$

The effect on the overall quality factor Q is then given by the contribution of Q_{sc} to

$$\frac{1}{Q} = \sum_i \frac{1}{Q_i} . \tag{2}$$

Eq. 2 follows from eq. 1 under simplifying conditions.

Relation of scattered power to Q_{sc}:

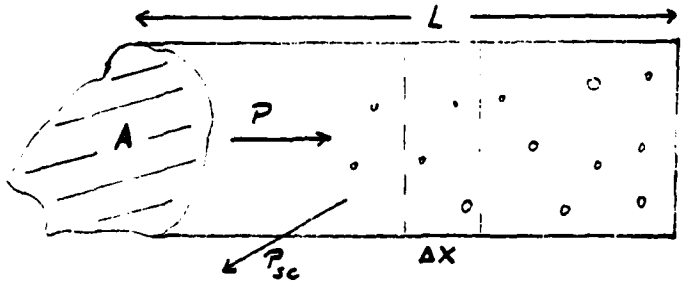

We will assume that the scattered power per interval Δx, ΔP_{sc}, is proportional to the incident power P:

$$\Delta P_{sc} = \frac{1}{\kappa_{sc}} P \Delta x . \tag{3}$$

We will also assume that the change of P due to scattering is negligible throughout the length L, i.e.

$$P_{sc} = \frac{1}{\kappa_{sc}} PL \ . \tag{4}$$

Here κ_{sc} = extinction length due to scattering.

The power P in the cavity is simply related to the energy W stored in the cavity through the following considerations:

Assume a monochromatic plane field with rms magnitudes E_{RMS} and H_{RMS} in vacuum. With the Poynting vector $\vec{S} = \vec{E} \times \vec{H} = (\varepsilon_0/\mu_0)^{1/2}$, the time-averaged power is

$$P = < \int \vec{S} \ . \ \vec{dA} > = (\varepsilon_0/\mu_0)^{1/2} \ E^2_{RMS} A \ . \ (\vec{E} \perp \vec{H} \perp \vec{A}) \tag{5}$$

On the other hand, the energy W is given by

$$W = \frac{1}{2} \int (\vec{E} \ . \ \vec{D} + \vec{H} \ . \ \vec{B}) dVol = \varepsilon_0 E^2_{RMS} Vol = \varepsilon_0 E^2_{RMS} LA \tag{6}$$

(cylindrical mode volume; this assumption is however not critical).

We have therefore from eq.'s 5) and 6):

$P = W/(L\sqrt{\varepsilon_0\mu_0}) = (c/L)W$ = (free spectral range)x(energy stored) (7)

From eq's 1), 4), and 7), we get then

$$Q_{sc} = \omega_0 \frac{W}{P_{sc}} = \omega_0 \frac{(L/c)P}{(PL/\kappa_{sc})} = 2\pi \frac{\kappa_{sc}}{\lambda} \tag{8}$$

We have thus to increase the scattering length κ_{sc} such that the resulting $Q_{sc} >> Q$. The fact that we see the sun indicates that this is easy.

In the following, the extinction length due to Rayleigh scattering is calculated.

Rayleigh Scattering

We assume dipole scattering only, because it usually has the largest scattering cross section.

We assume Rayleigh scattering off individual atoms, for two reasons:

1) The atomic dimensions d are small compared to the wavelength λ used (no complications from charge distribution in atom): $d_{AIR} = 3.03 \times 10^{-10}$ m, $\lambda \simeq 5 \times 10^{-7}$ m

2) the mean free path length ℓ is large compared to the wavelength used (no scattering from density fluctions)

$\ell = kT/(\sqrt{2}\,\pi\, d^2 p) \gg \lambda$ requires for air: $p \ll 18$ kPa (= 135 torr)

We have then for the total scattered power off one (induced) dipole

$$P_{sc,1} = (4\pi^3/3)(C/\varepsilon)(W_0^2/\lambda^4) \qquad (9)$$

where the dipole moment $W_0 = \alpha E_0 = \alpha\sqrt{2}\,E_{RMS}$ (9a) in an electric field E_0, with the polarizeability

$$\alpha = (\varepsilon_0/N_\nu)(\varepsilon - 1) = (\varepsilon_0/N_\nu)(n^2 - 1) \qquad (10)$$

$n^2 = \varepsilon$ (macroscopic) relative dielectric constant of gas,

$N\nu$ = volume density of scatterers, in an ideal gas: $p = N\nu\, kT$ (10a).

(p = pressure)

The (total) scattering cross section per molecule is

$$\alpha = \frac{8}{3}\pi^3 (\varepsilon - 1)^2 / N_\nu^2 \lambda^4, \qquad (11)$$

and the relation for the total scattered power on traversing a length L is, using equations 4, 5, 8, 9, 9a, 10, and $c\sqrt{\mu_0 \varepsilon_0} = 1$:

$$P_{sc} = P_{sc,1} N_\nu AL = \frac{8}{3}\pi^3 \frac{(n^2-1)^2 L}{N_\nu \lambda^4} P = \frac{1}{\kappa_{sc}} PL \ , \qquad (12)$$

from which the extinction length κ_{sc} can be calculated, with eq. 10a:

$$K_{sc}^{-1} = \frac{8}{3}\pi^3 \frac{(n^2-1)^2}{N_\nu \lambda^4} = \frac{32}{3}\pi^3 \frac{(n-1)^2 kT}{\lambda^4 p} \ ,$$

using $(n^2-1)^2 = (n-1)^2(n+1)^2 \approx (n-1)^2 4$.

Using the Lorentz-Lorenz formula and eq. 10a:

$$\frac{n^2-1}{n^2+1} \approx n-1 = \text{const}\, N_\nu = \text{const}\frac{p}{kT} \ , \quad \text{or}$$

$$(n-1)_{p,T,\lambda} = (p/p_0)(T_0/T)(n-1)_{p_0,T_0,\lambda} \ . \qquad (13)$$

At standard conditions (p_0 = 101 kPa = 1 atm, T_0 = 273 K = 0°C), and λ = 514.5 nm, $n_{AIR} - 1 = 2.79 \times 10^{-4}$, $n_{He} - 1 = 0.3500 \times 10^{-4}$.
We have finally

$$\kappa_{sc}^{-1} = \frac{32}{3}\pi^3 \frac{1}{\lambda^4} \frac{1}{N_0} \frac{T_0}{T} \frac{p}{p_0} (n-1)^2_{p_0,T_0,\lambda} \ , \qquad (14)$$

where $N_0 = p_0/kT_0 = 2.687 \times 10^{25}$ molecules/m^3 (= Loschmidt number)

Quality factor versus scattering:

The final result is then, using eq.'s 14 and 8):

$$Q_{sc} = 2\pi \frac{\kappa_{sc}}{\lambda} = \frac{3}{16} \frac{N_0}{\pi^2} \frac{\lambda^3}{(n-1)^2_{p_0,T_0,\lambda}} \frac{T}{T_0} \frac{p_0}{p} \ . \qquad (15)$$

Given the type of gas (which determines n):

Example: 1) Air-filling at standard conditions, $\lambda = 0.5145 \times 10^{-6}$ m

$$Q_{sc} = \frac{3}{16} \frac{2.678\times10^{25} \times (0.5145\times10^{-6})^3}{\pi^2 (2.940\times10^{-4})^2} = 8.0\times10^{11} .$$

Compare this to a square ring with overall finesse F = 20,000.

The latter results in a

$Q_{Mirror} = FL/\lambda = 1.2 \times 10^{12}$ (L = 31 m, $\lambda = 0.5145 \times 10^{-6}$ m)

which is about equal to the quality factor due to scattering by air at 1 atmosphere.

With very modest forepumping down to 1 torr = 133 Pa, $Q_{sc} \approx 6 \times 10^{14}$ i.e. negligibly large compared to even the best hoped-for (achieveable?) mirror quality factors.

Note also that the optimum pressure for HeNe-plasma for tubes of ~ 1 cm diameter is somewhat below 1 torr; this means that scattering losses are negligible even in active ring lasers, if the assumptions above are satisfied (however, scattering in an ionized gas, and at resonating atoms would have to be considered separately).

Example 2: A cavity of length L=52 cm produced by Rockwell has an evacuated finesse of $F_{vac} = 29800 \pm 400$ at $\lambda = 633$ nm. What is the finesse F_{sc} with air filling?

$(n-1)_{Air,\ T_0,P_0,\lambda = 633nm} = 0.00029170$, T=(273 + 25)K, $p=P_0$.

we get $Q_{sc} = 1.661\times10^{12}$, or $F_{sc} = Q_{sc}\lambda/L = 2.02\times10^{6}$.

From eq. 2 follows $\frac{1}{F_{Air}} = \frac{1}{F_{vac}} + \frac{1}{F_{sc}} = \frac{1}{29800} + \frac{1}{2.02\times10^{6}}$

or $F_{Air} = 29370$

(measured at Rockwell with air filling: 2900 ± 400)

The data are compatible with our calculations, although they are not conclusive. The same mirrors, put into a 30 m cavity, would have a finesse in vacuum of $29800 \times 30/0.52 = 1.719 \times 10^6$, and letting air in would reduce the finesse from

$F_{vac} - 1.72 \times 10^6$ to $F_{Air} = 0.929 \times 10^6$. , which would then mean a substantial reduction in over-all finesse, or quality factor.

III. D. Proposed calibration methods for large ring: Light drag through gas flow from switchable calibrated leaks, tilting (rocking) the ring base.

The dynamic range of a large stationary ring is, expressed in earth rotation rates Ω_E, from about $10^{-10}\Omega_E$ to $1\Omega_E$, or, expressed in optical beat frequencies, from about 100 nHz to 1 kHz, i.e. over 10 orders of magnitude. It turns out that low beat frequencies can easily be generated via air flow through calibrated leaks: The needed mass flow requires such low air pressures that the cavity quality factor (section III. C.) is not affected.

This contribution is already published (ref.'s 20 and 21). Rocking of the base is made possible at the base at the Seiler lab. It is useful for generating large signals.

Calibration of a large passive laser ring

H.R. Bilger

Department of Electrical and Computer Engineering, Oklahoma State University
Stillwater, OK 74078

G.L. Shaw

Frank J. Seiler Research Laboratory
USAF Academy, Colorado Springs, CO 80840

B.J. Simmons

Frank J. Seiler Research Laboratory
USAF Academy, Colorado Springs, CO 80840

Abstract

Two types of effects are investigated as to their potential for calibrating a large ring and for introducing test signals of known magnitude: 1) tilting the base of the ring by a known angle and with known time evolution, and 2) utilizing Fresnel drag from a controlled flow of gas.

Introduction

A large, 58 meter square, ring laser gyro (RLG) is being assembled on the pneumatic isolation platform at the Frank J. Seiler Research Laboratory. Two techniques for calibration of the RLG will be considered in this presentation. In the first method, the RLG would be tilted at a precisely known angle to vary the effective rotational rate. The second method discussed makes use of the Fresnel drag from a controlled flow of gas in the ring.

An adjustable effect to produce an RLG output is described for several reasons: 1) to check the linearity of the output, 2) to check properties in the frequency domain, 3) to calibrate the sensitivity and/or the noise sources acting in the ring, and 4) to introduce a probe signal during initial adjustments. The earth rotation naturally provides a sizeable rotation rate with a very good signal/noise ratio of the order of 10^{8};[1] but it has the disadvantages of not being adjustable and of being constant as opposed to an effect leading to a frequency modulation of the output. One advantage of basing the large RLG on a pneumatically supported platform is that the base can be tilted by small angles thus changing the effective rotational rate imposed on the ring. The isolation platform can be maintained at a known tilt to local level to and accuracy of the order of 10^{-3} arc seconds by means of closed loop control of pneumatic actuators[2]. The platform can be offset from level by as much as 6 arc minutes by means of these pneumatic actuators. The base can also be excited in 6 degrees of freedom at small amplitudes from DC to 10 Hz by means of electro-magnetic actuators.

The light path of the RLG is contained in tubing evacuated to about 10^{-8} torr. The Fresnel drag calibration technique would be performed by allowing a small gas flow parallel to the light beam, along a portion of the ring. A known gas flow rate establishes a calculable effect on the difference in velocity for the clockwise and counterclockwise light beams of the RLG, and an expected value for the non-rotating output under this condition.

Range of calibration

Large ring lasers are attractive because of their high sensitivity for rotation and low noise. In the following we will use a square ring laser of $A = 58\ m^2$ with perimeter $L = 4\sqrt{58}$ m, operating at a wavelength $\lambda = 514.5$ nm as basis for discussion. A two mode ring laser has a beat frequency output

$$\Delta f = 4\,\vec{A}\cdot\vec{\Omega}/\lambda\,L, \qquad (1)$$

where $\vec{A}$ = surface vector of ring, $\vec{\Omega}$ = angular velocity vector of absolute ring rotation.

As Equation (1) is linear in $\vec{\Omega}$, there is no obvious upper limit of output. However, for convenience we will limit the design considerations to bandwidths up to earth rate for the recording of the phase $\phi(t)$, [$\Delta f = (1/2\pi)(d\phi/dt)$], i.e., $\Delta f = 679$ Hz (latitude $\theta = 38^{\circ}\ 58'$). As to the lower limit we will assume that quantum noise limits the performance at high Fourier frequencies. The power spectral density is given by [3]

$$S_{\Delta f,W} = 2\ (hf_o^3/Q^2P) \tag{2}$$

with an estimate of finesse F = 1000 or a quality factor $Q = (L/\lambda)F = 5.9 \times 10^{10}$, and a power level of 500 mW, the white power spectral density would be, at the oscillation frequency $f_o = c/\lambda = 583$ THz,

$$S_{\Delta f,W} = 1.51 \times 10^{-10}\ (Hz^2/Hz),$$

which allows an accuracy of

$$\delta\Delta f = \sqrt{S_{\Delta f,W}/\tau} \tag{3}$$

for the measurement of the beat frequency over an integration time τ; e.g., with τ = 1 d, an rms frequency fluctuation of the order of 42 nHz can be anticipated. However, the open-ended limit set by Equation (3) is not realizable over arbitrarily long times. In practice, 1/f noise or even $1/f^2$ noise of the laser oscillators set a lower limit[4] to the attainable accuracy. In today's commercial ring laser gyros, the white quantum noise turns over into 1/f noise at corner frequencies of the order of 10-1000 µ Hz. Furthermore, the observed 1/f noise is always larger than the Gagnepain-Uebersfeld limit as observed in quartz oscillators[5].

$$S_{\Delta f,F} = A/f, \qquad A = f_o^2/Q^4 \tag{4}$$

For lack of better theory, we use Equation (4) to estimate the flicker floor. With f_o = 583 THz and $Q = 5.9 \times 10^{10}$, $S_{\Delta f,F} = 2.8 \times 10^{-14}/f$. The equivalent Allan standard deviation

$$\sigma_A(\tau) = \sqrt{2\ln 2 \times 2.8\times10^{-14}} = 197\ \text{nHz}.$$

The transition between white noise and 1/f noise appears at Fourier frequencies of about 200 µHz, requiring integration times of about 1 hour to arrive at this flicker floor; lower limits of beat frequency errors of the order of 10^{-8} Hz are theoretically feasible, and a dynamic range of over nine decades of beat frequency is possible, for which range calibration signals should be provided.

First calibration method: tilting the gyro base

A tilt modifies the output from earth rate. The surface vector $\vec{A}$ in Equation (1) is made time-dependent, $\vec{A} \rightarrow \vec{A}(t)$. This can be achieved by rotating an actively controlled pad around the east-west symmetry axis. A variety of factors have to be investigated in such a feasibility study: Reproducibility, adjustibility, hysteresis, effect on long-term stability. The change of beat frequency due to tilt in the meridional plane by an angle $\delta\alpha$ is

$$\delta\Delta f(\text{Hz}) = (4\ \vec{A}\cdot\vec{\Omega}/\lambda L)\ \cot\theta\ \delta\alpha = 4.1 \times 10^{-3}\ \delta\alpha\ (\text{arc second}) \tag{5}$$

in the example above. To change the beat frequency by 1 mHz, a lift of 9.1 µm of the 7.62 m - long pad is required. The "noise" of the tilt is 10^{-3} arc second which is transduced by the ring into a beat frequency fluctuation of 6.58 µHz, well above the limit given by the flicker floor.

There is also the possibility of rocking the pad, i.e., to introduce a sinusoidal tilt versus time. Provided that the excitation of eigenmodes of the pad can be sufficiently suppressed, this manner of introduction of an ac-modulated frequency becomes an excellent means of generating a calibration signal. An external measurement of the height by using high-performance levelling instruments by electrical or optical means can certainly be done with an error of 10 µm and possibly of 1 µm.

Second calibration method: Fresnel drag with gas flow

Light drag is a surprisingly simple means to introduce an anisotropy in the ring. Experimentally, some drag equations have been verified to the level of 0.1%.[6]

For a homogeneous velocity field $\vec{v}$ of a gas parallel to the light beam over a distance d, the beat frequency is to a good approximation given by[7]

$$\Delta f = (4/\lambda L)(n-1)vd, \tag{6}$$

where n = index of refraction. For helium this approximation is good to 1%. The quantity (n-1) is proportional to the gas pressure. For an ideal gas

$$(n-1)_{T,p,\lambda} = (T_o/T)(p/p_o)(n-1)_{T_o,p_o,\lambda} \tag{7}$$

T = absolute temperature of flowing gas, p = pressure of flowing gas, T_o, p_o = standard conditions. For stationary mass flow, the flow rate

$$M = d(pV)/dt = q(vp) = kT\,dN/dt = \text{constant} \tag{8}$$

(q = tube cross section, V = volume of gas, N = number of gas molecules, k = Boltzman constant), if a mass flow source is used, for example a calibrated leak as is used in vacuum work. It follows for the beat frequency due to light drag

$$\Delta f = (4/\lambda L)(d/q)(n-1)_{T_o,p_o,\lambda}(T_o/Tp_o)M \tag{9}$$

The beat frequency is therefore determined by the mass flow rate. The velocity vs length is arbitrary and need not be known; the drag is independent of pressure and pressure gradients along the path, as long as M is constant and the flow is stationary.

Estimate of required leak. Assume a helium-filled leak with $(n-1)_{T_o,p_o,\lambda} = 3.49 \times 10^{-5}$. The leak is to be injected into one leg of the ring having 1 cm tube diameter and d = 3.3 m length. At room temperature (T = 298 K), a flow rate of $M = 2.6 \times 10^{-4}$ Pa·m³/s is then required to produce $\Delta f = 1$ mHz. A calibrated He leak of 100 "micron cubic foot/hour" has a mass flow rate of 1.05×10^{-4} Pa·m³/s. If larger beat frequencies are required, air can be used with about eightfold increased drag.

Several calibrated leaks can be mounted in opposing legs of the ring, to change magnitude and sign of the drag. They can be switched off and on at any time. Commercially, a large range of 10^{-11} Pa·m³/s to 10^{-4} Pa·m³/s is available which will cover the entire range of beat frequencies from about 10 mHz down into the noise. It may also be mentioned that turbulent flow will remove the radial velocity profile and will produce a more uniform output frequency.[8]

Vacuum Requirements. Conversely, inadvertent drag due to moving residual gas has to be avoided. From the foregoing we can estimate upper limits of mass flow sources for negligible drag. To push drag effect below 10^{-7} Hz generally we require the sources (inadvertent leaks, outgassing, etc.) to have flow rates below 10^{-9} Pa·m³/s.

However, typical information about vacuum is given through pressure, which in turn is related to flow via the pump resistance of the ring.

It turns out that with mass flow rates even as high as 100 micron cubic foot per hour (10^{-4} Pa·m³/s) we are already in the high vacuum regime. In this regime, the pump resistance R (s/m³) of a cylindrical tube of cross section q and length d, molecular weight m is[9]

$$R(s/m^3) = (3\pi/4)(m/2kT)^{1/2}\, d/q^{3/2} \tag{10}$$

and the pressure difference along such a tube is

$$P_2 - P_1 = MR. \tag{11}$$

Assuming a worst case of "inadvertent" mass flow injection of $M = 10^{-9}$ Pa·m^3/s farthest away from the pump, $d = 7.6$ m, and a tube with 1 cm diameter as above, we obtain

$$P_2 - P_1 \simeq P_2 = 0.6 \times 10^{-4} \text{ Pa } (= 4.7 \times 10^{-7} \text{ torr})$$

whereby the pressure P_1 at the input of a 75 l/s pump would be 1.3×10^{-8} Pa ($\simeq 1 \times 10^{-10}$ torr), i.e., negligible.

From this we conclude that reasonable high vacuum conditions have to prevail, but also that the loading of vacuum pumps by Fresnel drag calibrations is not excessive.

References

1. N. Matsunami and K. Nakajima, "Noise Features of the Rotation of the Earth," Proc. Symp. 1/f Fluctuations, Tokyo, Japan, July 1977. Data on earth rotation and time scale: The American Ephemeris and Nautical Almanac 1980, Nautical Almanac Office, Washington

2. B.J. Simmons, "A Sub-seismic Test Platform as a Motion Exciter," Proceedings of the 25th International Instrumentation Symposium, Anaheim, California, May 1979.

3. Theory as well as experiments are given by T.A. Dorschner, H.A. Haus, M. Holz, I.W. Smith, and H. Statz, "Laser Gyro at a Quantum Limit," IEEE J. Qu. El. QE-16, pp 1376-1379, 1980.

4. H.R. Bilger and M. Sayeh, "Noise Phenomena in Ringlasers," 7th Int. Conf. Noise in Phys. Syst., Montpellier, France, May 1983; H.R. Bilger, "Possibility of Flicker Floor in Laser Gyros," 11th Winter Colloquium on Quantum Electronics, Snowbird, UT, Jan 1981.

5. J.J. Gagnepain, J. Uebersfeld, G. Goujon, and P. Handel, "Relation Between 1/f Noise and Q-Factor in Quartz Resonators at Room and Low Temperatures, First Theoretical Interpretation," Proc. 35th Ann. Freq. Contr. Symp., Ft Monmouth, NJ, May 1981, [illegible]

6. H.R. Bilger and W.K. Stowell, "Light Drag in a Ringlaser: An Improved Determination of the Drag Coefficient," Phy. Rev. A 16, pp 313-319, 1977.

7. E.J. Post, "Sagnac Effect," Rev. Mod. Phys. 39, pp 475-493, 1967.

8. P. Zeeman, "An Optical Method for Determining the Ratio Between the Mean and Maximal Velocities in the Turbulent Motion Fluids in a Cylindrical Tube. Contribution to the Experiment of Fizeau," Proc. Koninkl. Acad. Wet. Amsterdam 18, p 1240, 1916.

9. S. Dushman, Scientific Foundations of Vacuum Technique, 2d Ed., Wiley 1962.

References

1. W. W. Chow, J. Gea-Banacloche, L. M. Pedrotti, V. E. Sanders, W. Schleich, and M. O. Scully, "The ring laser gyro," Rev. Mod. Phys. 57, pp. 61-104, 1985.

2. J. Wahr, "The earth's rotation rate," American Scientist, Jan.-Feb. 1985, pp. 41-46.

3. H. R. Bilger and M. R. Sayeh, "Flicker noise in frequency fluctuations of lasers," (submitted to Phys. Rev. Lett., 16 March 1985).

4. A. H. Rosenthal, "Regenerative circulatory multi-beam interferometry for the study of light-propagation effects," J. Opt. Soc. Am. 52, pp. 1143-1148 (1982).

5. H. R. Bilger and M. Sayeh, "Noise phenomena in ringlasers," presented at the 7th Int.'l Colloq. on Noise in Phys. Systems, Montpellier, France, May 1983; printed in Noise in Physical Systems and 1/f Noise (eds. M. Savelli, G. Lecoy and J. P. Nougier), Elsevier Science Publishers B. V., 1983, pp. 325-328.

6. S. Ezekiel, "An overview of passive optical gyros," SPIE 487, pp. 13-20, 1984.

7. H. R. Bilger, "Low frequency noise in ring laser gyros," SPIE 487, pp. 42-48, 1984.

8. H. R. Bilger and M. R. Sayeh, "Flicker noise in frequency fluctuations of lasers," (submitted to Phys. Rev. Lett., 16 March 1985), ref. 3.

9. The first adaptation of Kogelnik's approach to circuits with finite enclosed area is probably W. W. Rigrod, "The optical ring resonator," B. S. T. J. 44, pp. 907-1965; the Seiler group produced: J. D. Keating and G. L. Shaw, "Programs to locate and decribe the mode matching lenses for the PRRLG," Document FJSRL-TM-82-0011, AF Systems Command, Aug. 82; T. D. Baxter, T. T. Saito, G. L. Shaw, R. T. Evans, and R. A. Motes, "Mode matching for a passive resonant ring laser gyroscope," Appl. Opt. 22, pp. 2487-2491, 1983; T. T. Saito and J. L. Gossner, "Mode sensitivity and matching for a passive ring resonant gyroscope with equal curvature mirrors." Seiler Lab (unclassified report), Aerospace-Mechanics Sciences,1983.

10. S. A. Collins, "Analysis of optical resonators involving focusing elements," Applied Optics 3, pp. 1263-1275, 1964.

11. A. E. Siegman, "An introduction to lasers and masers," McGraw-Hill 1971.

12. T. D. Baxter, T. T. Saito, G. L. Shaw, R. T. Evans, and R. A. Motes, "Mode matching for a passive resonant ring laser gyroscope," Appl. Opt. 22, pp. 2487-2491, 1983; see ref. 9.

13. H. R. Bilger and M. R. Sayeh, "Design considerations of a large laser ring," 15th Winter Colloquium on Quantum Electronics, Snowbird, UT, 9-11 Jan 1985.

14. N. Yamauchi, "Resonant modes in a ring laser resonator and their deformations by mirror rearrangements," Electr. and Comm. in Japan 57-C, No. 11, pp. 92-100, 1974.

15. H. A. Haus, "Waves and fields in optoelectronics," Prentice-Hall 1984.

16. J. A. Arnaud, "Beam and fiber optics," Academic Press 1976.

17. M. Abramowitz and I. A. Stegun (eds.) "Handbook of mathematical functions," Dover 1972, p. 773.

18. I. S. Gradshteyn and I. M. Ryzhick, "Tables of integrals, series, and products," 4th ed., Academic Press, 1965.

19. H. R. Bilger and T. Habib, "Knife-edge scanning of an astigmatic Gaussian beam," Appl. Opt. 24, pp. 686-690, 1985.

20. H. R. Bilger, G. L. Shaw, and B. J. Simmons, "Calibration of a large passive laser ring," SPIE 487, pp. 110-113,1984.

21. G. L. Shaw, B. J. Simmons, and H. R. Bilger, "Limits of sensitivity and calibration of a large laser ring," Workshop on Physics of optical ring gyros, Snowbird, UT, 7-10 Jan., 1984.

22. H. R. Bilger and W. K. Stowell, "Light drag in a ringlaser: An improved determination of the drag coefficient," Phys. Rev. A16, pp. 313-319, 1977; E. J. Post, "Sagnac effect," Rev. Mod. Phys. 39, pp. 475-493, 1967.

23. S. Dushman, "Scientific Foundations of Vacuum Technique," 2nd ed., Wiley 1962.

24. An early account of drag in a commercial ringlaser is given in J. Killpatrick, "The laser gyro," IEEE Spectrum, Oct. 1967, pp. 44-55.

25. M. Born and E. Wolf, "Principles of Optics" 5th ed., Pergamon, 1975.

END

FILMED

10-85

DTIC